SURVEY OF MICRORNA FUNCTIONS IN *DROSOPHILA MELANOGASTER*

PUSHPA VERMA

(M.Sc. GENETICS, UNIVERSITY OF DELHI, INDIA)

A THESIS SUBMITTED FOR THE DEGREE OF DOCTOR OF PHILOSOPHY

DEPARTMENT OF BIOLOGICAL SCIENCES

NATIONAL UNIVERSITY OF SINGAPORE

2013

DECLARATION

I hereby declare that the thesis is my original work and it has been written by me in its entirety. I have duly acknowledged all the sources of information, which have been used in the thesis.

This thesis has also not been submitted for any degree in any university previously.

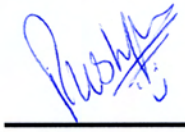

PUSHPA VERMA

3rd January 2013

ACKNOWLEDGEMENTS

I am incredibly thankful to my supervisor Dr Stephen Cohen for giving me opportunity to work in his lab, for his valuable insights, constant encouragement, support, guidance, discussions and for his patience. I am really thankful to him for having confidence in me and for giving me freedom to shape my projects. I will always cherish his immense scientific enthusiasm and motivation.

I would like to thank all past members of Cohen's lab: Thomas Sandmann for being a priceless friend, a cheerful colleague and an encouraging mentor. Jishy Varghese for his patience and insightful discussions, Ville Hietakangas and Sebastien Szuplewski for sharing their knowledge with me, Valerie Hilgers for being a valuable friend and for sharing her thoughts over the tea, Wanzhong Ge for his generosity and kindness and being extremely nice colleague to work with and a true friend, Marilou for her pleasant company and for her willingness to always discuss and listen to me.

I am grateful to all present members of Cohen's lab for their useful discussions and for making lab a pleasant place to work: Sherry Aw, Hector Herranz, Marita Buescher, Yawen Chen, Hong Xin, Ruifen Weng, Jan Kugler, Siew Choo Lim, Lynette Foo, Devika Garg. I would like to express my gratitude to David Foronda for introducing me to the world of histoblasts and for his time and suggestions. My sincere thanks go to Shilin Song, Kah Junn Tan and Singfee Lim for technical assistant. I would like to thanks Singfee for providing constant support and for lending an ear during my good and bad times during course of my Ph.D. I would always cherish her invaluable friendship. I am thankful to Zhang wei for being a very patient, a helpful friend and colleague and for giving me company for dinner during

my course of Ph.D. I would like to thanks Alice and Linda for providing assistance with fly food preparation and fly flipping.

I would like to thanks all past and present members of Pernille's lab for making fly room a pleasant place to work: Adam Cliffe, Smitha Vishnu, Hsin Ho Nachen, Rishita, Lara, Mikiko and Isaac.

My sincere thank goes to my graduate supervisory committee members, Pernille Rorth, Toshie Kai and Mohan Balasubramanian for their invaluable suggestions and great encouragement during the course of my work.

I am extremely grateful to Prof George Augustine for his help and for enlightening me with his knowledge about neurobiology during my stay in Korea and Singapore. I sincerely thank him for very patiently teaching me electrophysiology. I am thankful to his lab members in Korea for their help and cooperation.

I want to acknowledge my parents for always being very understanding, encouraging and supportive. I really admire them for giving me values, which helped me becoming a better human being. I am thankful to my sisters, brother and cousins to provide a cheerful environment at home. I am extremely grateful to my best friend and husband now, Vineet for his unconditional love, understanding and support during good and bad phases of my life.

I am thankful to my friends outside of the lab, Pooja, Ekta, Ramesh, Poornima, Amit, Priyanka, Anil, Roopali, Anindya and Veena for making my life cheerful. I also want to thanks all my friends from India for being excellent friends over the years: Nitin, Yatender, Vidhi, Navneet, Tanweer, Pallavi, Srikant, Babita, Yukti.

Last but not the least, I am thankful to Temasek Life Sciences Laboratory (TLL) and Institute of Molecular and Cellular Biology (IMCB) for providing excellent scientific infrastructure and financial support during the course of my Ph.D.

TABLE OF CONTENTS

SUMMARY

miRNAs (microRNAs) are endogenous small noncoding RNAs, which act as post-transcriptional regulators of gene expression. They play an important role in fine-tuning a broad range of biological processes like growth, development, metabolism, neurodegeneration etc. To date, miRNAs have been found in almost all organisms from plants to Humans. In *Drosophila* a total of 426 mature miRNAs have been identified, however the *in vivo* function of most of these miRNAs remains to be deciphered.

This thesis work aims to characterize functions of miRNAs, using reverse genetics in *Drosophila melanogaster*. This work was started by studying 53 novel miRNAs, newly predicted in 2007. *In-situ* hybridization in embryos was used for screening the novel miRNAs for their expression pattern. Based on their expression patterns and conservation (at least across 12 different *Drosophila* species), 8 miRNAs (*miR-252, miR-965, miR-927, miR-980, miR-993, miR-995, miR-998* and *miR-1000*) were selected for detailed functional analysis. Two knockouts were generated for each miRNA using the ends-out method of homologous recombination. miRNA GFP-knock-in, GAL4-knock-in and rescue alleles were generated by inserting GFP, GAL4 and the miRNA hairpin respectively, into the endogenous miRNA locus using recombinase mediated cassette exchange (RMCE). Most miRNA mutants showed subtle defects during phenotypic evaluation. This thesis describes in depth functional characterization of two of these miRNAs, *miR-1000* and *miR-965*.

Chapter 4 presents characterization of *miR-1000*. *miR-1000* is expressed in the nervous system throughout development, with reduced expression with age. The *mir-1000* mutants showed early onset neurodegeneration, marked by short lifespan, locomotion and coordination defects, accompanied by increased apoptosis in the brain. Overexpression of a nervous system specific gene, called Vesicular Glutamate Transporter (*VGlut*) was discovered to be the cause of neurodegenerative features of the *miR-1000* mutant. *VGlut* loads the excitatory neurotransmitter Glutamate, into synaptic vesicles. Increased expression of *VGlut* in the *miR-1000* mutant caused excess glutamatergic signaling and subsequent excitotoxicity in the brain. *VGlut* regulation by *miR-1000* in *Drosophila* showed functional conservation in mammals too. In summary, *miR-1000* was shown to play a neuroprotective role in the brain by regulating glutamatergic signaling.

Chapter 5 describes functional characterization of *miR-965*. *miR-965* is expressed in the histoblast cells (precursors of adult abdominal epithelium). *miR-965* mutant flies showed abdominal segment deformations in the adults. Asynchronous divisions of histoblast cells during early pupal stage and abnormal migration of these cells in the later stages was discovered to be the cause of abnormal segmentation defects in the *miR-965* mutant. *miR-965* was found to target two genes, *string (cdc25)* and *wingless (wg)* during histoblast development. In summary, *miR-965* controls adult segmentation formation by regulating *stg* and *wg* mediated cell division and migration processes.

LIST OF FIGURES AND TABLES

FIGURES:

ABBREVIATIONS

Abbreviations	**Full name**
Pri-miRNA	Primary miRNA
Pre-miRNA	Precursor of miRNA
RISC	RNA-induced Silencing Complex
dsRBD	double strand RNA Binding Domain
Loqs	Loquacious
3'UTR	3' Un-Translated Region
Ago	Argonaute
DGCR8	DiGeorge Syndrome Critical Region 8
P-bodies	Processing bodies
Df	Deficiency
CNS	Central Nervous system
NMJ	Neuro-Muscular Junction
FFL	Feed Forward Loop
SNPs	Single Nucleotide Polymorphisms
PCR	Polymerase chain Reaction
SLIC	Sequence and Ligation Independent Cloning
PNK	Polynucleotide Kinase
ATP	Adenosine Triphosphate
CIP	Calf Intenstine Phosphatase
RMCE	Recombination Mediated Cassette Exchange
KO	Knockout
rp49	Ribosomal Protein 49
S2 cells	Schneider cells
HL3.1 medium	Hemolymph Like medium
LNA	Locked Nucleic Acid
GFP	Green Florescent Protein
RFP	Red Florescent Protein
PFA	Paraformaldehyde
PBS	Phosphate Buffer Saline
PBT	Phosphate Buffer Triton-X
NGS	Normal Goat Serum
BSA	Bovine Serum Albumin
UTP	Uridine triphosphate
DIG	Digoxigenin
AP	Alkaline Phosphatase
EPSP	Excitatory Post-synaptic Potential
IPSP	Inhibitory Post-synaptic Potential
VGlut	Vesicular Glutamate Transporter
NMDAR	*N*-methyl-D-aspartate receptor
GluNR	Glutamate binding NMDA receptor subunit
AMPA	α-amino-3-hydroxy-5-methyl-4-isoxazolepropionic acid
ADAR2	Adenosine deaminase acting on RNA 2
ALS	Amyotrophic lateral sclerosis

KR	Kainate receptors
mGluR	Metabotropic receptors
iGluR	Ionotropic Glutamate receptors
GPCRs	G protein-coupled receptors
DHPG	3,5-dihydroxyphenylglycine
DCG-IV	2-(2,3-dicarboxycyclopropyl) glycine
L-AP4	2-amino-4-phosphonobutyrate
ROS	Reactive oxygen species
EAATs	Excitatory Amino Acid Transporters
mEJPs	miniature Excitatory Junction Potentials
DIAP1	Drosophila Inhibitor of Apoptosis1
APF	After pupa formation
LEC	Larval epidermal cells
en	*engrailed*
hh	*hedgehog*
stg	*string*
wg	*wingless*
AP	Anterior-posterior
DV	Dorsal-ventral
esg	*escargot*
EGFR	*epidermal growth factor receptor*
UAS	Upstream Activating sequence
Hb9	*Homeobox 9*
MHC	Myosin Heavy Chain
Dlg	Discs large

CHAPTER 1: INTRODUCTION

1.1 Functions of miRNAs in biological processes

Organisms use various mechanisms to maintain robust response to various environmental and biological fluctuations. Repression of gene expression through miRNAs is one such regulatory mechanism, which confers robustness in the biological systems.

miRNAs are small, endogenous, 20-24 nucleotide, non-coding RNAs. The first miRNA was discovered and characterized in 1993 in *C. elegans* (Lee at al 1993). Since then thousands of miRNAs have been discovered in various species. According to miRbase (release 18), the Human genome encodes 2042, mouse 1281, zebrafish 247, *Drosophila* 426 and *C. elegans* 368 miRNAs and their number has been increasing every year with the development of high throughput methods of small RNA sequencing and computational analysis.

Recently, miRNAs have emerged as important regulators of gene expression and their misregulation in various tissues often results in disease conditions. Increasing evidences indicate important roles of miRNAs in disease development, progression, diagnosis and treatments.

let-7 expression is often found to be reduced in lung cancer and its overexpression can dramatically inhibit tumor growth *in vivo* (Esquela-Kerscher et al 2008, Osada & Takahashi 2011, Wang et al 2012). Conversely, a subset of miRNAs, including *miR-21* and *miR-155* have been observed to be highly expressed in a variety of tumors and may serve to promote tumor growth (Caponi et al 2012, Grignol et al 2011, Lee et al 2012, Yang et al 2012). Global miRNA expression is frequently changed in tumor samples relative to normal tissues, thus emphasizing the importance of miRNAs in oncogenesis.

In the nervous system, *miR-9* was reported to be necessary for the proliferation of neural precursor cells (Laneve et al 2010). In human and mouse midbrains, *miR-133* was found to regulate dopaminergic neuron differentiation by targeting a transcription factor, *Pitx3*, which is known to promote dopaminergic neuron differentiation and survival (Kim et al 2007). *miR-8* and *miR-34* act as neuro-protective miRNAs by limiting expression of *atrophin* and *Eip74EF* respectively and their loss of function cause neurodegeneration (Karres et al 2007, Liu et al 2012). All these reports emphasize the importance of miRNAs in brain development and neuroprotection.

miRNAs are also found to be located at the sites of genomic instability, including duplications and fragile sites, thus contributing to disease pathogenesis. Chromosomal region 13q14 containing *miR-15* and *miR-16* was observed to be deleted in ~68% of chronic lymphocytic leukemia (CLL) patients (Calin et al 2002). Chromosomal rearrangement of *miR-142* located at the junction of the t(8;17) resulted in an aggressive B-cell leukemia (Gauwerky et al 1989).

The *miR-137* locus is observed to have Single Nucleotide Polymorphisms (SNPs) in schizophrenia patients (Cummings et al 2012). SNPs in the *miR-7* targeting site in *KRAS* 3'UTR acts as diagnostic markers in early-stage colorectal cancer and metastatic colorectal cancer (Ruzzo et al 2011, Smits et al 2011, Zhang et al 2011). SNP in *miR-7* targeting site is also associated with lung cancer risk (Chin et al 2008). The gene locus of *miR-224* is a candidate region for two neurologic diseases: early-onset Parkinsonism or Waisman syndrome (Gregg et al 1991) and X-linked mental retardation MRX3 (Sutherland et al 1991).

All above-mentioned evidences indicate a need for understanding the functions of miRNAs in various biological processes as well as in disease development.

1.2 Biological modes of miRNA function

Each miRNA can in principle target multiple genes. Functions of some miRNAs can be attributed to one or two target genes while for others, the function is a consequence of simultaneous down-regulation of multiple targets. There are various mechanisms known to determine modes of miRNA functions.

1.2.1 miRNAs as Developmental Switch

miRNAs may act as developmental switches, when they completely eliminate the expression of a target gene in particular tissues. Hence, often miRNAs and their targets have been observed to have mutually exclusive expression across tissues or different stages, where miRNA expression at a particular stage suppresses residual transcripts, required for a previous developmental stage (Farh et al 2005, Stark et al 2005, Tsang et al 2007).

The first miRNAs identified in *C. elegans*, *lin-4* and *let-7*, are examples of developmental switches, where they function as regulators of developmental timing (Lee et al 1993, Wightman et al 1993). Without *lin-4*, the animal was unable to make transition from the first to the second larval stage due to differentiation defects caused by lack of repression of *lin-14* and the deletion of *let-7* led to the failure of larval-to-adult transition due to misregulation of *lin-41* (Reinhart et al 2000). In *Drosophila*, *let-7* was observed to be required for maturation of neuro-muscular junction (NMJ)

during larva to adult transition. *let-7* targets a gene called *abrupt* during this transition and abolishes its expression (Caygill & Johnston 2008).

Mutually exclusive patterns of miRNAs and their targets can also result from Coherent Feed forward loop (Coherent FFL). A coherent FFL exhibits control through a transcription factor, which inhibits (or activates) a target gene but activates (or inhibits, respectively) the miRNA against the target gene (Fig 1a). This kind of loop provides extra fidelity to the system by having additional inhibitory mechanism for a particular target gene. For example, during granulopoiesis in mouse, CCAAT enhancer-binding protein alpha (C/EBPa) inhibits transcription of the cell-cycle regulator *E2F1*. C/EBPa also induces *miR-223*, which represses *E2F1*, post-transcriptionally. This feed forward loop is in turn interlocked with a feedback loop, where *E2F1* inhibits production of *miR-223* (Pulikkan et al 2010). Positive and negative feedback loops within this system, probably results in a better control over developmental fates.

Mutual negative feedback loops have been shown to underlie bi-stable genetic switches, which can be activated by a transient changes in gene expression. The transcription factor, *NFI-A* suppresses expression of primary *miR-223* transcript in undifferentiated myeloid precursors in humans. Upon retinoic acid-induced differentiation into granulocytes, *miR-223* accumulates and represses *NFI-A*, thereby helping to prevent a return to the precursor state (Fig 1b) (Fazi et al 2005).

Developmental decisions can also be reinforced by positive feedback loop, wherein a gene activates miRNA transcription, which in turn represses a negative regulator of the target gene, hence activating the target gene indirectly. In worms, the ‘‘2 degrees’’ vulval precursor cell fate is established, when *LIN12* activates transcription of *miR-61*, which then represses *vav-1*, a negative regulator of *LIN12*

activity (Fig 1c), hence *miR-61* positively control *LIN12* activity (Yoo & Greenwald 2005). In *Drosophila*, *miR-14* controls ecdysone signaling by repressing ecdysone receptor, *EcR,* which in turn down regulates *mir-14*, thus forming a positive autoregulatory loop (Varghese & Cohen 2007).

1.2.2 miRNAs as fine-tuner

miRNAs act as fine-tuners when they modulate the target gene expression to an optimal level. These miRNAs do not eliminate expression of their targets, but attenuate them to the required level. Generally, mutants of miRNA in this category produce subtle phenotypes because of their modulatory nature. Antisense-mediated silencing of the abundant liver-specific miRNA, *miR-122* in the mouse leads to significant upregulation of various targets. These mice were found to be healthy and showed substantially reduced levels of circulating cholesterol and triglycerides. Thus *miR-122* was shown to have a function in hepatic lipid metabolism and may be required to fine-tune this process without affecting overall morphology or health of the organism (Esau et al 2006). In *Drosophila miR-8* mutants, *atrophin* levels were high, which correlated with behavioral defects and neuro-degeneration. In contrast, lower than normal *atrophin* levels resulted in reduced viability of flies (Karres et al 2007). Therefore, *miR-8* acts as a fine-tuning miRNA, which maintains the optimal amount of *atrophin*, required for proper cellular function in flies. Similarly, *miR-14* maintains insulin dependent energy homeostasis in *Drosophila* by fine-tuning a target called *sugarbabe* (Varghese et al 2010).

1.2.3 miRNAs as buffers

Sometimes, miRNAs act as buffers counteracting variation in gene expression. Modulation of gene expression by a negative feedback loop, in which a target gene

activates miRNA and a miRNA inhibits the target gene is such a scenario. In mammals, methyl CpG-binding protein 2 (*MeCP2*) acts through BDNF to induce the neuronal *miR-132*, which then feeds back to repress *MeCP2* (Klein et al 2007). Homeostasis in the level of *MeCP2* expression is important, as overexpression or downregulation of this regulator causes neuro-developmental defects.

miRNAs can also buffer the system by incoherent Feed forward loop (incoherent FFL). This occurs when a gene is repressed by a co-regulated production of a miRNA, that targets the gene. In Zebrafish, an intronic miRNA, *miR-26b* provides a perfect example of incoherent FFL, where it targets its host gene *ctdsp2*, by repressing a cofactor gene called *REST* during neurogenesis (Fig 1d) (Dill et al 2012).

Since these miRNAs generally act as buffers to maintain homeostasis of a system, deletion of each of them might not produce a strong mutant phenotype under normal conditions. However, certain stress conditions may aggravate a phenotype with such miRNAs (Brenner et al 2010). For example, mouse embryonic stem cell-specific *miR-290-295* cluster is only required for cell viability under DNA damage stress conditions (Zheng et al 2011). In mice, deletion of the heart muscle-specific miRNA, *miR-208* causes minor phenotypic defects under normal conditions but results in a failure to induce cardiac remodeling upon stress induced by hypothyroidism or pressure overload (van Rooij et al 2007).

a) Coherent feed forward loop

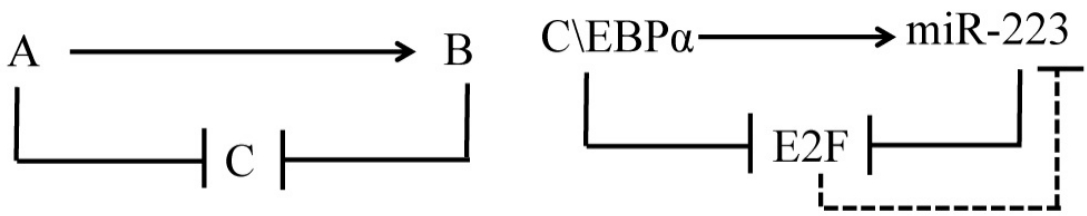

b) Mutual negative feedback

c) Positive feedback loop

d) Incoherent feed forward loop

Figure 1: Biological modes of miRNA function.

Examples of different modes of target regulation by miRNAs
a) Coherent feedback loop, b) Negative feedback, c) Positive feedback and d) Incoherent feed forward loop.

1.3 miRNAs biogenesis

miRNAs are produced by RNA polymerase II as a primary transcript called the pri-miRNA (Cai et al 2004, Kim 2005, Lee et al 2004) (Fig 2a). They may originate from independent transcriptional units at intergenic locations or from introns or exons of protein coding genes (Rodriguez et al 2004). Certain miRNAs are transcribed as poly-cistronic transcripts to allow coordinated expression (Altuvia et al 2005). The Pri-miRNA forms a stable hairpin structure, which is recognized by RNAse III enzyme, Drosha and nuclear protein DGCR8. Drosha and DGCR8 complex cleaves pri-miRNA into 70-80 nucleotide long pre-miRNA (Precursor miRNA) with a two-nucleotide overhang at the 3'end (Gregory et al 2006). miRNAs generated from short intronic hairpins are called "mirtrons". Mirtrons bypass drosha processing and are generated by action of splicing machinery that release pre-miRNA like hairpins from their host transcripts (Okamura et al 2007, Ruby et al 2007a). The pre-miRNA and mirtron-derived pre-miRNA are exported from the nucleus into the cytoplasm. This is achieved by the nucleo-cytoplasmic shuttle, Exportin 5 and Ran-GTP (Bohnsack et al 2004, Yi et al 2003). Exportin 5 recognises properly processed pre-miRNAs, which have 2 nucleotide overhangs at the 3'end and transport them to the cytoplasm.

In the cytoplasm, pre-miRNA is loaded onto the RISC (RNA-induced Silencing Complex) complex, consisting of RNAse III enzyme DICER and dsRBD (double strand RNA Binding Domain) protein, Loquacious (Loqs) (Forstemann et al 2005, Hutvagner et al 2001, Jiang et al 2005, Ketting et al 2001, Saito et al 2005). DICER-1 cleaves the pre-miRNA to give rise to ~22 nucleotide mature "miRNA-miRNA*" duplex, with 2 nucleotide overhang at the 3' ends and 5' terminal phosphates. The "miRNA*" strand of the duplex degrades during the final miRNA

maturation step. The “miRNA” strand gets incorporated into the RISC complex (Chendrimada et al 2005, Gregory et al 2005, Khvorova et al 2003, Maniataki & Mourelatos 2005, Matranga et al 2005, Schwarz et al 2003, Seitz et al 2011), where miRNA binds to its target mRNA to repress its expression.

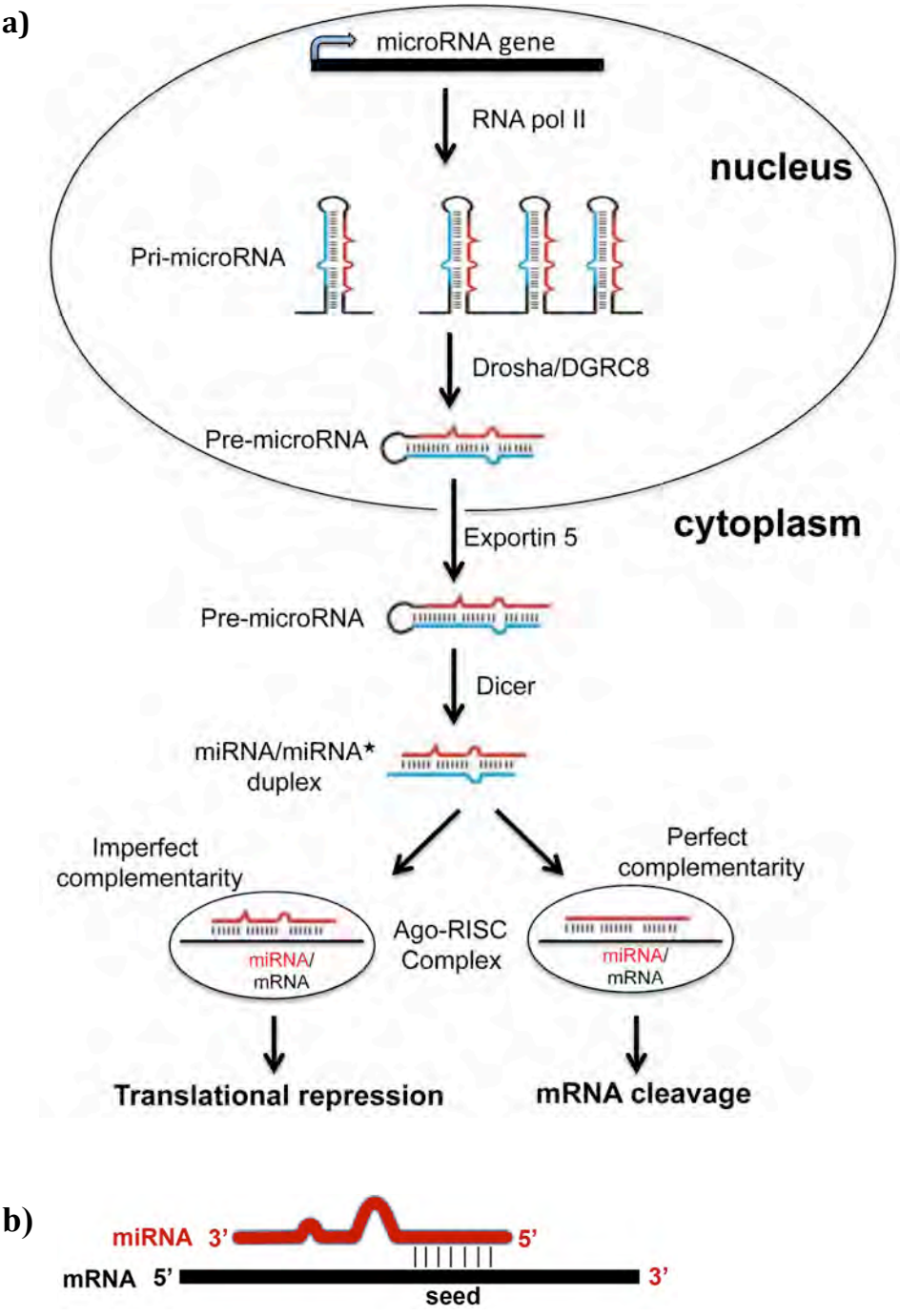

Figure 2: miRNA biogenesis and its action.

a) Description of miRNA biogenesis and mode of repression
b) Schematic showing a typical "seed" match of miRNA with its target mRNA

1.4 miRNA-mediated targeting of genes

miRNAs often repress their target genes by binding to the miRNA target site in the 3'UTR (3' Un-Translated) of a target gene. Approximately, 40-60% of genes are subjected to the miRNA regulation with their transcripts bearing at least one miRNA-binding site in their 3'UTR region (Friedman & Jones 2009).

1.4.1 miRNA target recognition elements

In plants, repression is achieved through complete complementarity between a miRNA and its target genes (Llave et al 2002, Reinhart et al 2002, Rhoades et al 2002), whereas in the animal system, miRNAs and their target mRNAs have imperfect complementarity. Repression in the latter case is mediated by a "seed" sequence, 2-7 bases from the 5'end of miRNA, which binds to the target site in the 3'UTR, 5'UTR or in coding regions of target transcript (Brennecke et al 2005, Doench & Sharp 2004) (Fig 2b).

Based on the seed sequence, the miRNA target sites on mRNA in animals can be categorized into three types:

1. Canonical sites: These sites form perfect 7-mer matches to miRNAs, mediated by perfect pairing of 2-8 or 1-7 nucleotide part at 5'end of miRNA (Brennecke et al 2005, Doench & Sharp 2004, Krek et al 2005, Lewis et al 2003).
2. Marginal sites: These sites form 6-mers of reduced efficacy by having matches to 2-7 or 3-8 nucleotide of miRNA seed region.
3. Atypical sites: These site form 3' supplementary sites, with seed match around 13-16 nucleotides at the 3'end. These sites compensate mismatch at the 5'end by providing perfect pairing at

the 3' end (Brennecke et al 2005, Doench & Sharp 2004, Grimson et al 2007, Krek et al 2005, Nielsen et al 2007).

In addition to the above-mentioned sites, there are reports of miRNA recognizing its targets by seedless but highly complementary sequence in the 3'UTR of the target gene (Lal et al 2009).

1.4.2 miRNA target prediction methods

Several computational algorithms have been developed to predict miRNAs and their targets based on their sequence complementarity, conservation, thermodynamic stability and more (Betel et al 2008, Lall et al 2006, Ruby et al 2007b, Stark et al 2005). Though there are many computational methods for target prediction, none of these methods alone is able to predict all biologically relevant miRNA targets with complete accuracy. Nevertheless, they provide putative miRNA target candidates for *in-vitro* or *in-vivo* confirmation.

Computational prediction methods used commonly for miRNA target prediction are mentioned below

1. Targetscan (http://www.targetscan.org): Targetscan predicts targets of miRNAs by looking for presence of conserved 8mer and 7mer miRNA seed sites in the UTRs of the target genes. It also identifies sites with mismatches in the seed region that are compensated by conserved 3' pairing. It calculates secondary structure of UTRs also. Predictions are ranked using site number, site type, and site context by considering factors that influence target-site accessibility. It incorporates five general features of site context that improve site efficacy:
    a) AU-rich nucleotide composition near the site.

b) Proximity to sites for co-expressed miRNAs, which leads to co-operative action.

c) Proximity to residues pairing to miRNA nucleotides 13-16.

d) Positioning within the 3'UTR at least 15 nucleotide from the stop codon.

e) Positioning away from the center of long UTRs.

(Grimson et al 2007, Lewis et al 2005).

Targetscan is the most commonly used prediction program but it does not take free energy of miRNA-mRNA interaction into account, thus misses certain important targets. It has 30% false prediction rate.

2. miRanda (http://www.miRNA.org/miRNA/home.do): The miRanda program (John et al 2004) is a three-step method for target identification in vertebrates, which is based on the following criteria.

   a) Sequence complementarity using a position-based alignment algorithm.

   b) miRNA-mRNA pair possibility based on free energies of RNA-RNA duplex formation (Wuchty et al 1999).

   c) Conservation of targets in related genomes.

   Limitation of this program is that it predicts targets of only human and mouse miRNAs and cannot be applied for invertebrates.

3. RNA hybrid (http://bibiserv.techfak.uni-bielefeld.de/rnahybrid): RNA hybrid is a computational program for finding the minimum free energy hybridization of a long and a short RNA. Free energy is calculated by energy gained from the formation of the miRNA-target duplex and amount of energy spent to

unpair the target to make it accessible to the miRNA. It takes candidate target sequences and a set of miRNAs and searches for energetically favorable binding sites (Rehmsmeier et al 2004). RNA hybrid is used to predict *Drosophila* miRNA targets in the 3' UTRs and coding sequence but it often predict sites in UTRs, which are not typical seed matches for miRNAs.

4. PicTar (http://pictar.mdc-berlin.de): PicTar identifies miRNA targets by searching for both perfect and imperfect seed in the 3'UTR alignment across different species (Krek et al 2005). It filters the target sites by calculating free energy of hybridization. In addition, this algorithm takes both miRNA and target gene expression profiles into consideration. PicTar predicts targets for human, mouse, flies and worms.

5. PITA (http://genie.weizmann.ac.il/pubs/mir07/mir07_prediction.html): This algorithm is based on calculating free energy of miRNA-target interaction. This miRNA target prediction method considers that target accessibility is a critical factor for miRNA function (Kertesz et al 2007). Besides that, this algorithm considers seed sequences of 6-8bp, beginning at position 2 of miRNA with no mismatches or loops allowed, thus it misses genes targeted by atypical miRNA seed sites.

6. DIANA-microT-Analyzer (http://www.diana.pcbi.upenn.edu/cgi-bin/micro_t.cgi): This algorithm takes both 5' and 3' ends of miRNAs into consideration for the prediction of miRNA targets (Kiriakidou et al 2004), but it is limited to target prediction of human and mouse miRNAs only.

7. RNA22 (http://cbcsrv.watson.ibm.com/rna22.html): RNA22 is pattern-based algorithm for prediction of miRNA target sites and miRNA:mRNA hetero-duplex formation. This method does not rely on conservation across different species. It first identifies potential miRNA binding sites in a gene of interest and then its targeting miRNA, thus permiting identification of targeting site in a gene that may not be present in closely related species (Miranda et al 2006). It has an additional advantage of predicting non-canonical target sites in 3'UTRs (Lal et al 2009).

For better prediction of miRNA targets, a combinatorial approach is often taken including two or more of above-mentioned programs, which encompass all important features including conservation, seed sequences and free energy of miRNA-mRNA. Targetscan and RNA hybrid methods are used in the present investigation to predict targets of miRNAs in *Drosophila melanogaster*.

1.5 Mechanism of miRNA repression of target genes

miRNAs repress expression of their target mRNA by incorporating them into the RISC complex. In *Drosophila*, miRNA can be loaded into Ago1 (Argonaute1) or Ago2 (Argonaute2) containing RISC complex, depending upon their complementarity. The RISC containing Ago1, represses mRNAs that have partial seed match with miRNA, whereas Ago2-RISC silences perfectly or near-perfectly matched target mRNAs (Forstemann et al 2007, Hutvagner & Zamore 2002a, Okamura et al 2004, Tomari et al 2007). RISC incorporated mRNAs are repressed by either translational inhibition or mRNA degradation.

1.5.1 Translational Inhibition of targets

Translation inhibition of targets results in reduction in protein product than its corresponding transcript due to post-transcriptional regulation. Translation inhibition by miRNA has been reported to take place either at the translation initiation step or the elongation step. At the initiation step, miRNAs have been observed to prevent binding of ribosomes to mRNA (Chendrimada et al 2007, Pillai et al 2005, Thermann & Hentze 2007, Wang & Proud 2008). At the elongation step of translation, miRNAs repress translation either by co-translational protein degradation (Maroney et al 2006, Nottrott et al 2006, Petersen et al 2006) or by premature termination via high rate of ribosomal drop off, resulting in incomplete protein products that would be rapidly degraded (Hendrickson et al 2009, Petersen et al 2006).

1.5.2 mRNA degradation or cleavage

Repression of many miRNA targets is frequently associated with their destabilization. mRNA decay is initiated by recruitment of GW182 protein by Ago to the targeted mRNA. The degradation, or at least its final steps, occurs in P-bodies (Processing bodies) that are enriched in mRNA-catabolizing enzymes and translational repressors (Bagga et al 2005, Behm-Ansmant et al 2006, Coller & Parker 2004, Eulalio et al 2007, Filipowicz et al 2008, Guo et al 2010, Jing et al 2005, Wakiyama et al 2007, Wu et al 2006).

mRNA endonucleolytic cleavage occurs, when miRNA is perfectly or near-perfectly complementary to its target. Cleavage generally occurs between nucleotides 10 and 11 on the target mRNA sequence complementary to the miRNA strand, and is catalyzed by the Ago proteins. mRNA cleavage was shown to be very common for plants, but only a few cases of endogenous mRNA-mediated cleavage have been

reported in animals (Bagga et al 2005, Hutvagner & Zamore 2002b, Khraiwesh et al 2010, Llave et al 2002, Valencia-Sanchez et al 2006, Yekta et al 2004).

Recent reports suggest that co-ordination of several mechanisms of miRNA action is responsible for effective target mRNA repression. mRNA degradation has usually been found coupled to translational inhibition. Translational inhibition is reported to be the primary event, which depends on miRNAs impairing the function of the eIF4F initiation complex and is subsequently followed by mRNA degradation (Morozova et al 2012, Meijer et al 2013).

To summarize, miRNAs play a widespread roles in controlling various aspects of development and disease pathogenesis. In the beginning, to access the global roles played by miRNAs, the miRNA biogenesis pathway was targeted. The Dicer (a main player of the miRNA biogenesis pathway) was mutated in various species. This provided valuable information about roles of miRNAs in various biological processes. In *C. elegans*, *dicer-1* mutants displayed defects in the germ-line development and a burst vulva phenotype (Ketting et al 2001). Simultaneous removal of the maternal and the zygotic dicer-1 resulted in embryonic lethality, suggesting an essential role for miRNAs during embryogenesis (Grishok et al 2001). In *Drosophila*, the *dicer-1* mutant germ-line stem cells displayed cell division defects (Hatfield et al 2005) and depletion of Loquacious, the partner of Dicer-1, caused female sterility (Forstemann et al 2005). Also, double mutant of *Ago1* and *dicer-1* exhibited strong segmentation defects (Meyer et al 2006). Role of a dicer-dependent miRNA biogenesis was also reported in mouse oocytes to support normal development of the embryo (Murchison et al 2007).

The analysis of *dicer* or *ago* mutants has shed light on the types of biological processes that can be regulated by miRNAs. However, the contributions of individual miRNAs remain to be studied. Use of mutants that remove individual miRNAs is the preferred way to address its function. In this study, I have characterized a subset of miRNAs in *Drosophila melanogaster* by generating mutants and exploring their roles in various aspects of development.

CHAPTER 2: MATERIALS AND METHODS

2.1 Molecular biology methods

2.1.1 Cloning strategies and recombination DNA methods

For high fidelity PCR, Phusion enzyme (Thermo Scientific) was used. Go green taq (Promega) was used for colony PCR. TAKARA taq (TAKARA bio) was used for long range PCR. All PCR primers were ordered from 1st base (http://www.base-asia.com/oligo_synthesis). All restriction enzymes were used from New England Biolabs (NEB). All restriction digestions were carried out using appropriate buffer and BSA from NEB at specified temperature. Dephosphorylation of vectors was done using Calf Intenstine Phosphatase (CIP, NEB). Ligation was done by using T4 DNA ligase (NEB) for normal ligation and by using T4 DNA polymerase and recA (NEB) for SLIC (Sequence and Ligation Independent Cloning) method of cloning. SLIC method of cloning is based on recombination between single stranded complementary sequences between vector and PCR amplified insert (Li & Elledge 2007). All ligated reactions were transformed into competent *E. Coli* cells unless otherwise indicated. Ligation mix was transformed by mixing with *E. Coli* DH5α competent cells. Reaction was put on ice for 30 minutes, heat shocked for 45 seconds and recovered on ice for 2 minutes. Ligation mix was plated on LB agar (LB containing 1.5% bacto-agar) supplemented with appropriate antibiotics and grown at 37°C overnight. Positive clones were checked by colony PCR.

2.1.1.1: Cloning for in-situ probes

For cloning of in-situ hybridization probes, DNA fragments corresponding to the miRNA primary transcript were generated by PCR using Phusion enzyme. A 3’

A-overhang was added to the blunt-ended PCR product using Taq polymerase with its buffer and dATP at 72°C for 15 minutes and cloned into TOPO-TA vector (Invitrogen). The table below shows the primers used for PCR.

Primers for in-situ probes

miRNA name	**In-situ probe Primers**
miR-1	F- CCGAAAAGCAGAAACAAAGC R- TTATACACCAGGGCCCACAT
miR-316	F- TTCTCTGCCTTGGTGTTTGA R-GTAGGTGGATGGCGGTCTTA
miR-252	F- AGGACCTGCACTCTTCCAGA R- TGTTCTGCGATGACAAAAGC
miR-375	F- CGCACCACTACCTGTTCTGA R- TCGTTCCCAAGTCAGTTTCC
miR-927	F- CCAACAGGACTTTCTTCATTCC R- CTGTGCGTTTTCGTCACATC
miR-929	F- AAAAGGCAGAGGAGGAGGAG R- AGTTCGGTTAGTGGGCAGTT
miR-932	F- GGGGAATCGTGCAGTGTAAT R- GTTACCTAAGTGGCCGGTGA
miR-956	F- CAATAAGTTCGGCCACGAAT R- TCCAATCTCGAGTCGCTTTT
miR-958	F- GTGGACTTGGGGTATCTGGA R- GGGCTCTGTCCTCCCTAGTT
miR-959, miR-960	F- CGTGGTCGGAGCTCATTTAT R- CGTTGAACTGACCCCTTTGT
miR-962	F- AGCCACGCAATCTAGGAGAA R- CGGGCTTTCCTTTTTGGATA
miR-963	F- ACAAAGGGGTCAGTTCAACG R- AGCATGTCAGCGACAAACAG
miR-964	F- TCAGGTTGTTTCCTGTATTCGAT R- CACAAATCTGTTGCATACTTGC
miR-965	F- AATGAAAAACACTTTTCGTTGC R- CTGGAGGGAACCAACACAAT
miR-968	F- CAAAAATGGCAGTGATGTGG R- AGGGTCTGCCTCCTATTCGT
miR-971	F- GGCCATTTGACTGCTCGTAT R- TTCCCAAGCCAGCAAATAGT

miR-976	F-TTCCAGGACATTGAGCTGTG R- CCCAAAAATCATCGAAGTCAA
miR-975,miR-977	F- AATACGAAAGTGCGGACCAC R- AGACGTTTCGTTTGCTTGCT
miR-980	F- GCACTCCACCATCTCCGTAT R- GTGCCATCGATGACCTTCTT
miR-981	F- GATTCCGATAGGTGGGATTG R- TTTCTTGCTTGTCGCCTTTT
miR-992	F- GCGAGGAAATCGAAGGAAT R- AACGAGCAATTGTTTGTATTGG
miR-993	F- AGTGGGTTTGTTTGGTGTCC R- CTCGCAGAGGAAGTGAAACC
miR-994, miR-318	F- TCTTGAATCCCACAACGTGA R- AAACTTGATCCAAGAAATTCAAATG
miR-995	LNA probes: UAGCACCACAUGAUUCGGCUU
miR-998	LNA probes: UAGCACCAUGAGAUUCAGCUC
miR-999	F- TGAAAACGACCTGCTGTCAC R- AATCGAATGCAAACCGTAGC
miR-1000	F- AAATCAGGGAGTGGTCGTTG R-ACCACCCTCGAATGTGTAGC
miR-1002	F- TTCTGCTTGCTTGACACTGC R- TGATTGCTGCTGGGATTATG

2.1.1.2: Cloning miRNA-GFP sensors

miRNA sensors were used to visualize expression pattern of miRNA by negatively marking their expression domain by GFP or lacZ. miRNA-GFP sensors were generated by placing a miRNA complementary target site into the 3' UTR of a ubiquitously expressed EGFP expression vector (Mansfield et al 2004). The host plasmid consisted of EGFP under control of the tubulin promoter and with the 3'UTR and polyA addition site from SV40 (Fig 23a). Positive and negative strand's sequence of mature miRNAs was taken as forward and reverse oligonucleotide with attached digested site for XbaI and XhoI respectively. Forward and Reverse primers were mixed in equimolar ratio and annealed using boiling water method. Oligonucleotide

mixture was kept in boiling water for 5 minutes on a heat block and then gradually allowed to cool down to room temperature. Annealed oligos was then phosphorylated using T4 PNK (Polynucleotide Kinase) with its buffer, supplemented with 1mM ATP for 30' at 37°C for addition of 5' phosphate group. PNK was heat inactivated at 65°C for 15 minutes. Ligation of annealed oligos with XbaI-XhoI digested vector was done using T4 ligase (NEB) enzyme with its buffer at room temperature for 30 minutes. Ligation mix was transformed and grown on LB agar plates with ampicillin. Positive clones were sequenced with primers from EGFP.

Oligonucleotides used for miRNA-GFP sensors

miRNA	**GFP-sensor Oligonucleatides**
miR-252	F- CTAGATCCTGCGGCACTAGTACTTAGC R- TCGAGCTAAGTACTAGTGCCGCAGGAT
miR-927	F- CTAGAGGTAAAGCGTAGGAATTCTAAAC R- TCGAGTTTAGAATTCCTACGCTTTACCT
miR-929	F- CTAGACAATCTGACTCCGTTAGGGAGC R- TCGAGCTCCCTAACGGAGTCAGATTGT
miR-932	F- CTAGACTGCAATGCACTACGGAATTGAC R- TCGAGTCAATTCCGTAGTGCATTGCAGT
miR-959	F- CTAGATTCATAATACCCCCGATGACAAC R- TCGAGTTGTCATCGGGGGTATTATGAAT
miR-960	F- CTAGAGCTATGCAATCTGGAATACTCAC R- TCGAGTGAGTATTCCAGATTGCATAGCT
miR-962	F-CTAGAGACAGCATCAATTTCTCTACCTTATC R-TCGAGATAAGGTAGAGAAATTGATGCTGTCT
miR-963	F- CTAGAGAAACAACCTGATATTTACCTTGTC R- TCGAGACAAGGTAAATATCAGGTTGTTTCT
miR-964	F-CTAGAAAGTTAAGCTCCCCTATTCTAATCCCCTATTCTAAC R-TCGAGTTAGAATAGGGGATTAGAATAGGGGAGCTTAACTTT
miR-965	F- CTAGAAAGGGGAAAAGCTATACGCTTAC R- TCGAGTAAGCGTATAGCTTTTCCCCTTT
miR-968	F- CTAGACAACCCTTTAATGGATACTACTTAC R-TCGAGTAAGTAGTATCCATTAAAGGGTTGT
miR-975	F- CTAGAATACAGGATGTAGGAAGTGTTTAC R- TCGAGTAAACACTTCCTACATCCTGTATT
miR-976	F- CTAGAGCATTGATGATAACTAATCCAAC R- TCGAGTTGGATTAGTTATCATCAATGCT
miR-977	F- CTAGATTAGACAACGTGAATATCTCAC R- TCGAGTGAGATATTCACGTTGTCTAAT

miR-980	F- CTAGATAAGCCCTTCACAAGGCAGCTAC R- TCGAGTAGCTGCCTTGTGAAGGGCTTAT
miR-981	F- CTAGATGCAGGTTTCGTCGACAACGAAC R- TCGAGTTCGTTGTCGACGAAACCTGCAT
miR-993	F- CTAGAAGATACCTGTAGAGACGAGCTTCC R- TCGAGGAAGCTCGTCTCTACAGGTATCTT
miR-994	F- CTAGAATCACGGCTACTATTTCCTTAGC R- TCGAGCTAAGGAAATAGTAGCCGTGATT
miR-995	F- CTAGAAAGCCGAATCATGTGGTGCTAC R- TCGAGTAGCACCACATGATTCGGCTTT
miR-998	F- CTAGAAGCTGAATCTCATGGTGCTAC R- TCGAGTAGCACCATGAGATTCAGCTT
miR-1000	F- CTAGAACTGCTGTGACAGGACAATATC R- TCGAGATATTGTCCTGTCACAGCAGTT
miR-1002	F- CTAGATCGCCCTTTGTATCCACTACTTAAC R- TCGAGTTAAGTAGTGGATACAAAGGGCGAT
	Sequencing primers for miRNA GFP sensors
EGFP-C_down	CATGGTCCTGCTGGAGTTCGTG
EGFP-N_down	CTGGTCGAGCTGGACGGCGACG

2.1.1.3: Cloning of miRNA knockout constructs

Two independent knockout mutants were generated for each of the 8 miRNAs selected for detailed functional analysis. Deletion mutant for knockouts will be refer as knockouts (KO1) and RMCE (Recombination Mediated Cassette Exchange) knockouts as KO2 in this thesis.

For knockout alleles KO1, left and right homology arms were amplified using primers incorporating NotI and AscI restriction enzyme sites. A-overhang was added to each arm by treating PCR fragment with Taq polymerase (with Taq buffer and dATP) at 72°C for 15 minutes. PCR fragments were then cloned into TOPO-TA vector (Invitrogen) according to manufacture's protocol. Positive clones were sequenced. Fragments without PCR generated mutations, were cloned into the pW25 targeting vector (Gong & Golic 2003). Vector pW25 contains the mini-white marker gene flanked by loxP sites, multiple cloning sites for cloning of homologous arms,

restriction sites for nuclease I-sceI, FRT recognition site for FLP recombinase and P-elements ends for genomic integration of vector.

For RMCE knockouts KO2, the left homology arm was recloned from pW25 vector into the pW25-2XattP vector (Weng et al 2009) using NotI sites. For the Right arm, PCR fragments were amplified using Phusion enzyme and cloned into the SbfI site by the SLIC method of recombination cloning. Positive clones were confirmed by colony PCR. Final targeting constructs were purified by Midi prep DNA extraction kit and sequenced.

Primers for miRNA knockouts (KO1)

Homology arms for miRNA KO1	**Primer sequences**
miR-252 left arm	F- TA GCGGCCGC TCAGTGTTTCGATTCCATTTAGTT R- TA GCGGCCGC AAGGTTTGATTCGCTTAAAAATCC
miR-252 right arm	F- TA GGCGCGCC GTCGGATGCTCACTGATATTGTAG R- TA GGCGCGCC ACATCCAATATTCACCCTTGATCT
miR-927 left arm	F- TA GCGGCCGC ACCGATCCATTATCATGTTAAAAA R- TA GCGGCCGC GTAAGGTCGGAGAAAAACTTGAAA
miR-927 right arm	F- TA GGCGCGCC GTTACTCCATTTGATCGGGAATAG R- TA GGCGCGCC GCTTGCGCAATTACAACAAATTA
miR-965 left arm	F- TA GCGGCCGC TTAGAGCTATTGCAACGAAAAGTG R- TA GCGGCCGC GTGTAACGGGGATAATAGGATCTG
miR-965 right arm	F- TA GGCGCGCC AACACACACAGATGCAGATACAGA R- TA GGCGCGCC AAATAAACGGTTCACTTCTTCTGC
miR-980 left arm	F- TA GCGGCCGC GCAGTTCGACTCCCGAATAA R- TA GCGGCCGC CCGCACAACACTGCTTTTAG
miR-980 right arm	F- TA GGCGCGCC TGTTGAAAAGCGAATGTGGA R- TA GGCGCGCC CTAGCCAGGCCAAATGAAAA
miR-993 left arm	F- TA GCGGCCGC GTTACATTAAAATGTTGCCATCCA R- TA GCGGCCGC ATTTAAACAAAAGCCCGGAACTAC
miR-993 right arm	F- TA GGCGCGCC CACAGGGTAGAAAGAAACCTCAAT R- TA GGCGCGCC AGTCCAGAAGAGGAAGAACTGAAA
miR-995 left arm	F- TA GCGGCCGC TCGGAAATTATGAAAGTGTAGCAA R- TA GCGGCCGC CATTCGTCAAGGATAATATGTCCA
miR-995 right arm	F- TA GGCGCGCC CACGATTGCCAGTATTTAGCTTTA R- TA GGCGCGCC ACTTGTTTTCCTTCGACTTAGGTG
miR-998 left arm	F- TA GCGGCCGC AACATCTCTCGCTCTATCAGCTCT R- TA GCGGCCGC ATCGTGGGTGTATCTTTATCTCGT
miR-998 right arm	F- TA GGCGCGCC AAATGTCCAAGTTCTTTGTGAATG R- TA GGCGCGCC CAAAATGAATTTGACACGAGGAC

miR-1000 left arm	F- TA GCGGCCGC TTAACATTGTTGAGCGTCATTAGC R- TA GCGGCCGC ACGAAGGTAACCATATCTCAGACC
miR-1000 right arm	F- TA GGCGCGCC AATACTGTGGCGACTTTAGGTAGG R- TA GGCGCGCC CAGCACTTTATTCAATTCACTTGG

Primers for miRNA RMCE knockouts (KO2)

Homology arms for miRNA KO2	**Primer sequences**
miR-252 left arm	F- TA GCGGCCGCTCAGTGTTTCGATTCCATTTAGTT R- TA GCGGCCGCAAGGTTTGATTCGCTTAAAAATCC
miR-252 right arm	F-GTCCGTCAGTACCTGCAACATCCAATATTCACCCT TGATCT R- GATCACGTACGGGCGCGCCGTCGGATGCTCACTG ATATTGT
miR-927 left arm	F- TA GCGGCCGC ACCGATCCATTATCATGTTAAAAA R- TA GCGGCCGC GTAAGGTCGGAGAAAAACTTGAAA
miR-927 right arm	F- GTCCGTCAGTACCTGCAGCTTGCGCAATTACAACA AATTAG R- GATCACGTACGGGCGCGCCGTTACTCCATTTGATC GGGAATA
miR-965 left arm	F- TA GCGGCCGC TTAGAGCTATTGCAACGAAAAGTG R- TA GCGGCCGC GTGTAACGGGGATAATAGGATCTG
miR-965 right arm	F- GGTGTGTCCGTCAGTACCTGCAGGAAATAAACGG TTCACTTCTTCTGC R- ACGTACGGGCGCGCCTGCAGGAACACACACAGAT GCAGATACAGA
miR-980 left arm	F- TA GCGGCCGC GCAGTTCGACTCCCGAATAA R- TA GCGGCCGC CCGCACAACACTGCTTTTAG
miR-980 right arm	F- GGTGTGTCCGTCAGTACCTGCAGGGGCGCGCCCT AGCCAGGCCAAATG R- CCATTACCCTGTTATCCCTAGGGGCGCGCCTGTTG AAAAGCGAATGTG
miR-995 left arm	F- TA GCGGCCGC TCGGAAATTATGAAAGTGTAGCAA R- TA GCGGCCGC CATTCGTCAAGGATAATATGTCCA
miR-995 right arm	F- GGTGTGTCCGTCAGTACCTGCAGGCACGATTGCC AGTATTTAGCTTTA R- ACGTACGGGCGCGCCTGCAGGACTTGTTTTCCTTC GACTTAGGTG
miR-998 left arm	F- TA GCGGCCGC AACATCTCTCGCTCTATCAGCTCT R- TA GCGGCCGC ATCGTGGGTGTATCTTTATCTCGT
miR-998 right arm	F- GGTGTGTCCGTCAGTACCTGCAGGAAATGTCCAAG TTCTTTGTGAATG R- ACGTACGGGCGCGCCTGCAGGCAAAATGAATTTG ACACGAGGAC
miR-1000 left arm	F- TA GCGGCCGC TTAACATTGTTGAGCGTCATTAGC R- TA GCGGCCGC ACGAAGGTAACCATATCTCAGACC

miR-1000 right arm	F- GGTGTGTCCGTCAGTACCTGCAGGAATACTGTGG CGACTTTAGGTAGG R- ACGTACGGGCGCGCCTGCAGGCAGCACTTTATTCA ATTCACTTGG

Primers for colony PCR

Primer name	**Sequence**
Left_993 F	TCGCAGTTCTGTTATTGTTATGGT
Left_995 F	GATAGAGGCGAGAATCAACGTATT
Left_993/995 R	CTTATATAGCGAGCACAGCTACCA
Left_998 F	GTTTTCGTTTTGTTTCGCTTAAAT
Left_998 R	AATAGAGAATAACGGGGCATGATA
Left_1000 F	TGTGAGCTTTGAATTAAAAATGGA
Left_927 F	AGCTCTTTGATTGATTCGCTAAGT
Left_1000/927 R	CTTATATAGCGAGCACAGCTACCAG
Left_252 F	GGTTTTCTGAGATTCTCCCTGTAA
Left_252 R	TGGTTGATTTCAGTAGTTGCAGTT
Left_965 F	GAAGTTTCACTTCTCAGGGGATAA
Left_965 R	ACCAGAATAATCTGTTTCGTGTCA
Left_980 F	ATAACACACATACACACTCACAAAGAAA
Left_980 R	CTATTCAGAGTTCTCTTCTTGTCTTCAA
Right_993 F	GAAAGTGACATCCAGTGTTTGTTC
Right_993 R	ATTAATAATTCAGGCCCACGTAAA
Right_995 F	CTCAAATGGTTCCGAGTGGT
Right_995 R	GTTTCGCTGTGAATCGGAAT
Right_998/980 F	AAAAATGGTGGGCATAATAGTGTT
Right_998 R	CGATGCATTTAGATCTATGTGAGG
Right_980 R	GAATAAGTAGGGCCAAGTTTCAGA
Right_927/252 F	GAAAGTGACATCCAGTGTTTGTTC
Right_927 R	AATTCCCATTCTCGTTATGGTTTA
Right_252 R	GTACACGACTTGCAATGATACACA
Right_965/1000 F	TTTTACTGTTGTTAAAATTCGATCATTC
Right_965 R	TAATAATAATGGCAAGAGCTGAAACTAA
Right_1000 R	CTACAATCATCCAATCTATTTCTCAATC

2.1.1.4 Cloning for RMCE miRNA rescue constructs

For generating miRNA RMCE rescue constructs, genomic DNA containing the miRNA hairpin was PCR amplified using Phusion enzyme and cloned into pIB vector, (digested with SalI-BamHI enzymes) by SLIC cloning. Positive clones were confirmed by colony PCR.

Primers for RMCE miRNA rescue

Primer name	Sequence
927 RMCE res SLIC F	GCGGGCATGTCGAGGTCGACTGTAATTGCGCAA GCGATTATT
927 RMCE res SLIC R	GCTCTAGAACTAGTGGATCCTTAACATGATAAT GGATCGGTAGG
965 RMCE res SLIC F	GCGGGCATGTCGAGGTCGACAAGTAAAATAGC GGAATCAAAATAAT
965 RMCE res SLIC R	GCTCTAGAACTAGTGGATCCAACACTTTTCGTT GCAATAGCTC
980 RMCE res SLIC F	GCGGGCATGTCGAGGTCGACGCGTGTGAAATA CGAAGTTGAT
980 RMCE res SLIC R	GCTCTAGAACTAGTGGATCCTTTATTATTCGGG AGTCGAACTG
995 RMCE res SLIC F	GCGGGCATGTCGAGGTCGACTAATCCAGGTGG AGCAGGAC
995 RMCE res SLIC R	GCTCTAGAACTAGTGGATCCGCTAAATACTGGC AATCGTGA
998 RMCE res SLIC F	GCGGGCATGTCGAGGTCGACTCGTCCTCGTGTC AAATTCA
998 RMCE res SLIC R	GCTCTAGAACTAGTGGATCCCGATTTCATCTGG ACAACCA
252 RMCE res SLIC F	GCGGGCATGTCGAGGTCGACCTTACCAAGTTCG CTTTCCTAAGT
252 RMCE res SLIC R	GCTCTAGAACTAGTGGATCCGAACGGTAAAAC GCAAAGATTAGT
1000 RMCE res SLIC F	GCGGGCATGTCGAGGTCGACTGCGAAATAAAT CACTCCAACTAA
1000 RMCE res SLIC R	GCTCTAGAACTAGTGGATCCGTTTTTCTCAGGTT TTCCTGTCC

Colony PCR primers for RMCE miRNA rescue

Primer name	Sequence
927 RMCE res colony F	AATAGACCGAGATAGGGTTGAGTG
927 RMCE res colony R	TTAACATGATAATGGATCGGTAGG
965 RMCE res colony F	CCGTAAAGCACTAAATCGGAAC
965 RMCE res colony R	TCACAGAAGGGCACATATAACG
980 RMCE res colony F	TCAAAAGAATAGACCGAGATAGGG
980 RMCE res colony R	GCCAAATGAAAAACTGACATACAA
995 RMCE res colony F	TCAAAAGAATAGACCGAGATAGGG
995 RMCE res colony R	ATATTTCCTATGGTTGCCATGAAC
998 RMCE res colony F	CCGTAAAGCACTAAATCGGAACC
998 RMCE res colony R	TCCAAAATGAATTTGACACGAGGA
252 RMCE res colony F	GAACCATCACCCTAATCAAGTTTT
252 RMCE res colony R	GAACGGTAAAACGCAAAGATTAGT

1000 RMCE res colony F	TCAAAAGAATAGACCGAGATAGGG
1000 RMCE res colony R	TACTGCTGTGACAGGACAATATCA

2.1.1.5 Cloning for miRNA genomic rescue constructs

The Genomic rescue (GR) construct was generated for *miR-965* by cloning 336bp of upstream genomic DNA and 7754bp containing the *miR-965* hairpin (from the *kismet* intron) into pCasper4 vector. For control of genomic rescue (CGR), the same genomic fragments were cloned except lacking miRNA hairpin. The region was divided into three parts for SLIC cloning.

Primers for genomic rescue and Control genomic rescue

Primer name	**Sequence**
Upstream kis F	CGTTAACGTTCGAGGTCGACTCTAGACGAAAGCCGGCTAACGTAAC
Upstream kis R	CTTAAAATACGCTCAACTCCGATCCACACATCAAAGACCTCCATTT
Kis intron 1F	ATGGAGGTCTTTGATGTGTGGATCGGAGTTGAGCGTATTTTAAG
Kis intron 1R	ATATCGTGATGCCTTTTGTTTGTACATGT
Kis intron 2F	ACATGTACAAACAAAAGGCATCACGATAT
Kis intron 2 + 965GR	GGGATCAGATCCGCGGCCGCTTGATCTGGAAAGAGAAGACAAAA
Kis intron2 R	GGGATCAGATCCGCGGCCGCAAATACGAGTGCGAAAGTTAAAGG

Colony PCR primers

Primer name	**Sequence**
pCas-up kis F	GAGACAGCGATATGATTGTTGATT
pCas-up kis R	AATCGATGGTTCTTCTTTTTATGC
Up kis-intron1 F	AAAGGTCGACAGTTTTACTTCAGC
Up kis-intron1 R	AAATGTATGCTACAAGCGTTACGA
Kis intron2-pCas F	CCTTTAACTTTCGCACTCGTATTT
Kis intron2-pCas R	ACTTTGTGTTTAATTGATGGCGTA

2.1.1.6 Cloning of miRNA overexpression constructs

For generation of miRNA overexpression constructs, genomic portion containing miRNA hairpin was amplified using Phusion enzyme and Cloned into

NotI-XbaI digested pUAST-DsRed vector. NotI and XbaI sites were added to forward and reverse primer respectively. Positive clones were checked by colony PCR, using DsRed forward primer and miRNA-UAS reverse primers. Same forward primer from DsRed was used for sequencing.

Primers for miRNA overexpression

Primer name	Sequence
252-UAS F	TATAGCGGCCGCCTTACCAAGTTCGCTTTCCTAAGT
252-UAS R	TATATCTAGAGAACGGTAAAACGCAAAGATTAGT
927-UAS F	TATAGCGGCCGCTGTAATTGCGCAAGCGATTATT
927-UAS R	TATATCTAGATTAACATGATAATGGATCGGTAGG
965-UAS F	TATAGCGGCCGCAAGTAAAATAGCGGAATCAAAATAAT
965-UAS R	TATATCTAGAAACACTTTTCGTTGCAATAGCTC
980-UAS F	TATAGCGGCCGCGCGTGTGAAATACGAAGTTGAT
980-UAS R	TATATCTAGATTTATTATTCGGGAGTCGAACTG
993-UAS F	TATAGCGGCCGCGGATGGGATCTCCAATTGTAAC
993-UAS R	TATATCTAGAATTGAGGTTTCTTTCTACCCTGTG
995-UAS F	TAGCGGCCGCTAATCCAGGTGGAGCAGGAC
995-UAS R	TATCTAGAGCTAAATACTGGCAATCGTGA
998-UAS F	TAGCGGCCGCAATCGTCCTCGTGTCAAATTCAT
998-UAS R	TATCTAGAGGAGAGAGAGAGAGAGAGAGCTGA
1000-UAS F	TAGCGGCCGCTGCGAAATAAATCACTCCAACTAA
1000-UAS R	TATCTAGAGTTTTTCTCAGGTTTTCCTGTCC
UAS-DsRed colony/seq F	GAAGCTGAAGGTGACCAAGG

2.1.1.7 Cloning of miRNA luciferase reporter constructs

miRNA expression plasmids were generated by cloning miRNA hairpin into pCasper-tubulin promoter-SV40 vector using XbaI-XhoI sites.

For target gene luciferase reporter constructs, pCasper4-tubulin-Fluc-SV40 vector was used. The vector contains firefly luciferase (Fluc, from pG5luc, Promega) cloned downstream of tubulin promoter using NotI-XbaI sites. SV40 polyadenylation signal (SV40 pA, from N1, Clontech) was cloned after luciferase using XhoI-SalI sites. PCR generated 3'UTRs of target genes were amplified using Phusion enzyme

and cloned downstream of luciferase using XbaI-XhoI sites. Mutations were introduced into the miRNA target sites in the 3'UTRs by PCR, incorporating mutated seed sequences in the primers. The 3'UTRs were amplified in at least two PCR fragments, using the site mutant primers and assembled using SLIC cloning.

Renilla luciferase expression vector was used as transfection control, which was generated by replacing firefly luciferase with Renilla luciferase (Rluc, from pRL-CMV, Promega) in pCasper-tub-Fluc-SV40 vector using NotI-XbaI sites.

Primers for miRNA expression vector

Primer name	**Sequence**
miR-1000 F	TATATCTAGATGCGAAATAAATCACTCCAACTA A
miR-1000 R	TATACTCGAGGTTTTTCTCAGGTTTTCCTGTCC
miR-965 F	TATATCTAGACTTTCATTTTAAGTAAAATAGCGG
miR-965 R	TATACCTCGAGAACACTTTTCGTTGCAATAGCTCT
Hsa-miR-137 F	TATATCTAGACAGCTTGGTCCTCTGACTCTCT
Hsa-miR-137 R	TATACTCGAGAAGAAAGTGCTACCTTGGCAAC

Primer for 3'UTR luciferase reporter constructs

Primer name	**Sequences**
Pc 3'UTR F	GATCGCCGTGTAATTCTAGACCAAACAAATGTCGGGAAA A
Pc 3'UTR R	GGCTGCAGGTCGACCTCGAGCGCTTTGAATTGCTGTTTTG
Jumu 3'UTR F	GATCGCCGTGTAATTCTAGAAGCCCAAAAACCCATTACA TTA
Jumu 3'UTR R	GGCTGCAGGTCGACCTCGAGTTGGTTTCAATTTGTTTTTG TCA
Stg 3'UTR F	GATCGCCGTGTAATTCTAGAGATGATCGTGCAGTTCGTT ATC
Stg 3'UTR R	GGCTGCAGGTCGACCTCGAGTTCTTTTTCGTCGTGTATTA ATGT
Hsp83 3'UTR F	GATCGCCGTGTAATTCTAGAGCGACCAGTCGAAACAAA
Hsp83 3'UTR R	GGCTGCAGGTCGACCTCGAGGATTTTTAAAACACATTTG CTTGTTG
Tor 3'UTR F	GATCGCCGTGTAATTCTAGAGTCAACCGATCCGGCATAG A
Tor 3'UTR R	GGCTGCAGGTCGACCTCGAGTTTTAGAACGTTGATTGTTT CACG
Wg 3'UTR F	GATCGCCGTGTAATTCTAGACCGCCCTCTTCGTTCTTTGT
Wg 3'UTR R	GGCTGCAGGTCGACCTCGAGACTCATTGTCGTTTTGTGTT

	TTT
Hth 3'UTR F	GATCGCCGTGTAATTCTAGAGGAAATGAAACTGGAACTG GAAC
Hth 3'UTR R	GGCTGCAGGTCGACCTCGAGTCATATATGCATTTTGTTTT CATCA
Kis 3'UTR F	GATCGCCGTGTAATTCTAGACAGCGCTAGCAGAATGACA C
Kis 3'UTR R	GGCTGCAGGTCGACCTCGAGTAGTTGATGCTTGGGTGTT TC
VGluT UTR F	GATCGCCGTGTAATTCTAGATCATAGCTTTTAGTTGTAGT CGGAAA
VGluT UTR R	GGCTGCAGGTCGACCTCGAGTTCGTTGGGACTTGTACAA ATAAATA
Hsa-VGluT2 UTR F	TAATTCTAGAAAACTTGCAAGCATATCAACCA
Hsa-VGluT2 UTR R	GACCTCGAGTGTATGATTAATGCACTGCTTT

Primers for colony PCR

Primer name	**Sequence**
pNB11 seq up F	AGATCCTCATAAAGGCCAAGAAG
Colony pNB11 F	AGGTCCTATGATTATGTCCGGTTA
Colony kis 3'UTR R	CAGAGGAAGGGACACTATTGACTT
Colony pc 3'UTR R	TTTCGCCTATTCACTAAATGACAA
Colony jumu 3'UTR R	AAACAAAAGGGCACAAGTTATCTC
Colony stg 3'UTR R	CAAATGATTAAGGGGTCTGATTTC
Colony Hsp83 3'UTR R	CTTAAAACGACAACTGCTCTTGAA
Colony Tor 3'UTR R	TTTTAGAACGTTGATTGTTTCACG
Colony Wg 3'UTR R	ACAAAGGCTAAGCGTAGACAAAAT
Colony Hth 3'UTR R	GTTTCTTTTTGATGTGGTTTGTTG
pNB11 up F	GAA AAA GAG ATC GTG GAT TAC GTC
VGlut luc cln up R	CAT CAA CGG TAA TAA AAC TTG CAG
VGlut luc cln down F	GCC CCT ATT CAT TTA AAG ACA GAA
pNB11 down R	ATT TCG GAT ATA TGT CGG CTA CTC
HSa-VGlut2 Clny F	GAAAAAGAGATCGTGGATTACGTC
HSa-VGlut2 Clny R	TTTGTAGGATGAGATGTTGTGCTT

Primers for mutated 3'UTR luciferase reporters

Primer name	**Sequences**
Stg mut UTR up F	GGGCGGAAAGATCGCCGTGTAATTCTAGAGATGA TCGTGCAGTTCG
Stg mut UTR up R	CAAATAATGATCATAAATTGTACCTAGCAGAAGT T
Stg mut UTR down F	TTATGATCATTATTTGTTTATTTTTATGTAATCCG
Stg mut UTR down F	ATAAACAAATAAAATTGTACCTAGCAGAAGTT
Stg multiple mut 1F	GATCGCCGTGTAATTCTAGAGATGATCGTGCAGT

	TCGTTATC
Stg multiple mut 1R	CATCACTTAGGCGTAATGTCGGATAAATAAAGTTTTATGG
Stg multiple mut 2F	ACGCCTAAGTGATGCCAGATGTACCCTACTGCTAGGTACAATTTA
Stg multiple mut 2R	GGCTGCAGGTCGACCTCGAGTTCTTTTTCGTCGTGTATTAATGT
Wg mut up sphI F	GAACTGCCTGCGTGAGATTCTCGCATGCCAGAGATCCTA
Wg mut up R	CTAATAACAAAGGCTGAGTGGAGACAAAATACATAACACA
Wg mut down F	TGTGTTATGTATTTTGTCTCCACTCAGCCTTTGTTATTA G
Wg mut down R	GGCTGCAGGTCGACCTCGAGACTCATTGTCGTTTTGTGTTTTT
VGlut 1 mut up F	GATCGCCGTGTAATTCTAGATCATAGCTTTTAGTTGTAGTCGGAAA
VGlut 1 mut up R	ACTAGGCTTACTTCACTAGGTTTAGACGCTTACACAAGCAGTATTGTTGT
VGlut 1 mut down F	ACAACAATACTGCTTGTGTAAGCGTCTAAACCTAGTGAAGTAAGCCTAGT
VGlut 1 mut down R	TGGTTAACATATTTATGTTATTTTAGACCACACAGCCCCGAGAGCTTAAG
VGlut 2 mut up F	TGGTCTAAAATAACATAAATATGTTAACCAGAAAGCCACGGTTAAACTTT
VGlut 2 mut up R	GGCTGCAGGTCGACCTCGAGTTCGTTGGGACTTGTACAAATAAATA
Hsa-VGlut2 mut1 up F	GATCGCCGTGTAATTCTAGAAAACTTGCAAGCATATCAACCA
Hsa-VGlut2 mut 1 up R	GGAATCCTCATCTCGATGGGTACACAAATGTTGCAATTCTTG
Hsa-VGlut2 mut 1 down F	CCATCGAGATGAGGATTCCATAAAATTTCCTGTCTGTATATTACC
Hsa-VGlut2 mut1 down R	GGGCTGCAGGTCGACCTCGAGTGTATGATTAATGCACTGCTTTTT

2.1.1.8 Cloning of GFP 3'UTR reporter constructs

All 3'UTR GFP constructs were made by cloning 3'UTR of target gene downstream of EGFP, using XbaI-XhoI site into pCasper-tubulin-EGFP vector. Same wild type and mutated 3'UTRs were used for luciferase and GFP reporter constructs clonings. EGFP from N1, Clontech was cloned using KpnI-NotI site into pCasper-tubulin vector.

2.1.2 Plasmid DNA Preparation

2.1.2.1 Plasmid Mini Prep

A 5ml liquid LB culture of the appropriate plasmid containing cells was set up with the appropriate antibiotic. Culture was shaken vigorously for 14-16 hours at 37°C. The cells were pelleted down at maximum speed (14,000 rpm) in microfuge for 1 minute. DNA extraction was carried out according to manufacturer's protocol, using Qiagen Miniprep kit.

2.1.2.2 Plasmid Midi Prep

A 50-100 ml liquid LB culture of plasmid containing cells was set up with the appropriate antibiotic. Culture was shaken vigorously for 14-16 hours at 37°C. The cells were pelleted at 14,000 rpm for 1 minute in Falcon tubes. DNA extraction was carried out according to manufacturer's protocol, using Qiagen Miniprep kit and DNA was dissolved in water or TE (Tris-EDTA) buffer.

2.2 Fly DNA extraction

2.2.1 Single fly DNA extraction

DNA was extracted from single flies for PCR analysis. Single flies were homogenized for 5 - 10 seconds in a microfuge tube with a pipette tip containing 50µl of "squishing" buffer (10 mM Tris-Cl pH 8.2, 1 mM EDTA, 25 mM NaCl, and 200 µg/ml Proteinase K). Proteinase K was added to the buffer before use. The sample was incubated at 37°C for 30 minutes. Proteinase K was heat inactivated by incubating at 85°C for 10 minutes. The sample was centrifuged at 14000 rpm for 1 minute. The supernatant was transferred into a fresh tube. 1-2µl of supernatant was used for PCR.

2.2.2 Fly DNA extraction for long range PCR

15-20 flies were placed in a microfuge tube on ice. Flies were crushed with lysis buffer, provided with DNeasy Blood and Tissue extraction kit from Qiagen. Proteinase K was added and the homogenized mix was spun at 10000 rpm for 30 sec to remove debris. Supernatant was taken and DNA was extracted according to manufacture's protocol.

2.3 Fly RNA Analysis

2.3.1 RNA extraction

For total RNA extraction, 10-15 flies were crushed into 600µl of TriZol reagent (Invitrogen). For total head RNA extraction, 15-20 flies were placed into microfuge tube and thrown into liquid nitrogen. Tube was taken out and shaken vigorously for 30 second for detaching heads from the body. Heads were collected and homogenized into 600µl of TriZol reagent. The homogenized mix was vortexed and kept at room temperature for 5 minutes. 400µl of chloroform was added and phase separation was done by high-speed centrifugation. The aqueous phase was taken and RNA was precipitated with isopropanol, followed by centrifugation at maximum speed for 20 minutes. The RNA pellet was washed twice with 70% ethanol and air-dried. RNA was dissolved in RNAse-free water.

2.3.2 miRNA RT-qPCR

20-50ng of RNA was used for miRNA RT-qPCR. miRNA RT and qPCR primer sets were obtained from Applied Biosystems (ABI). Reverse transcription and qPCR was done according to manufacture's protocol by using TaqMan miRNA assay kit (ABI). miRNA qPCR results were normalized to U27 and U14 control primers.

2.3.3 Target gene RT-qPCR

Total RNA was treated with DNAse (Promega) to avoid DNA contamination. First strand synthesis was done using oligodT primers and superscriptIII enzyme (Invitrogen). Real time PCR was done using POWER SYBR green (ABI) in an ABI7500 fast real time thermal cycler (ABI). Q-PCR primers were designed by Primer3 software (http://frodo.wi.mit.edu) and ordered from 1st base (Sigma). Results were normalized to endogenous control, ribosomal Protein (rp49).

Primers for qPCR

Primer name	Sequence
kis F	TTCACGGAAATCATCAAGGA
kis R	CTGTTGCTGTAGCGGATGTG
Pc F	TCGTGGAGTACCGTGTCAAG
Pc R	CGGAGGATTTGTTCGTTTGT
jumu F	CAAAACAAAGTGCATGCTAAAAAC
jumu R	GCATCGAGTCGGATACATAAAAGT
Hsp83 F	CAACAAGCAGCGTCTGAAAA
Hsp83 R	CCTGGAATGCAAAGGTCTCT
stg F	ATTCTCCCATTTTCCCAGTTTT
stg R	CTTCCCATCCTATCCTTTCCTT
Wg F	GTC AGG GAC GCA AGC ATA AT
Wg R	GCG AAG GCT CCA GAT AGA CA
Tor F	GAGTTCGACCATCACATTTTC
Tor R	AGTAAGACTGCCCTCGCAGTTA
EGFP F	GCAGTGCTTCAGCCGCTA
EGFP R	AGCCTTCGGGCATGGC
VGlut F	TACTAGCTGAGCAGCAAGATGAAG
VGlut R	TGCGATATCTCAAACTTCTCCATA
Nplp1 F	CGAAATGGAGTCCCTTATAAATCA
Nplp1 R	GTCTTTCCCGAAGTAAGTTTTTCA
slgA F	CCATCAAGGATCTCGAAAAGTATT
slgA R	ACAAATGCAAAATTCCCTCCTTAT
Pdk F	AAAGCAGTTCATGGACTTTGGT
Pdk R	GGCGATCTCCTTCATGATATTC
Rodgi F	AAGTACACGCGATACTGAAGCA
Rodgi R	TTCTCAGTCTTCTTTCCCTCGT
Eaat2 F	GCCGTAGTCGAGGAGTTGTC
Eaat2 R	AAGTCCTCCATCGTGGTGTC
Nmda1 F	CTCAGTCGTTCTTAATGGGAGTTT
Nmda1 R	TAAAGTCGTACTTTGTCTGCAAGG

mGluR1 F	TGTATAATCTGGCTTGCGTTTG
mGluR1 R	GCCACTGACGCACTTAGACTTA
Glu-R1 F	ATTATGATAAAGAAGCCCGTGAAA
Glu-R1 R	GTGGGAAACGTGTAACAAAGTACA
Eaat1 F	AGATTTTCTTGCGAATGCTTAAAT
Eaat1 R	AGTAATGGCTCTGGTAGCAATCTT
rp49 F	GCTAAGCTGTCGCACAAA
rp49 R	TCCGGTGGGCAGCATGTG

2.4 Cell transfection and luciferase assay

2.4.1 Cell transfection

Drosophila Schneider cells (S2) were grown at 25°C in serum free medium (SFM, Gibco) supplemented with L-Glutamine. 2 X 10^6 cells were seeded per well in 24 well plates and cultured for 24 hours before transfection. S2 cells were transfected in 24-well plates with 25ng each of the firefly luciferase reporter and the *Renilla* luciferase control plasmids, and 250ng of the miRNA-expression plasmid or empty vector. Transfection was done using Cellfectin II reagent (Invitrogen). All transfections were performed in triplicate. Each experiment was performed at least three separate times.

2.4.2 Luciferase assay

Dual-luciferase assays (Promega) were performed 2.5 days after transfection. Cells were lysed using 100µl passive lysis buffer (Promega) and shaken at room temperature for 20 minutes. 3-5µl of lysed cells supernatant was taken for luciferase readings. Readings were taken using Infinite 200 multimode reader (Tecan), according to manufacturer's protocol.

2.5 Immunocytochemistry and Confocal microscopy

2.5.1 Fixing Drosophila embryos

Embryos were collected on apple juice agar plates, by housing flies in a cage at 25°C. Embryos were washed in PBT (1X PBS and 0.1% Triton X-100), dechorionated in 50% bleach, rinsed in PBT, fixed in 1:1 heptane: 4% methanol free paraformaldehyde (4% PFA with 0.1M Hepes pH 7.4) for 15 min while shaking, devitellinated in 1:1 heptane: methanol for 1 min and stored in 100% ethanol at -20°C.

2.5.2 Fixing larval and adult tissues for staining

Third instar larvae were dissected in ice cold Phosphate Buffered Saline (1X PBS) and fixed in 4% Paraformaldehyde (PFA) for 20 min at room temperature. Adult brains were dissected in ice cold PBT (PBS+ 0.1% Triton-X) and fixed in 4% PFA for 30 min at room temperature.

2.5.3 Antibody staining for fixed tissues

For immunostaining, embryos were rehydrated in PBT and blocked in 3% BSA-PBT. Samples were incubated with primary antibodies overnight at 4°C. After 4-5 washes in PBT, samples were incubated for 2 hours at room temperature with secondary antibodies (Alexa Fluor, 1:500, Invitrogen).

For Immunostaining, fixed larval tissues were washed three times with PBT and blocked for 1 hour in blocking buffer (PBS+0.2% Triton-X, 0.1g BSA). Samples were incubated with primary antibody in blocking buffer overnight at 4°C. samples were washed 3-4 times with PBT and incubated for 2 hours at room temperature with secondary antibodies (Alexa Fluor, 1:500). Samples were washed with PBT and incubated for 15-20 minutes at room temperature with DAPI (1:1000) for nuclear staining.

For Immunostaining, adult brains were washed several times with PBS+ 0.1% Triton-X (PBT) before blocking with 5% NGS (Normal Goat Serum) for 16hrs at 4°C. Brains were incubated with primary antibody for 36-48hrs at 4°C. Brains were washed several times in PBT and incubated with secondary anitbodies (Alexa Fluor, 1:500) for 16 hours at 4°C. Samples were washed with PBT and stained with DAPI (1:1000) for 20 minutes.

The following antibodies were used.

Antibody name	**Dilution**	**Source**
Mouse anti-Dlg	1:10	Developmental Studies Hybridoma Bank (DSHB)
Rabbit anti-caspase3	1:50	Cell Signaling
Chicken anti-GFP	1:2000	Abcam
Mouse anti-wg	1:10	DSHB
Rabbit anti-VGlut	1:10000	DiAntonio's lab
Mouse anti-MHC	1:50	Daniel Kiehart

Samples were mounted in Vectashield (Vector Laboratories) and analyzed under confocal microscope (Zeiss LSM700). Confocal images were processed using ImageJ and photoshop.

Number of cells with positive staining was counted from stacks of confocal sections using Imaris software (http://www.bitplane.com/go/products/imaris). Cells more than 2μM in size were counted after background subtraction. Two filters of equal quality and constant mean intensity were used for all samples.

2.5.4 Live imaging of pupae

For movies of histoblast proliferation, 0 hour white pupa were taken and washed with PBS. Pupae were dried and stuck to glass bottom microwell imaging dish (MatTek) with the help of mineral oil. For movies of histoblast migration, pupae were staged by picking white pupae at 0hrs APF and allowed to age for 15-16

hours at 25°C. The brown pupal cuticle was removed without damaging internal tissues. Pupae were mounted in the imaging dish with mineral oil for live imaging.

Zeiss LSM700 and Leica SP5 were used for live imaging and movies were processed using imageJ and photoshop.

2.6 miRNA in-situ hybridization

2.6.1 Generation of in-situ probes

Probes were PCR amplified using M13 forward and reverse primers and gel purified before subjecting to *In-vitro* transcription. *In vitro* transcription using digoxigenin (DIG) labeled UTP's (Uridine triphosphate) was done as per the manufacturers protocol (Roche) using SP6 or T7 polymerase based on the probe strand desired. The mix was incubated at 37°C for 2 hours, following which 1µl of DNaseI was added and incubated for another 15 min. RNA was cleaned by RNAeasy kit from Qiagen.

2.6.2 *In-situ* hybridization

1-2µg of RNA probe was used for *in-situ* hybridization of embryos. pri-miRNA transcripts probes and Locked Nucleic Acid (LNA) probes were used and embryo *in-situ* for all miRNA probes was performed as described (Stark et al 2005). Probe were detected with AP-coupled anti-DIG Fab fragments (Roche #1093274; 1:2000; overnight at 4°C) and visualized with NBT/BCIP (Roche #1682326; 30–120 min). A Zeiss Axioplan microscope was used to capture images.

2.7 Fly Genetics

2.7.1 Fly husbandry

Flies were grown in plastic vials or bottles at 25°C under controlled temperature and humidity. Flies were maintained on standard cornmeal food containing cornmeal, dextrose, brewer's yeast, 10% Nepagin and 0.8% agar. All crosses were carried out at 25°C. Stocks were kept at 18°C and flipped every 6 weeks into new food vials.

2.7.2 Generation of transgenic flies

For generation of transgenic flies, P-element system was used for random integration. P-element ends present in the vector helped in plasmid integration into the genome. Plasmids were injected into blastoderm stage embryos at their pole cells end, which resulted in germ line transmission of plasmid. Injected flies were crossed to wild type or balancer flies and screened for presence of red eyes. Red eyes indicated transformation event because of the presence of mini-white gene marker. Red-eyed flies were crossed to balancer flies to map their chromosomal location.

For site-specific injection, plasmid carrying an attB site was injected into phiC31 integrase flies (Groth et al 2004). Transformants were identified as red-eyed flies in the next generation.

2.7.3 Generation of miRNA knockouts

For generation of miRNA knockouts, the targeting vector was randomly integrated into the genome, using the p-element method for generating red-eyed "donor transgenic flies". The P-elements were mapped and donors that were not on the same chromosome as the target miRNA were selected for use. Donors were

crossed with flies carrying heat shock FLP recombinase and endonuclease I-SceI. Progeny were given heat shock at 37°C for 1 hour at the 2nd instar larval stage to generate a linear extra-chromosomal DNA fragment, carrying the targeting cassette. White or mosaic eyed female flies from this cross was mated and red eyed flies were selected in the next generation. Presence of red eye indicated homologous recombination event. Red eye events located on miRNA bearing chromosome were further confirmed by genomic PCR and finally by miRNA qPCR.

2.7.4 Generation of GFP knock-in, GAL4 knock-in and RMCE miRNA rescue flies

miRNA knockout flies carrying mini-white gene with two flanking attP sites were crossed to phiC13 integrase flies. Embryos from this cross were injected with plasmid carrying GFP, GAL4 or miRNA hairpin flanked by attB sites, for generation of GAL4 knock-in, GFP knock-in and RMCE rescue flies respectively. Progeny was screened by loss of the red eye marker, resulted from replacement of mini-white gene by GFP, GAL4 or the miRNA hairpin. Replacement of the mini-white gene by the desired fragment was confirmed by single fly PCR.

2.7.5 Excision of mini-white marker to generate clean knockouts

Presence of mini-white gene often disturbs flanking genes or other non-coding RNAs in the vicinity of deleted miRNA, so to rule out any disruption to the flanking genomic portion by mini-white gene, we excised mini-white from miRNA knockouts. Excision was done using loxP-CRE system of site-specific recombination. Knockouts carrying mini-white gene, flanked by loxP sites, were crossed to CRE recombinase expressing flies. Following recombination, clean white-eyed knockouts with presence of only one loxP was obtained.

2.8 Phenotypic analysis

2.8.1 Embryo hatching, pupariation and adult eclosion assays

Embryos were collected on apple juice plates at 25°C under controlled humidity. Mutants were balanced using florescent balancer chromosomes in order to genotype embryos. 200-300 embryos were transferred to fresh apple juice plate and aged for 2 days at 25°C. The number of hatched embryos was counted.

For pupariation rate, 50 larvae were transferred per vial and grown under control and uncrowded condition.

For adult eclosion rate, the number of adult's eclosed from the pupae in the pupariation sample was counted. Counts were normalized to the number of pupae in the samples. Each experiment was repeated at least three times and the average was determined.

2.8.2 Lifespan assay

Flies were reared under conditions of controlled crowding (50 larvae/vial), temperature and humidity. Groups of 20 male or female flies were collected at eclosion and aged separately. Flies were transferred to fresh vials every 2nd day and the number of dead flies was recorded. The experiment was repeated with at least three independently reared biological replicates and the average was taken.

2.8.3 Climbing assay

Groups of 20 male or female flies, reared under conditions of controlled crowding, were collected when freshly emerged. Flies were aged for 2 day or 10 days without further exposure to CO_2. Before testing, flies were transferred to a graduated cylinder made from a 25ml plastic pipette, and allowed to rest for half an hour before the assay. Flies were tapped down to the bottom of the tube and allowed to climb.

Three trials were done for each sample and the results averaged. The experiment was repeated with 3 independently reared biological samples. Assay was always performed between 2-5pm to avoid differences in activity due to circadian cycles.

2.9 Drug feeding

Memantine hydrochloride (Sigma) was dissolved in water and added to a final concentration of 0.01mM in standard fly food. Food was stored overnight to ensure even distribution of the drug before use. Climbing assays were performed after 24hrs on drug-treated and mock-treated flies.

2.10 Electrophysiology

Spontaneous miniature excitatory junction potential (mEJP) events were recorded from muscle 6 of segment A3 and A4 from third instar larvae. Larvae were dissected in cold calcium free HL3.1 (Hemolymph like) medium (70mM NaCl, 5mM KCl, 4mM $MgCl_2$, 10mM $NaHCO_3$, 5mM Trehalose, 115mM Sucrose, 5mM HEPES, pH-7.2). Segmental nerves and brain were removed before electrophysiology recording. Recordings were done using HL3.1 medium with 0.8mM $CaCl_2$, pH-7.2 at room temperature. A sharp glass electrode filled with 3M KCl was used for recording. Spontaneous events were recorded by Clampex 6 and analyzed by mini-analysis software (http://www.synaptosoft.com/MiniAnalysis).

2.11 Fly strains

Mutant, Deficiencies and transgenic fly strains for various genes were obtained from Bloomington stock center (BL) and DGRC Kyoto, Japan (DGRC). RNAi lines were obtained from Vienna *Drosophila* RNAi stock center (VDRC).

List of flies ordered from stock center

Stock number	Genotype	Purpose
BL7682	Df(3R)Exel6203, /TM6B, Tb	Df (*miR-1000*)
BL7772	Df(2L)Exel7002/CyO	Df (*miR-965*)
BL26566	Df(1)BSC714/ /Binsinscy	Df (*miR-927*)
BL1901	Df(3R)MAP11/TM3 sb	Df *(miR-993)*
BL9289	Df(3R)BSC124/TM6B, Tb	Df*(miR-995)*
BL7665	Df(3R) Exel6186/ TM6B, Tb	Df (*miR-998*)
BL4777	P{w[mC]=UAS-stg.N}16	*UAS-stg*
BL5918	P{w[mC]=UAS-wg.H.T:HA1}6C	*UAS-wg*
BL2075	P{w[+mC]=UAS(-FRT)wg.ts}M7-2.1	*UAS-wg*
BL5919	P{UAS-wg.H.T:HA1}3C	*UAS-wg*
BL405	wgSp-1/SM5	*wg* mutant allele
BL2500	$ru^1h^1th^1st^1cu^1$ sr^1e^s stg4 ca^1/TM3, Sb Ser	*stg* mutant allele
BL29556	P{TRiP.JF03235}attP2	*stg*-RNAi
BL21049	P{wHy}stgDG05404	*stg* mutant allele
BL20349	P{EPgy2}stgEY12388	*stg* mutant allele
BL4160	msi[1]/TM3, Sb[1]	*msi* mutant allele
BL4161	msi[2]/TM3, Sb[1]	*msi* mutant allele
BL26160	$P\{GawB\}VGlut^{OK371}$	*VGlut*-GAL4
BL18860	$PBac\{w[+mC]=WH\}Glu\text{-}RI^{[f05411]}$	*GluR1* mutant
BL32252	Df(2R)BSC888 /SM6a	Df (*miR-137*)
BL7798	Df(2L)Exel8016/CyO	Df (*GluRIIA,GluRIIB*)
BL7783	Df(2L)Exel7011/CyO	Df (*VGlut*)
V13352	P{GD5007}v13352	*wg-RNAi*
V39676	P{GD5007}v39676/TM3	*wg-RNAi*
V2574	P{GD834}v2574/TM3	*VGlut-RNAi*
V1793	P{GD707}v1793	*mGluR-RNAi-1*
V1794	P{GD707}v1794	*mGluR-RNAi-2*
DGRC114042	$P\{GawB\}esg^{NP7011}$/CyO,P{UASlacZ.UW14}UW14	*esg-GAL4*
DGRC105323	$P\{GawB\}mGluRA^{[NP6701]}$	*mGluR-GAL4*
BL32830	$Mi(MIC)mGluRA^{MI02169}$	*mGluRA* allele

CHAPTER 3: RESULTS

CHARACTERIZATION OF miRNAs

For characterization of individual miRNAs, expression and functional analysis was done for each miRNA.

3.1 Expression analysis of miRNAs

The expression of miRNAs is under strict regulation both spatially and temporally. The expression profiles of miRNAs were first inferred from small RNA sequencing and northern blotting studies (Aravin et al 2003, Berezikov et al 2006, Chen et al 2005b, Lagos-Quintana et al 2001, Lau et al 2001, Lee & Ambros 2001, Ruby et al 2007b). RNA sequencing identified new miRNAs and provided quantitative information about their expression levels. miRNA microarrays, qRT-PCR, *in situ* hybridization and miRNA sensors provide more detailed information about temporal and spatial expression of miRNAs and their possible role in controlling a biological process during development.

The miRNAs with sequences conserved through evolution show similar expression patterns across species. Conservation of expression might indicate conservation of function. The conserved miRNA, *miR-1* is expressed in muscles from *Drosophila* to human and controls muscle specific functions (Biemar et al 2005, Chen et al 2006, Kwon et al 2005, Townley-Tilson et al 2010, Wienholds et al 2005, Zhao et al 2007). *miR-124* shows CNS (Central Nervous System) specific expression in all species to control neuronal functions (Cheng et al 2009, Lagos-Quintana et al 2002, Makeyev et al 2007).

Patterns of miRNA expression also proved to be useful for disease diagnostics. Changes in expression levels of *miR-1*, *miR-133* and *miR-499* were found to act as biomarkers for myocardial infarction and atrial fibrillation (D'Alessandra et al 2010, Girmatsion et al 2009, van Rooij et al 2006). Several miRNAs were shown to express differentially in various types of cancers also (Iorio et al 2005, Lu et al 2005, Mattie et al 2006, Volinia et al 2006).

Generating information about the expression pattern of miRNAs can help us to predict the relevance of individual miRNAs in biological processes. Therefore, I chose to survey the expression of 53 novel miRNAs predicted in 2007 (Ruby et al 2007b, Sandmann & Cohen 2007). 30 of these miRNAs were selected for detailed expression pattern analysis based on their conservation across at least 12 *Drosophila* species.

3.1.1 *In-situ* expression of miRNAs in embryo

The expression pattern of the 30 miRNAs was studied in embryos, using *in-situ* hybridization. The probes designed to include the primary transcript containing the miRNA hairpin, were generated using PCR or used in the form of LNA (Locked Nucleic Acid) probes (Chapter 2). The miRNAs, *miR-1* and *miR-316* were used as positive controls because of their well-known mesodermal expression pattern (Aboobaker et al 2005) (Fig 3a, 3b). Out of the 30 miRNAs studied, 4 miRNAs, *miR-252* (Fig 3c), *miR-927* (Fig 3d), *miR-993* (Fig 3e) and *miR-1000* (Fig 3f) showed expression in embryonic CNS. *miR-1002* showed expression in the yolk nuclei and hemocytes (Fig 3g). *miR-995* and *miR-998* showed faint ubiquitous expression. The remaining 23 miRNAs showed no specific expression pattern.

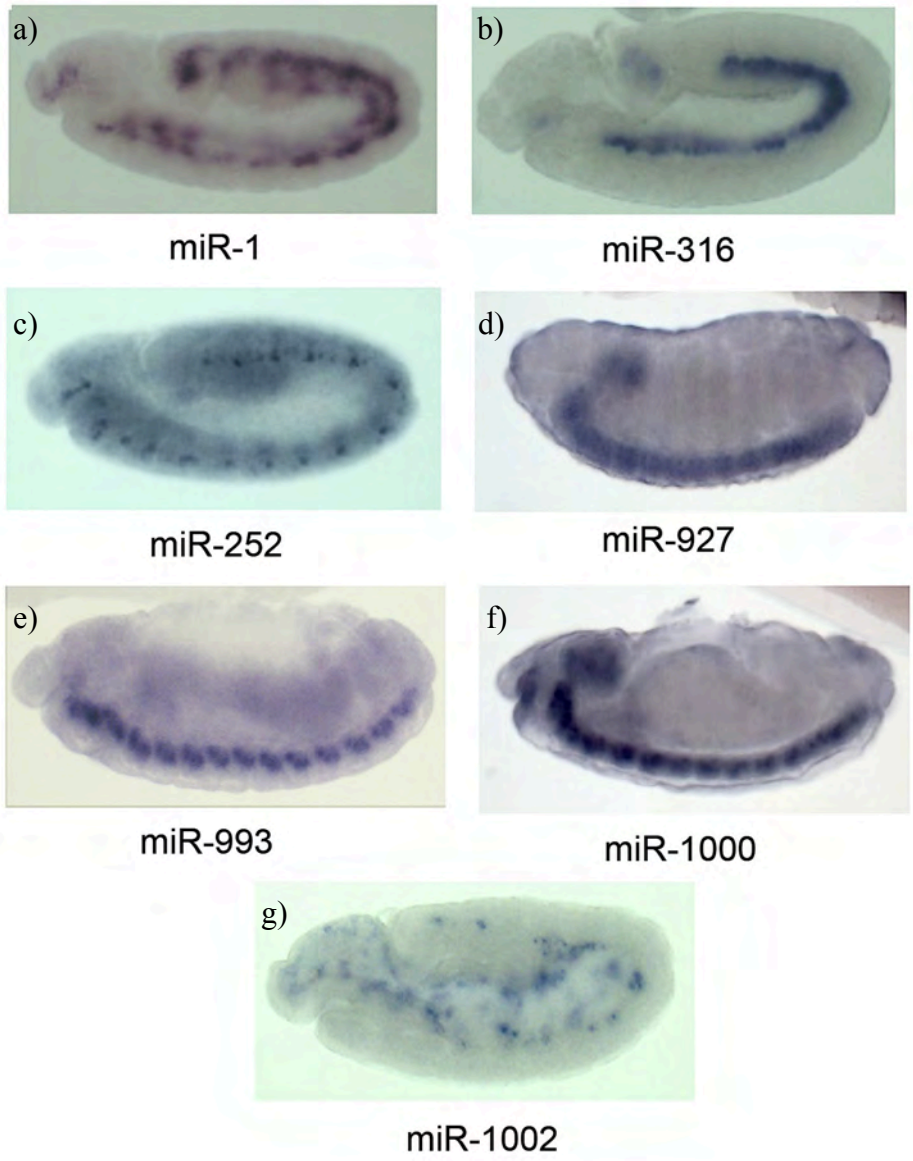

Figure 3: Embryo *In-situ* hybridization of miRNAs.

Control miRNAs, *miR-1* (Fig 3a) and *miR-316* (Fig 3b), showing mesodermal expression, *miR-252* (Fig 3c) expression in some specific cells in brain and ventral nerve cord, *miR-993* (Fig 3e) expression in ventral nerve cord, *miR-927* (Fig 3d) and *miR-1000* (Fig 3f) expression in brain and ventral nerve cord, *miR-1002* (Fig 3g) expression in hemocytes and yolk nuclei.

Table 1: Expression analysis of miRNAs in embryos by *in situ* hybridization

miRNA name	**In-situ expression pattern**
miR-1	Embryonic mesoderm
themiR-316	Embryonic mesoderm
miR-252	Embryonic CNS
miR-375	No specific expression
miR-927	Embryonic CNS
miR-929	No specific expression
miR-932	No specific expression
miR-956	No specific expression
miR-958	No specific expression
miR-959, miR-960	No specific expression
miR-962	No specific expression
miR-963	No specific expression
miR-964	No specific expression
miR-965	No specific expression
miR-968	No specific expression
miR-971	No specific expression
miR-976	No specific expression
miR-975,miR-977	No specific expression
miR-980	No specific expression
miR-981	No specific expression
miR-992	No specific expression
miR-993	Embryonic ventral cord
miR-994, miR-318	No specific expression
miR-995	Ubiquitous
miR-998	Ubiquitous
miR-999	No specific expression
miR-1000	Embryonic CNS
miR-1002	Hemocytes and yolk nuclei

3.1.2 miRNA GFP sensor for expression studies

To study expression patterns of miRNAs at other developmental stages, miRNA-GFP sensors were generated by introducing a miRNA target site in the 3'UTR of a GFP reporter transgene (Brennecke et al 2003). GFP was driven by the tubulin promoter for ubiquitous expression. GFP sensor transgenes lacking miRNA target sites were used as a control (Fig 4a, 4b). miRNA binds to the target site in the 3'UTRs and causes down regulation of GFP in miRNA-expressing cells. Thus, the expression pattern of a miRNA is determined by the presence of low GFP fluorescence in miRNA sensor, compared to the control sensor (Fig 4). The GFP-sensor constructs were generated for 30 miRNAs (Chapter 2) but generation of sensor transgenic flies and detailed analysis was only performed for 8 miRNAs (*miR-252, miR-965, miR-980, miR-927, miR-995, miR-998* and *miR-1000*). No specific expression pattern was detected in imaginal discs for all 8 miRNAs studied. *miR-965, miR-927, miR-995, miR-998* and *miR-1000* showed widespread expressions in various parts of larval brain and ventral nerve cord (Fig 4d, 4e, 4g, 4h, 4i, 4j), whereas *miR-252* and *miR-980* showed expression in limited number of cells in the brain (Fig 4c, 4f). The *miR-965* sensor also showed expression in histoblast cells (precursor of adult abdominal segments), which will be described in Chapter 5 (Fig 27b).

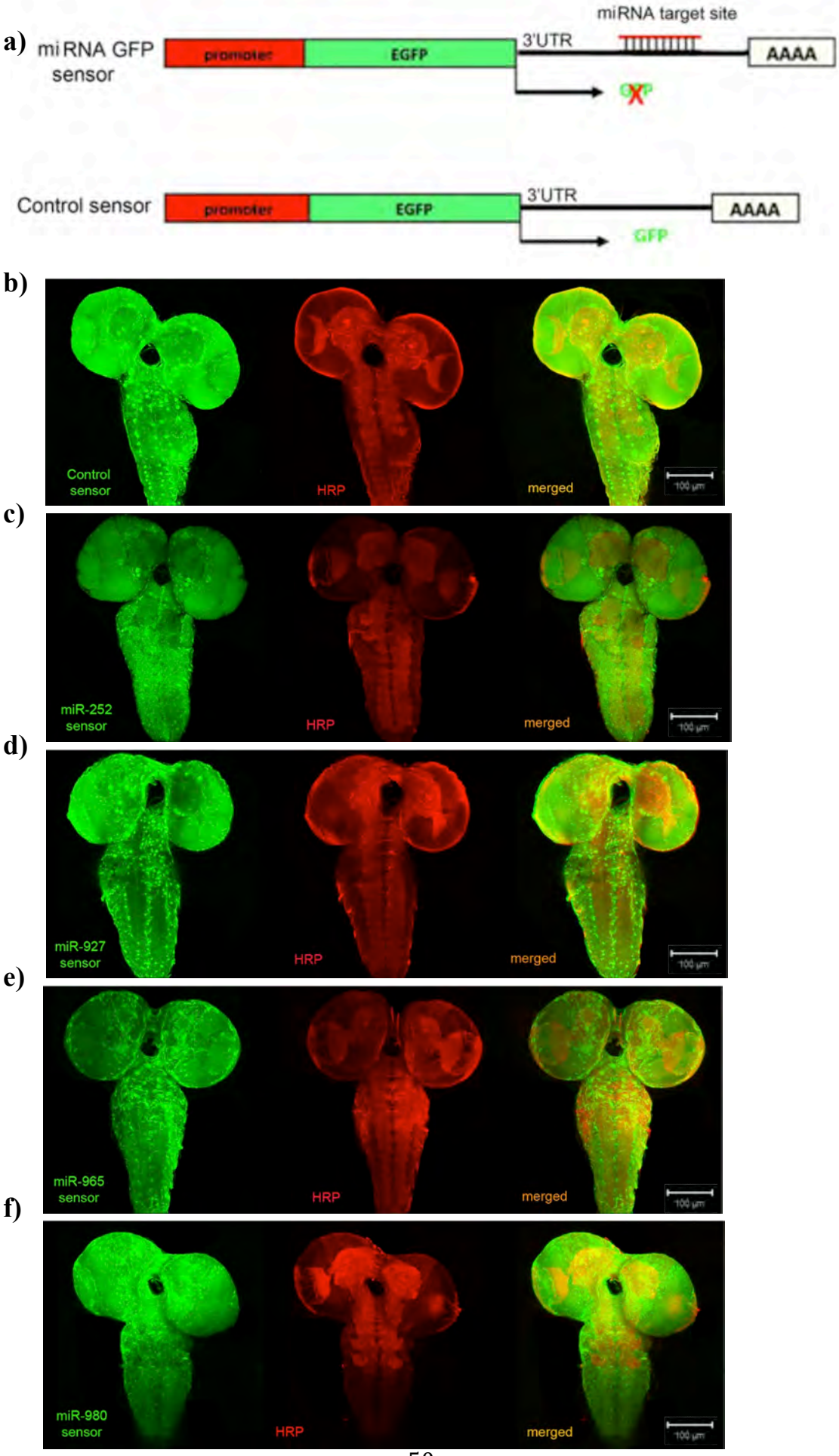
a)
miRNA GFP sensor
promoter
EGFP
miRNA target site
3'UTR
AAAA
GFP
Control sensor
promoter
EGFP
3'UTR
AAAA
GFP
b)
Control sensor
HRP
merged
c)
miR-252 sensor
HRP
merged
d)
miR-927 sensor
HRP
merged
e)
miR-965 sensor
HRP
merged
f)
miR-980 sensor
HRP
merged

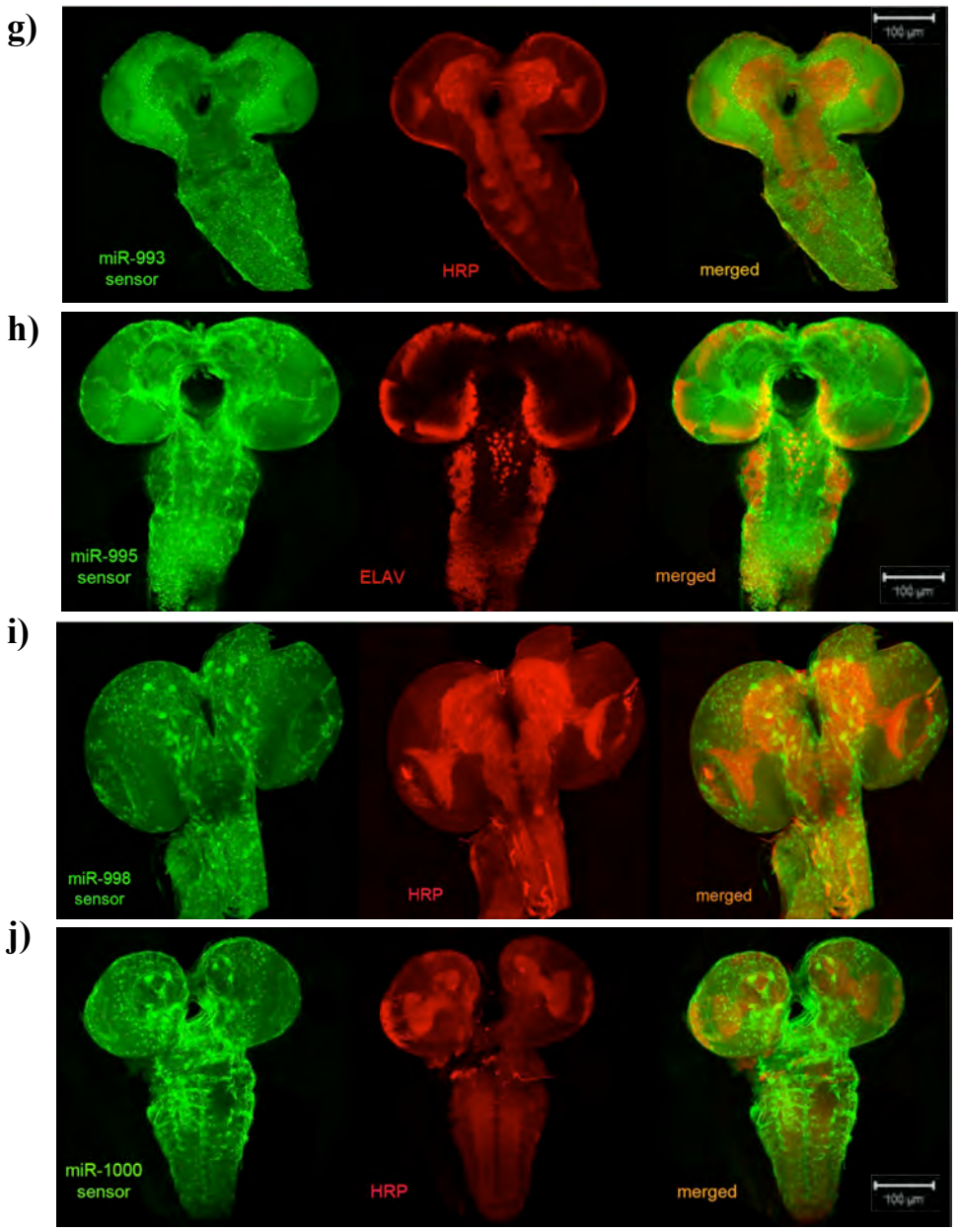

Figure 4: Generation of miRNA-GFP sensor and expression pattern in brain

a) Schematic of miRNA-GFP sensor construct with tubulin promoter (red), EGFP (green), 3'UTR (black line) with miRNA target site, polyA tail. Lower panel shows control GFP sensor without miRNA target site in the 3'UTR of EGFP.
b) Control GFP sensor, showing expression in larval CNS. Bright GFP dots indicate site-specific expression of control sensor.
c) Expression pattern of *miR-252* sensor, d) *miR-927* sensor e) *miR-965* sensor, f) *miR-980* sensor, g) *miR-993* sensor, h) *miR-995* sensor, i) *miR-998* sensor and j) *miR-1000* sensor in larval CNS, showing expression of respective miRNA by lack of GFP in the left panels. Middle panels show HRP staining and ELAV (Fig 4h) staining in larval CNS. Scale bar- 100µM.

3.1.3 Tissue specific expression using GAL4-UAS system or miRNA-GFP

The tissue-specific expression of miRNAs was also studied using GAL4-UAS system. The GAL4-UAS system consists of two components: GAL4, a transcriptional activator protein from yeast and UAS (upstream activation sequence) transgenes, having binding sites for GAL4. When the two components are brought together, the UAS transgene is expressed in cells, where GAL4 is present (Brand & Perrimon 1993) (Fig 5a). I used miRNA-GAL4 with UAS-GFP or UAS-RFP to detect miRNA expression. An example of miRNA-GAL4 knock-in is shown in Fig 5b, where *miR-1000*-GAL4 with UAS-RFP showed expression in embryonic CNS. In addition, miRNA-GFP lines, where GFP was inserted into the endogenous miRNA locus, were also used. The miRNA-GFP flies expressed GFP under the control of miRNA regulatory elements (Fig 5c). An example of miRNA-GFP knock-in is shown in Fig 5d, where *miR-980*-GFP knock-in showed expression in salivary glands of larva.

I will describe expression pattern of two miRNAs, *miR-965* and *miR-1000* in detail in Chapter 4 and 5 respectively.

a) miRNA-GAL4 knock-in

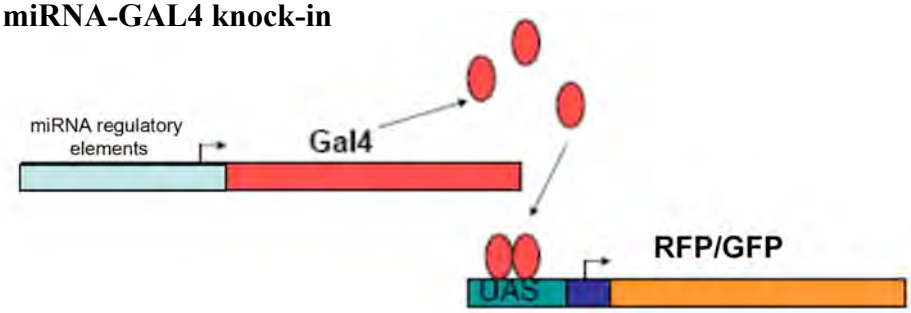

b)

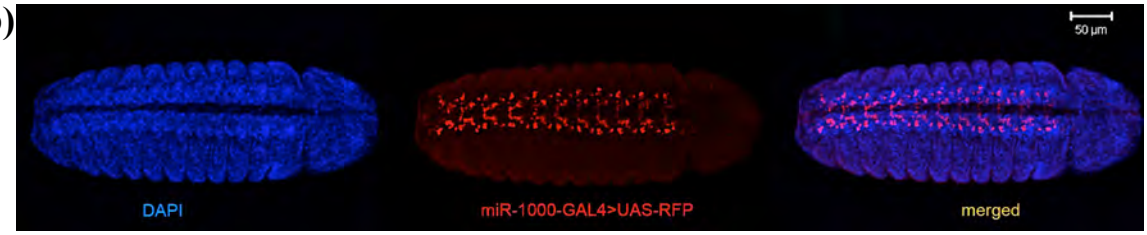

c) miRNA-GFP knock-in

d)

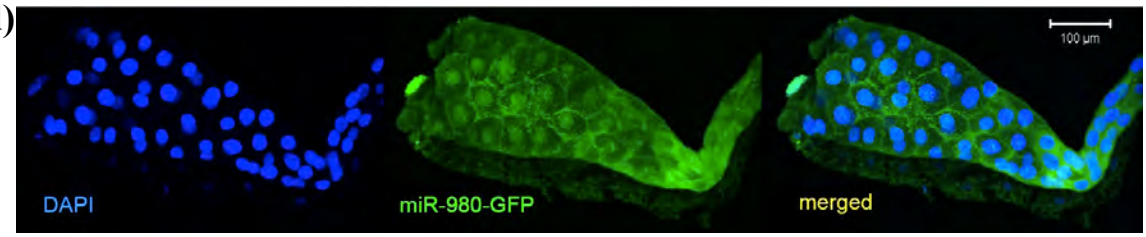

Figure 5: Generation of miR-GAL4 and miR-GFP knock-in

a) Schematic showing GAL4-UAS system. GAL4 is driven by miRNA regulatory elements and express after binding to UAS-GFP or UAS-RFP.
b) *miR-1000*-GAL4 driven by *miR-1000* regulatory elements, showing expression in embryonic CNS by UAS-RFP (red). Nuclear staining is shown by DAPI (blue). Scale bar- 50 µM
c) Schematic of miRNA-GFP knock-in construct, expressing GFP under the control of miRNA regulatory elements.
d) *miR-980*-GFP knock-in expressing GFP under the control of *miR-980* regulatory elements, showing expression in salivary gland of larva (green). Nuclear staining is shown by DAPI (blue). Scale bar - 100 µM.

3.2 Functional analysis of miRNAs

Deletion of individual miRNAs is the most preferred way to address their biological functions. In this study, I have characterized a subset of miRNAs in *Drosophila melanogaster* by generating precise deletion mutants using homologous recombination methods.

Eight miRNAs (*miR-252, miR-927, miR-965*, *miR-980, miR-993, miR-995, miR-998* and *miR-1000*) were selected for mutant production from the 30 miRNAs used for expression analysis. These miRNAs were chosen based on their nervous system specific expression and high conservation across at least 12 different *Drosophila* species. Two independent mutants were generated for each miRNA: a targeted knockout allele (KO1) and an RMCE knockout (KO2).

3.2.1 Ends-out method of homologous recombination for miRNA deletion mutant (KO1)

For the knockout allele (KO1), ends-out homologous recombination was used to make a small deletion at the miRNA locus (Fig 6a). The construct contained a mini-white gene (shown in red) that was used to replace the miRNA hairpin. For intronic miRNAs, the mini-white gene was excised, using CRE-LoxP system, leaving behind a single loxP site in place of the miRNA hairpin.

3.2.2 RMCE (Recombination Mediated Cassette Exchange) knockout (KO2)

RMCE knockout is also based on ends-out homologous recombination technique but with additional features of site-specific recombination and systematic modification of the targeted cassette (Weng et al 2009). After the initial targeting event, the mini-white cassette (flanked by an attP site, shown in pink in Fig 6b) was precisely replaced by another cassette, carrying a gene of interest flanked by attB sites

(shown in dark red). Cassette exchange was carried out by phiC31 integrase. In RMCE miRNA mutants, mini-white was replaced by GFP (shown in green) or GAL4 (shown in grey) cassettes to generate miRNA-GFP and miR-GAL4 knock-in alleles at the endogenous miRNA locus (Chen et al 2011). miR-GFP and GAL4 knock-in alleles provided valuable tools for studying expression of miRNAs and for manipulating expression of other genes in the expression domain of miRNAs. The RMCE method also provided a reliable way to generate miRNA rescue flies by restoring the miRNA hairpin at the endogenous locus, by replacement of the mini-white cassette in RMCE mutant. RMCE homologous recombination and cassette exchange is shown in Fig 6b.

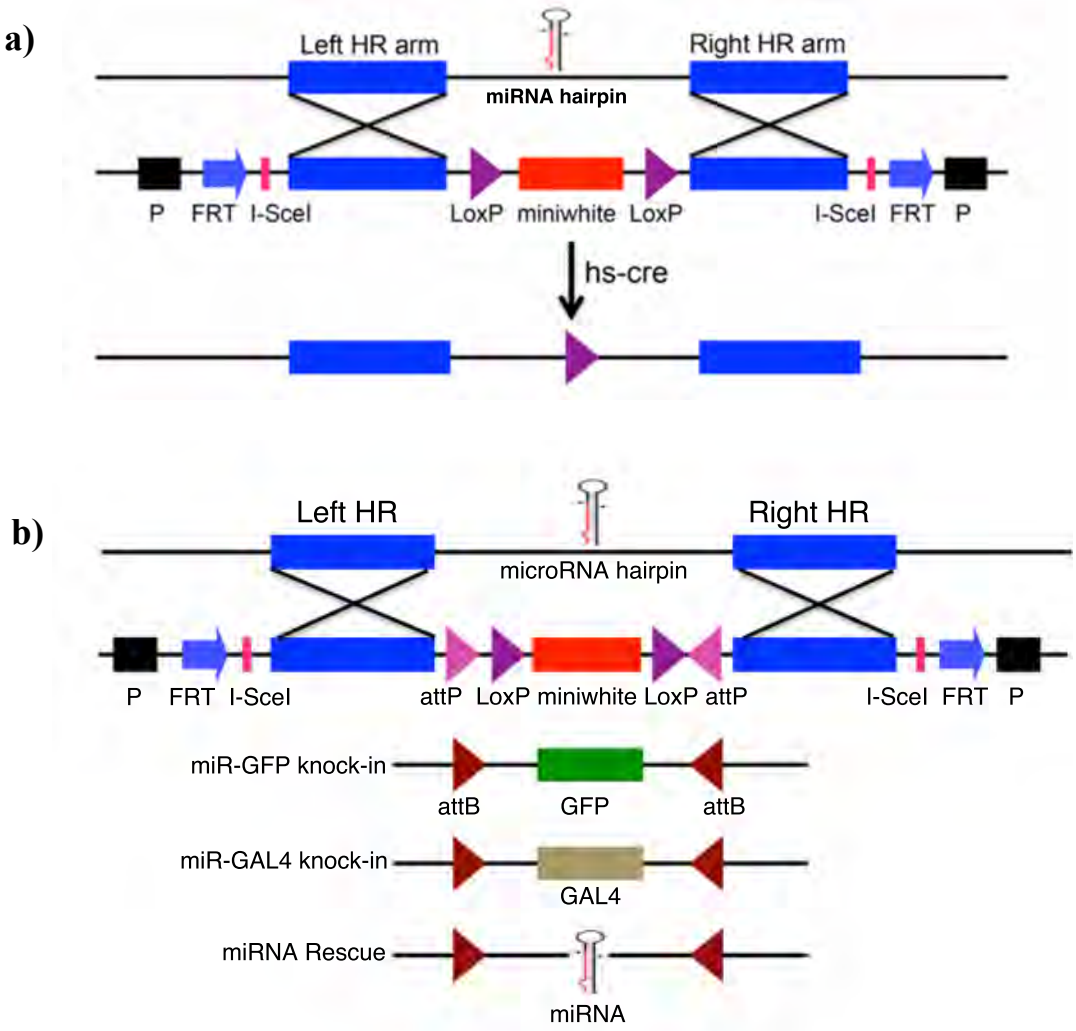

Figure 6: Strategy for ends-out method of homologous recombination

a) Generation of miRNA deletion mutant (KO1) by homologous recombination method. Homologous arms flanking miRNA hairpin are shown in blue. Left HR and Right HR indicates left and right homology arm respectively. Mini-white gene cassette (shown in red) replaced miRNA hairpin. Mini-white gene excised by hs-cre (heat shock CRE) to generate clean miRNA knockout with one loxP site (shown in purple) remaining.

b) RMCE method of homologous recombination to generate RMCE miRNA mutant (KO2). Miniwhite gene cassette replaced by GFP (green), GAL4 (grey) or miRNA rescue (hairpin), mediated by attP-attB recombination to generate miR-GFP knock-in, miR-GAL4 knock-in and miRNA rescue respectively.

3.3 Phenotypic analysis of miRNA mutants

The miRNA mutants were subjected to a panel of functional tests to identify defects. Mutants were tested in trans-heterozygous allelic combinations (KO1/KO2 or KO/Df) to minimize genetic background effects. KO1/KO2 refers to combinations of two independent miRNA mutants (e.g. KO/RMCE allele). KO/Df indicates one mutant allele in trans to a chromosomal deficiency lacking the miRNA locus. All tests were done using w^{1118} or *yw* fly strains as controls.

Seven miRNA mutants *(miR-927, miR-965, miR-980, miR-993, miR-995, miR-998* and *miR-1000*) were subjected to the basic phenotypic analysis. The *miR-252* mutant could not be studied because of background lethality and is being cleaned by backcrossing with wild type flies.

3.3.1 Morphological defects

Mutant flies were analyzed for morphological defects, which included looking for changes in eye shape and size; wing size and shape; morphology, number, shape and size of bristles present on various parts of the body; leg morphology, antenna size and shape; thorax and abdominal segment size and morphology; haltere shape and size and overall size of the organism. Upon morphological analysis, *miR-995* mutant showed cross-vein defect in the wings (Fig 7a), *miR-980* mutant showed melanotic tumors from larval stage onwards (Fig 7b), *miR-965* mutant showed adult segmentation defect (Fig 7c) and *miR-927* mutant showed disorganized ommatidial bristles in the eye (Fig 7d). *miR-993, miR-998* and *miR-1000* mutants showed no obvious morphological defects.

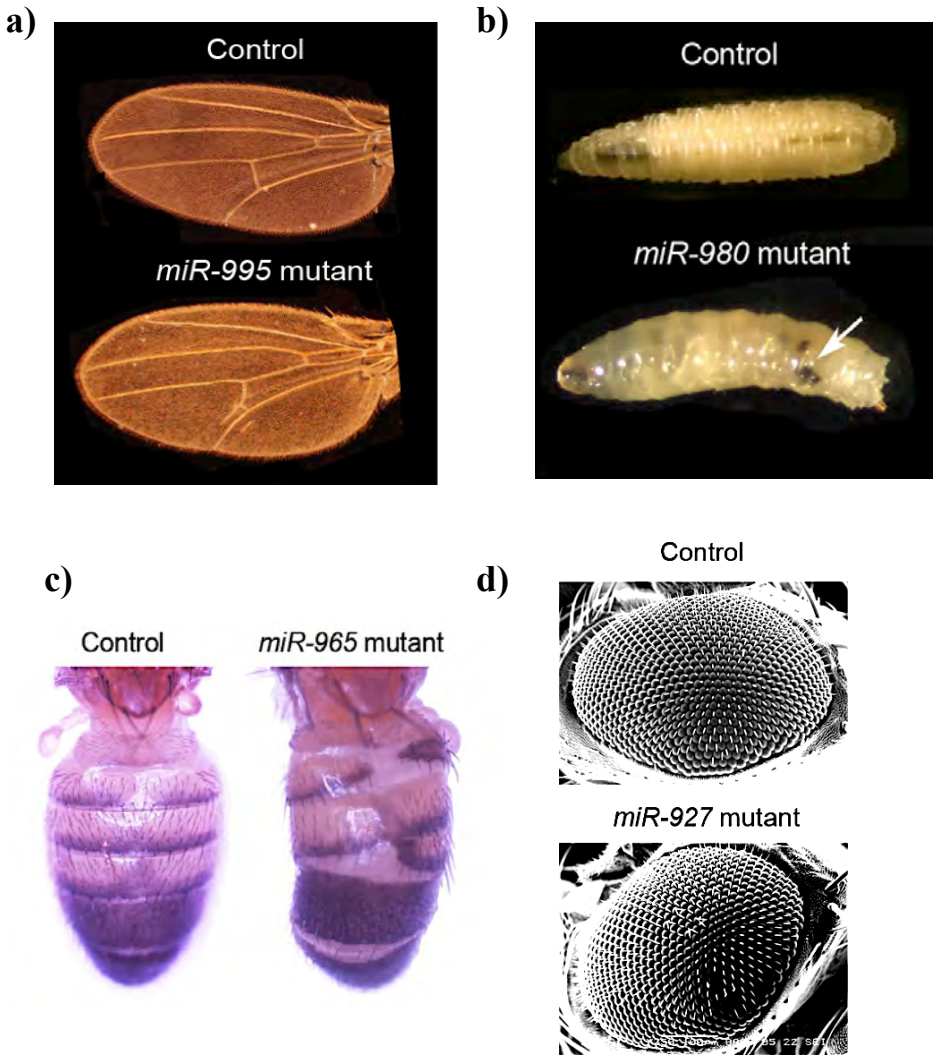

Figure 7: Morphological defects in miRNA mutants

a) *miR-995* mutant showing extra growth in cross-vein of wings (lower panel). Upper panel shows wings with normal cross-vein in control flies.
b) *miR-980* mutant larva showing melanotic tumors (black spots showed by arrow) in lower panel. Upper panel shows control larva.
c) *miR-965* mutant showing abnormal segmentation in adult flies (right panel) compared to normal segmentation in control flies (left panel).
d) *miR-927* mutant showing duplication and deletion of ommatidial bristles in the eye of adult fly (lower panel) in scanning electron micrograph (SEM). Upper panel shows eye of control flies.

3.3.2 Survival/viability defects

Survival defects were scored for all developmental stages from embryo to larval (embryo hatching), larva to pupa (pupariation) and pupa to adults (adult eclosion). Adult survival was scored by lifespan assays.

In embryo hatching assay, *miR-993* mutants showed ~30-60% embryo survival ($p=0.17$). *miR-995* and *miR-998* mutants showed ~80% embryo survival ($p\leq0.2$). Embryo hatching of *miR-927* and *miR-980* mutants was comparable to wild type embryos (Fig 8a).

In pupariation assay, *miR-927, miR-980* and *miR-993* showed normal pupariation (>90%) whereas *miR-998* and *miR-995* mutants showed ~60% ($p\leq0.01$) and ~83% ($p=0.02$) survival of pupae respectively (Fig 8b).

In adult eclosion assay, most mutants showed normal eclosion (>90%) except *miR-998* mutant, which showed ~75% eclosion of adults from pupae ($p=0.06$) (Fig 8c).

In adult lifespan assays, *miR-993, miR-998* and *miR-927* mutants showed shorter lifespan compared to wild type flies ($p\leq0.1$). *miR-980* mutant showed normal lifespan ($p=0.6$), whereas *miR-995* mutant showed longer lifespan ($p<0.01$) (Fig 8d).

Detailed phenotypic analysis of *miR-1000* and *miR-965* will be addressed in the subsequent chapters (Chapter 4 and 5) of this thesis.

a)

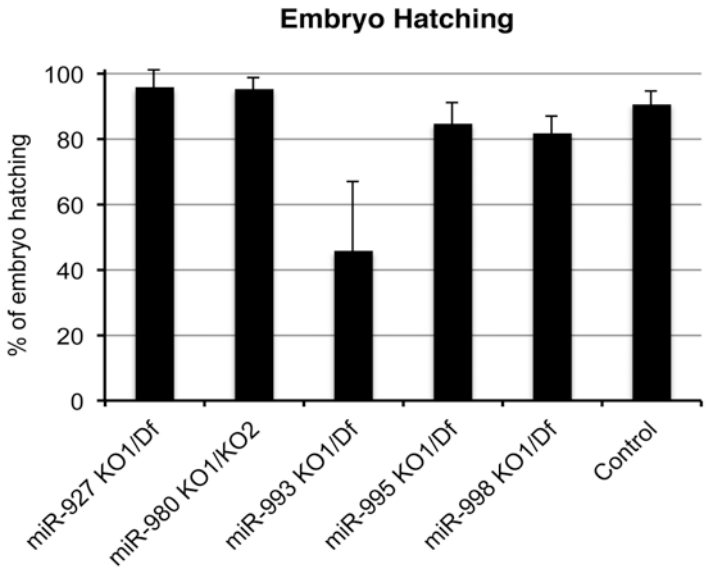
Embryo Hatching
% of embryo hatching
100
80
60
40
20
0
miR-927 KO1/Df
miR-980 KO1/KO2
miR-993 KO1/Df
miR-995 KO1/Df
miR-998 KO1/Df
Control

b)

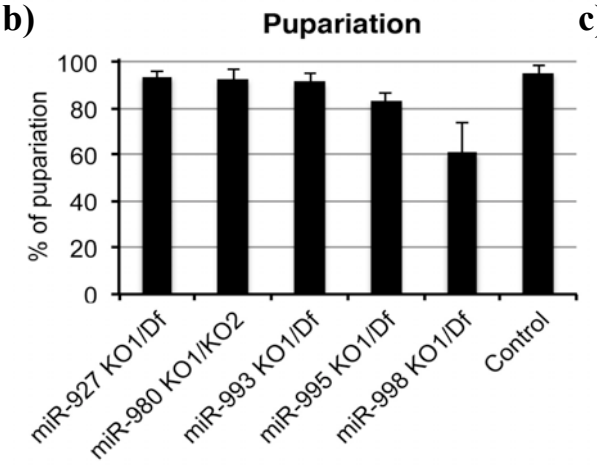
Pupariation
% of pupariation
100
80
60
40
20
0
miR-927 KO1/Df
miR-980 KO1/KO2
miR-993 KO1/Df
miR-995 KO1/Df
miR-998 KO1/Df
Control

c)

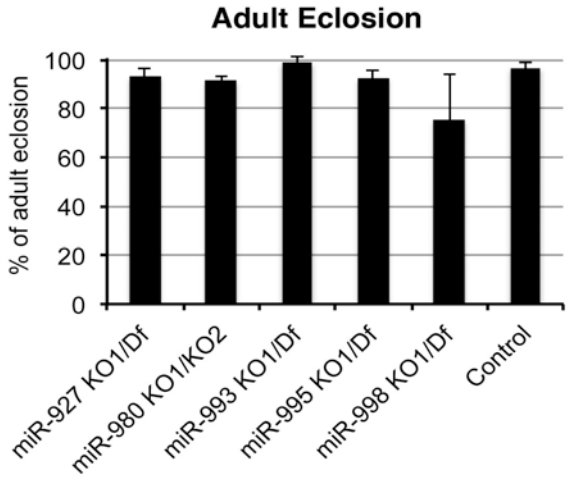
Adult Eclosion
% of adult eclosion
100
80
60
40
20
0
miR-927 KO1/Df
miR-980 KO1/KO2
miR-993 KO1/Df
miR-995 KO1/Df
miR-998 KO1/Df
Control

d)

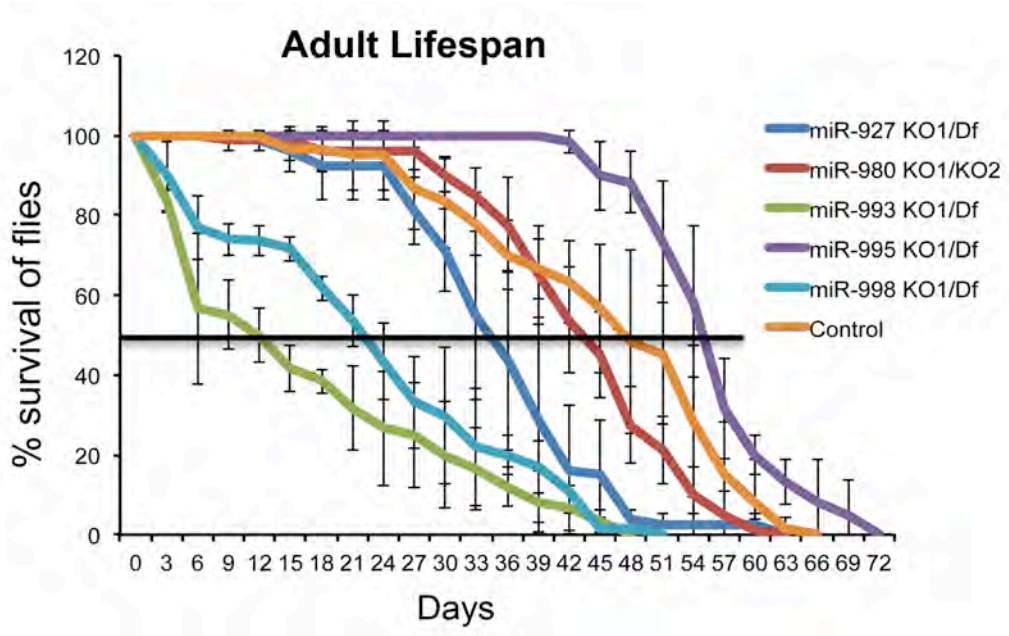
Adult Lifespan
% survival of flies
120
100
80
60
40
20
0
0 3 6 9 12 15 18 21 24 27 30 33 36 39 42 45 48 51 54 57 60 63 66 69 72
Days
miR-927 KO1/Df
miR-980 KO1/KO2
miR-993 KO1/Df
miR-995 KO1/Df
miR-998 KO1/Df
Control

Figure 8: Survival /viability defects of miRNA mutants

a) Embryo hatching of transheterozygous *miR-927* mutant (*miR-927* KO1 in trans to Df(1) BSC715), *miR-980* mutant (*miR-980* KO1/RMCE KO2), *miR-993* mutant (*miR-993* KO1 in trans to Df(3R)MAP11), *miR-995* mutant (*miR-995* KO1 in trans to Df(3R)BSC124), *miR-998* mutant (*miR-998* KO1 in trans to Df(3R) Exel6186) and control flies. Data represent average of at least three biological replicates (n≥150 for each replicate). *yw* flies were used as a control.
b) Pupariation of transheterozygous mutants as indicated above. Data represent average of at least three biological replicates (n≥50 for each replicate).
c) Adult eclosion of transheterozygous mutants as indicated above. Data represent average of at least three biological replicates (n≥50 for each replicate).
d) Survival of transheterozygous mutant flies shown in lifespan assays. Median lifespan of *miR-927* mutant (dark blue) = 36.6±4.6 days, *miR-980* mutant (red) = 43±7.5 days, *miR-993* mutant (green)= 11.3±2 days, *miR-995* mutant (purple)= 73±1.3 days, *miR-998* mutant (light blue)= 21.6±3.5 days and control (orange)= 46.5±7.8 days. Data represent average of at least three biological replicates (n≥20 for each replicate).

3.3.3 Fertility defects

Male and female fertility was scored by crossing mutant males with wild type females and mutant female with wild type males respectively. At least 100 flies were checked for their ability to produce progeny. All miRNA mutants analyzed were fertile except *miR-1000* mutants, where mutant females were 100% sterile and mutant males showed ~30-40% sterility (Fig 12c in Chapter 4).

3.3.4 Behavioral defects

Mutant flies for nervous system specific miRNAs were subjected to behavioral assays to find defects.

a) Climbing assay to determine motor coordination defect in mutants, which might indicate problems with the muscles or neurotransmission from brain.
b) Open field assay to determine walking ability of mutants.
c) Phototaxis assay to determine ability of mutants to perceive light properly.
d) Geotaxis assay to determine their ability to move against gravity.

All miRNA mutants analyzed, showed normal behavior at age of 2 day except *miR-1000* mutants, which will be described in details in Chapter 4.

3.3.5 Stress related defects

For scoring stress resistance or sensitivity of mutants, flies were subjected to following stress assays. Only two mutants (*miR-995* and *miR-1000*) were subjected to stress assays so far.

a) Starvation stress: Flies were grown on 1% agar without any nutrient to determine their abilities to withstand food related stress.
b) Oxidative stress: oxidative stress was given by exposing flies to free radicals, by feeding food along with 2.5% H_2O_2.

An example of starvation and oxidative stress is shown in Fig 9 for *miR-995* mutants. *miR-995* mutant males behaved like control flies ($p=0.77$) when subjected to starvation stress (Fig 9a), whereas *miR-995* mutant females showed increased resistance to starvation ($p\leq0.001$) (Fig 9b).

Similarly, *miR-995* mutant females showed resistance to oxidative stress when grown on food containing H_2O_2 ($p\leq0.001$) (Fig 9d), whereas *miR-995* mutant males exhibited similar tolerance towards oxidative stress as heterozygous controls ($p=0.5$)(Fig 9c).

Results of starvation and oxidative stress for *miR-1000* mutants will be described in Chapter 4.

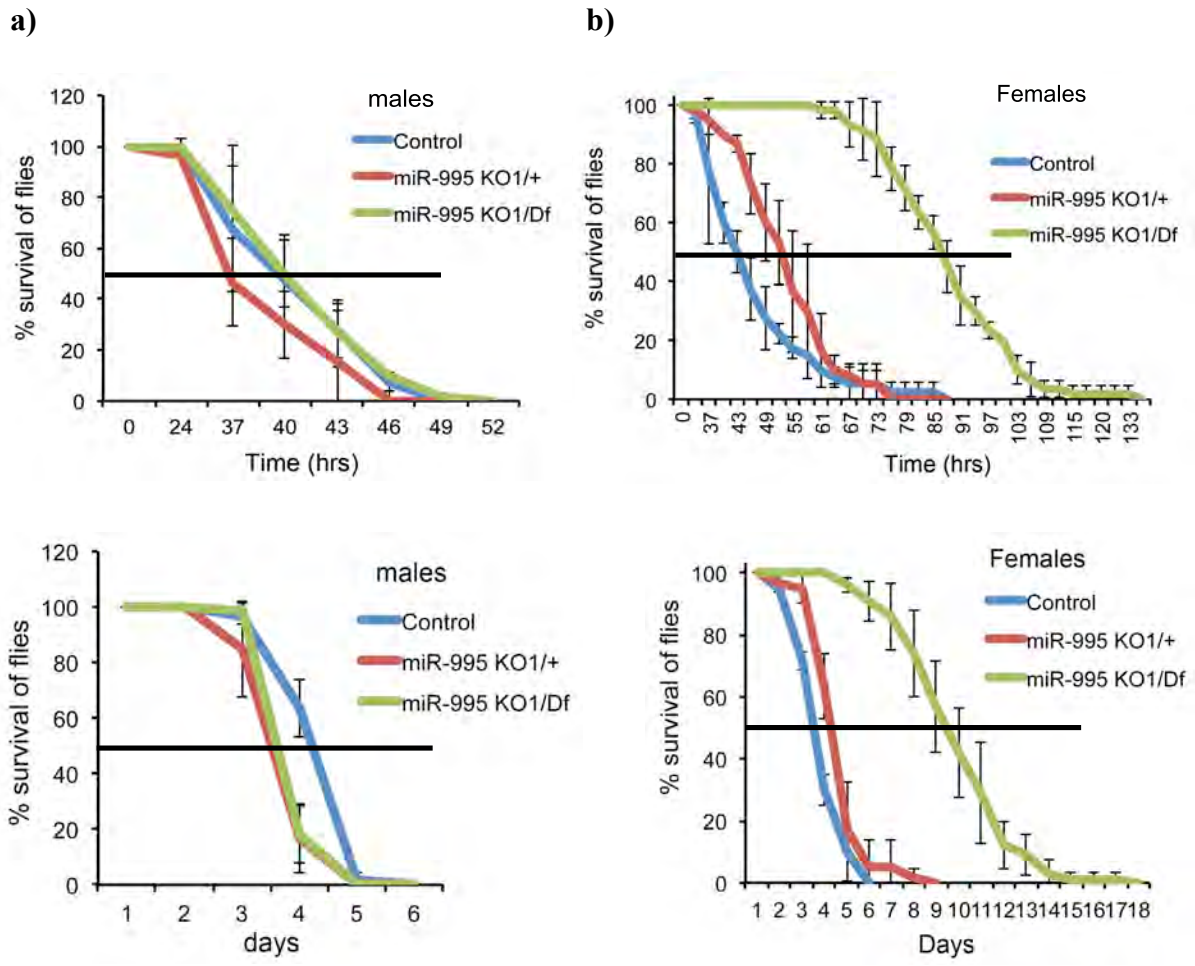

Figure 9: Stress related defects of miRNA mutants

a) Graph showing survival of *miR-995*/Df male mutants (green), Control (blue) and heterozygous (red) flies upon starvation stress. Median survival upon starvation for *miR-995*/Df = 41.85±1.1hrs, for *miR-995*/+ = 39.1±1.9 hrs and for control = 42.8±5.4 hrs. Data represent average of at least three independent experiments (n≥60). W^{1118} flies were used as a control.

b) Graph showing survival of *miR-995*/Df female mutants (green), Control (blue) and heterozygous (red) flies upon starvation stress. Median survival upon starvation for *miR-995*/Df = 86.3±2.8hrs, for *miR-995*/+ = 51.9±5.6 hrs and for control = 43±1.1hrs. Data represent average of at least three independent experiments (n≥60).

c) Graph showing survival of *miR-995*/Df male mutants (green), Control (blue) and heterozygous (red) flies upon oxidative stress. Median survival upon oxidative stress for *miR-995*/Df = 2.6±0.08 days, for *miR-995*/+ = 2.5±0.23 days and for control = 3.2±0.1 days. Data represent average of at least three independent experiments (n≥60).

d) Graph showing survival of *miR-995*/Df female mutants (green), Control (blue) and heterozygous (red) flies upon oxidative stress. Median survival upon oxidative stress for *miR-995*/Df = 8.5±0.9 days, for *miR-995*/+ = 3.3±0.3 days and for control = 2.5±0.04 days. Data represent average of at least three independent experiments (n≥60).

To summarize, 30 novel miRNAs were selected for screening by expression pattern analysis in embryos using *in situ* hybridization and miRNA-GFP sensors. Eight miRNA, *miR-252, miR-927, miR-965, miR-980, miR-993, miR-995, miR-998* and *miR-1000* were then selected for detailed functional analysis by generation of deletion mutants for each miRNAs. Characterization of two miRNAs, *miR-965* and *miR-1000* (which showed interesting phenotypes in the initial phenotypic screen) and their role in biological process will be described in depth in this thesis.

CHAPTER 4: CHARACTERIZATION OF *miR-1000*

4.1 Expression analysis of *miR-1000*

4.1.1 Nervous system specific expression pattern of *miR-1000*

In-situ hybridization, *miR-1000*-GFP and *miR-1000*-GAL4 driving UAS-H2-RFP were used to determine the *miR-1000* expression pattern at different stages of development.

I did *in-situ* hybridization using a probe against the primary transcript of *miR-1000* to see the expression pattern in embryos. *miR-1000* showed expression in the embryonic CNS (Fig 3). Double staining of *miR-1000*-GAL4 expressing UAS-H2-RFP alongwith antibody against Hb9 (Homeobox gene 9), showed overlapping expression in motor neurons of embryos (Fig 10a). *Hb9* expresses in developing motor neurons in CNS of mammals as well as flies (Arber et al 1999).

miR-1000-GFP showed expression in the nervous system throughout development from embryo to adult. *miR-1000* was also expressed in the neurons at NMJs in the larval body wall, but no expression was detected in the muscles (Fig 10b). In larvae, *miR-1000* expression was observed in different parts of the brain and ventral nerve cord with strong expression in mushroom bodies, optic lobes and Bolwig's nerve (Fig 10c). Adult brain also showed widespread expression of *miR-1000* with most prominent expression in mushroom bodies (Fig 10d, left panel). Mushroom bodies are the region of the brain, involved in learning and memory. *miR-1000* expression was also observed in different layers of the adult eye (Fig 10d, middle and right panel).

The level of *miR-1000* expression in adult flies of different ages was quantified by qPCR. *miR-1000* levels decreased by 50% between day 2 and day 15 and 30 in wild type flies (Fig 10e).

a)

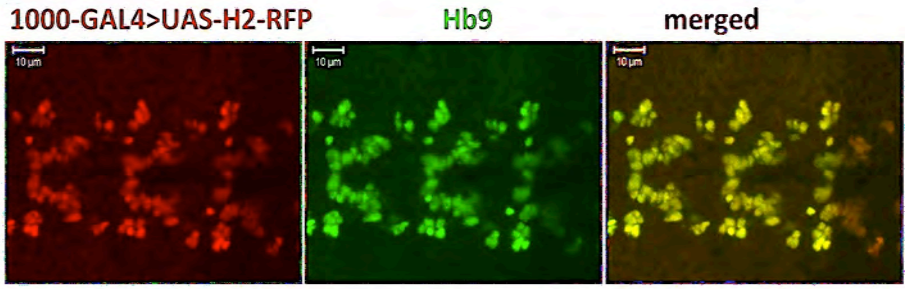
1000-GAL4>UAS-H2-RFP
Hb9
merged

b)

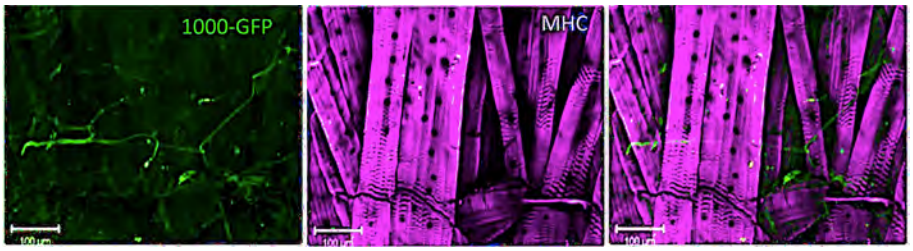
1000-GFP
MHC

c)

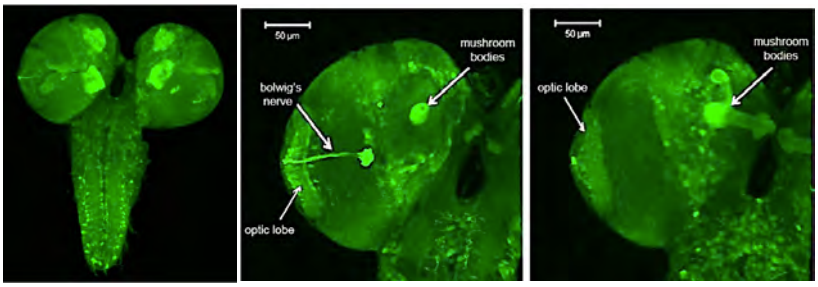
mushroom bodies
bolwig's nerve
optic lobe
mushroom bodies
optic lobe

d)

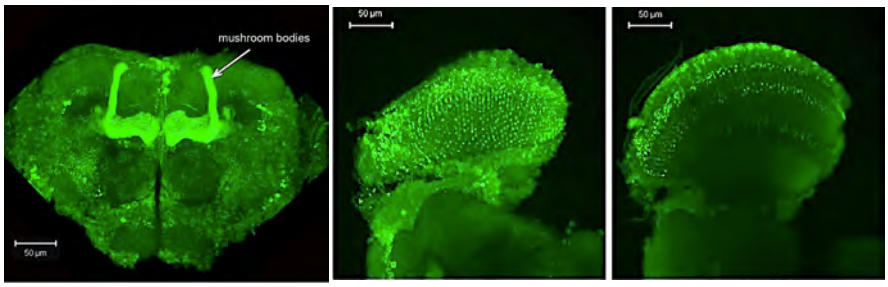
mushroom bodies

e)

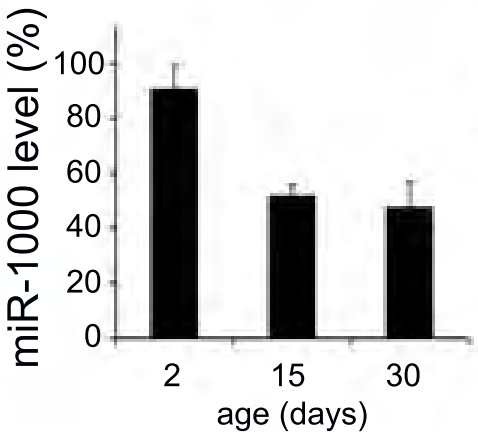
miR-1000 level (%)
100
80
60
40
20
0
2
15
30
age (days)

Figure 10: Spatial and temporal expression of *miR-1000* in different stages

a) Expression of *miR-1000* (red, left panel) by *miR-1000*-GAL4 driving UAS-H2-RFP in embryonic ventral nerve cord. Hb9 antibody (green, middle panel) showing expression in motor neurons. Merged (yellow, right panel) showing overlapping expression of *miR-1000* in embryonic motor neurons with Hb9. Scale bar- 10μM
b) Expression of *miR-1000* in larval NMJs, shown by *miR-1000*-GFP (green, left panel) and expression in the muscles by MHC antibody (purple, middle panel). Merged (right panel) showing non-overlapping expression of *miR-1000* and muscles. Scale bar – 100μM.
c) *miR-1000*-GFP showing widespread expression of *miR-1000* in the larval brain and ventral nerve cord (left panel, Scale bar- 100μM), enlarged brain lobe with expression of *miR-1000* in the optic lobe and Bolwig's nerve (middle panel, shown by arrow) and mushroom bodies (right panel, shown by arrow). Scale bar – 50μM.
d) *miR-1000* expression in the adult brain (left panel) with bright mushroom bodies (shown by arrow), expression of *miR-1000* in upper (middle panel) and middle layers (right panel) of adult eye. Scale bar – 50μM.
e) *miR-1000* expression in the wild type flies of age 2, 15 and 30 day by *miR-1000* qPCR, performed using head RNA. Expression level normalized to 1 day old flies and U14 and U27 control primers. Graph represents qPCR results from three independent samples and error bars are ± SD.

4.2 Generation and validation of *miR-1000* mutants and Rescue flies

The *miR-1000* (KO1) and *miR-1000* RMCE (KO2) mutants were generated as described in Chapter 3. *miR-1000* is located in the first intron of the *msi* gene, but represents an independent transcription unit, transcribed from the opposite strand of the DNA (Fig 11a). 4436bp left homology and 4199bp right homology arms were used to generate deletion of 141bp region, containing the *miRNA-1000* hairpin (sequences mentioned in Chapter 2). To prevent disruption to host gene *msi,* the *mini-white* marker was excised, leaving a single LoxP site in the *msi* intron. Genetic complementation tests with an *msi* mutant allele showed that *msi* function was not compromised in the *mini-white*–excised *miR-1000* mutants. Deletion of the *miR-1000* in the both mutants was confirmed by genomic DNA PCR and miRNA qPCR (Fig 11b).

For the *miR-1000* RMCE (KO2) alleles, *mini-white* was replaced by Gal4 to generate *miR-1000*-GAL4; by GFP to generate *miR-1000*-GFP and by a 202bp *miR-1000* hairpin to generate the *miR-1000* rescue allele. *miR-1000*-GFP and *miR-1000*-GAL4 were used for expression analysis shown previously. *miR-1000* level was restored to 50% of normal in the rescued mutant (Fig 11b). This allele was used in subsequent phenotypic analysis to test functional rescue for *miR-1000* mutants. All phenotypic analysis was done using *miR-1000* mutant flies carrying two independently generated alleles (KO1/KO2) or an allele in trans to a chromosomal deletion, Df{3R}Exel6203, removing the *miR-1000* locus (KO1/Df or KO2/Df). Flies carrying Df{3R}Exel6203 will be referred to as "Df", unless otherwise indicated. Control and rescue flies were always used along with mutants to confirm that lack of miRNA was the cause of the phenotype. Two-tailed student's T-test was used for most of the statistical analyses.

a)

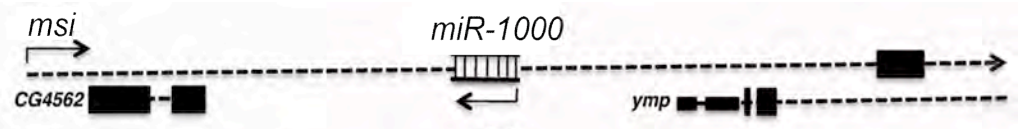

b)

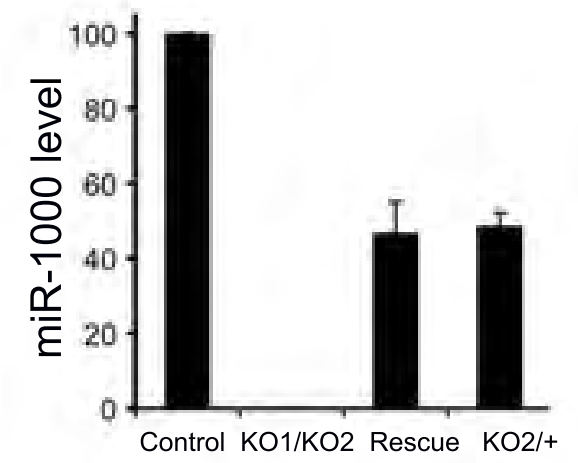

Figure 11: *miR-1000* locus and validation of *miR-1000* mutants

a) *miR-1000* genomic locus, showing *miR-1000* hairpin in the first intron of *msi* gene. Arrows indicate opposite directions of transcription of *msi* and *miR-1000.*

b) Validation of *miR-1000* trans-allelic combination of two mutants (KO1/KO2) and *miR-1000* rescue by *miR-1000* qPCR. Results were normalized to wild type head RNA and endogenous controls U14 and U27. Rescue flies show 50% level of *miR-1000*, similar to heterozygous mutant (KO2/+). KO1 indicates the mini-white excised deletion mutant allele and KO2 is the mini-white excised RMCE mutant allele.

4.3 *miR-1000* mutant phenotypes

4.3.1 Reduced viability of *miR-1000* mutants

Three trans-allelic combinations (KO1/Df, KO2/Df, KO1/KO2) of *miR-1000* mutants were analyzed for developmental progression: embryo hatching to larva, larval survival to pupa and pupal survival to adults. Trans-allelic combination of mutants showed ~20-30% lethality at the embryonic stage (Fig 12a). However, when grown under controlled conditions, with limited crowding, their survival from larva to pupa and from pupa to adulthood was normal (Fig 12b).

4.3.2 Reduced fertility of *miR-1000* mutants

Male and female fertility of *miR-1000* mutant was checked by crossing mutant flies to wild type flies. Percentage fertility was calculated by counting the number of flies capable of producing progeny. *miR-1000* mutant females produced no progeny, whereas mutant males were capable of producing progeny in 60% (KO1/Df) to 80% (KO2/Df) of crosses (Fig 12c). Mutant female ovaries were dissected and analyzed for possible defects. Mutant ovaries were normal in appearance with a morphologically normal oviduct attached to it, when compared with wild type ovaries (Fig 12d, A, B). No obvious problem with egg production was observed, as eggs of all stages were present in the mutant ovaries. However, the mutant females seemed to have a problem in egg laying as many mature eggs were observed to be present inside mutant ovaries (Fig 12d,C).

a)

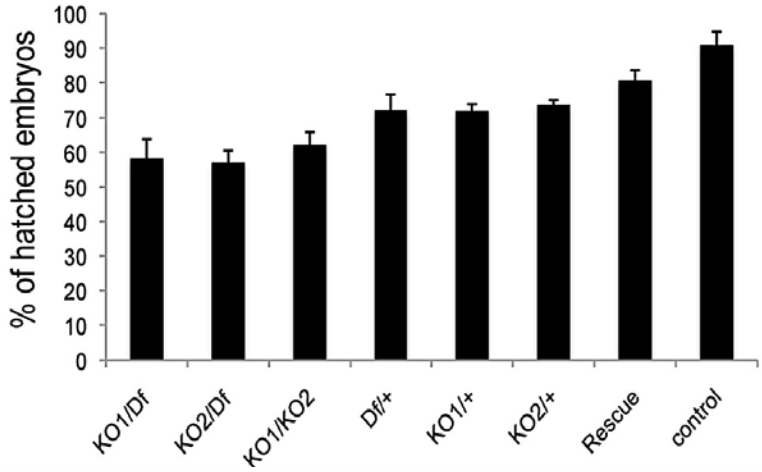
% of hatched embryos
100
90
80
70
60
50
40
30
20
10
0
KO1/Df
KO2/Df
KO1/KO2
Df/+
KO1/+
KO2/+
Rescue
control

b)

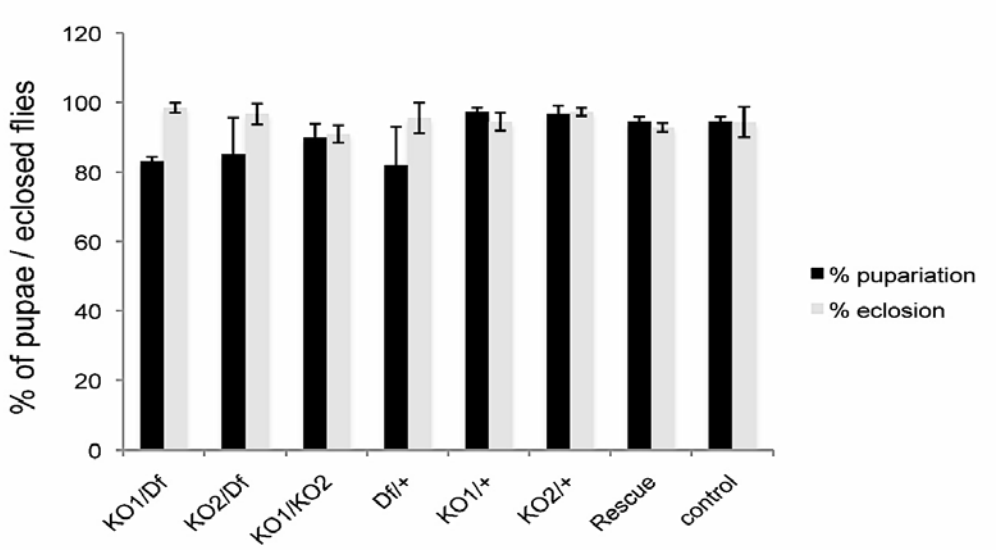
% of pupae / eclosed flies
120
100
80
60
40
20
0
KO1/Df
KO2/Df
KO1/KO2
Df/+
KO1/+
KO2/+
Rescue
control
% pupariation
% eclosion

c)

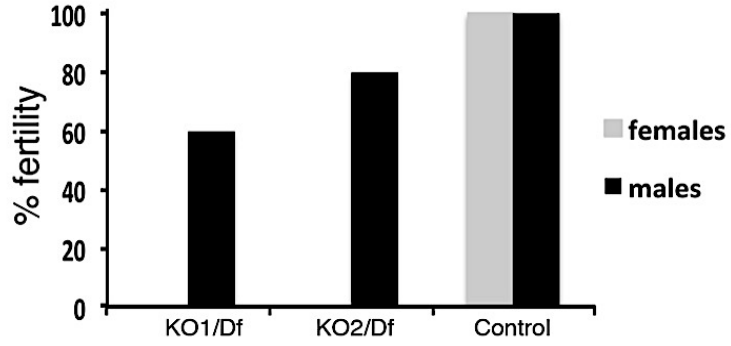
% fertility
100
80
60
40
20
0
KO1/Df
KO2/Df
Control
females
males

d)

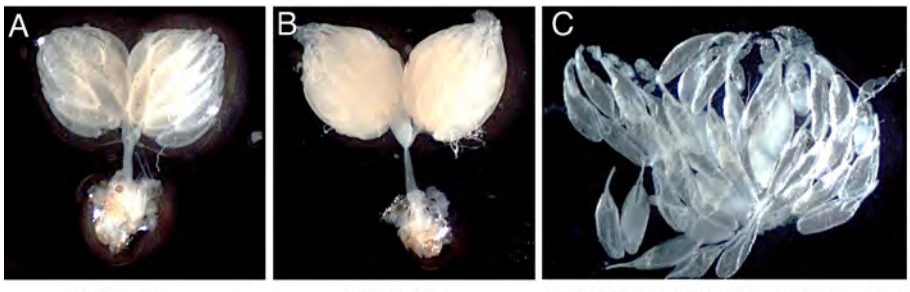
A
B
C
Wild type
KO1/KO2
KO1/KO2 ovary with mature eggs

Figure 12: Viability and fertility defects of *miR-1000* mutant

a) Embryo hatching rate of three mutant combinations (KO1/Df, KO2/Df and KO1/KO2) and rescue. Heterozygous ((KO1/+, KO2/+ and Df/+) were used as additional controls. p-value of all mutant combinations (KO1/Df, KO2/Df and KO1/KO2) is <0.01 when compared to control and rescue. Data represent average of three different experiments and error bar is ±SD.
b) Graph showing Pupariation (larva to pupa formation) in black bars and adult eclosion (pupa to adult formation) in grey bars in flies of indicated genotypes. Data represent average of three different experiments and error bar is ±SD.
c) Graph showing fertility for *miR-1000* mutant males (in black bar) and females (in grey bar). n=100 for each group.
d) Images of female ovary from wild type (A) and *miR-1000* mutant (B). Panel C shows presence of mature eggs in *miR-1000* mutant ovary.

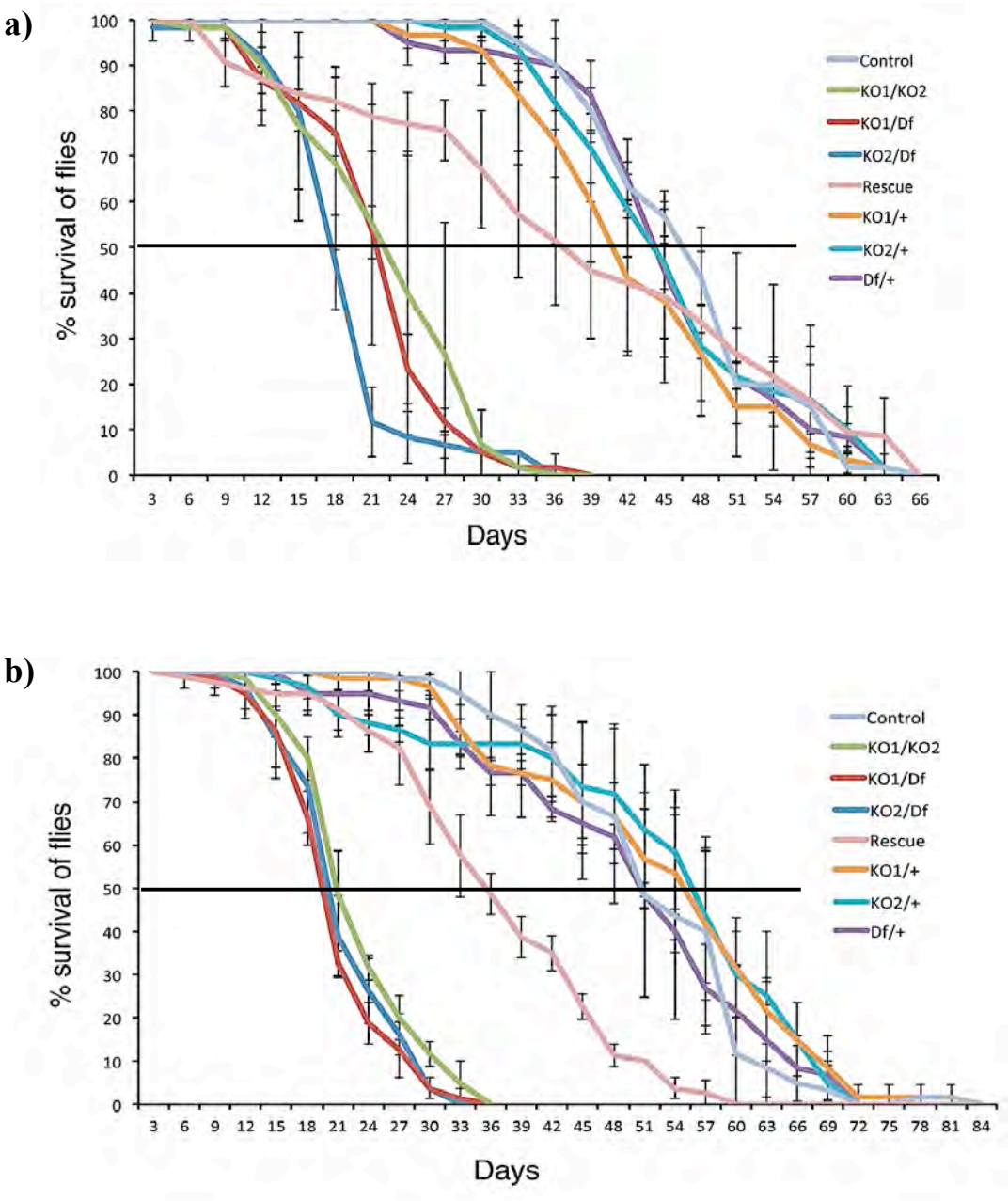

Figure 13: Longevity of *miR-1000* mutants

a) Adult male lifespan and b) female lifespan for *miR-1000* mutants in trans-allelic combinations (KO1/KO2, KO1/Df, KO2/Df) showing reduced lifespan as compared to rescue, control and heterozygous controls (KO1/+, KO2/+, Df/+). $p<0.05$ comparing KO1/KO2, KO1/Df , KO2/Df with rescue and $p<0.01$, when comparing the same mutant combinations to control. Data represent average of at least 3 independent biological replicates and error bars are ± SD.

4.3.3 Shortened lifespan of *miR-1000* mutants

miR-1000 mutants had shortened life span when grown under controlled conditions without any competition-induced stress (Fig 13). This was observed in all trans-allelic combinations tested. Reduced life span was observed in both males and females (Fig 13a and 13b), with survival rapidly declining by 2 weeks of age. Lifespan was improved using the RMCE rescue allele, confirming lack of *miR-1000* as the cause of reduced lifespan in mutants.

4.3.4 Movement disability of *miR-1000* mutants

The *miR-1000* mutants showed early onset movement disorder. At 2 days of age, 50-60% flies were impaired in their ability to climb above 5cm in a climbing assay, indicating motor coordination defect. They also showed progressive deterioration of climbing ability, as 80% of mutant flies were unable to climb above 5cm at 10 days. The climbing defect was rescued by restoring *miR-1000* expression using the RMCE rescue allele (Fig 14a).

miR-1000 mutants also displayed poor walking behavior, when made to walk on a horizontal surface in an open field assay. Age-dependent impairment in walking ability was also observed, with average speed of walking going down at day 10, compared to day 2 (Fig 14b,c). Age-dependent speed reduction was not observed in rescue and control flies.

a)

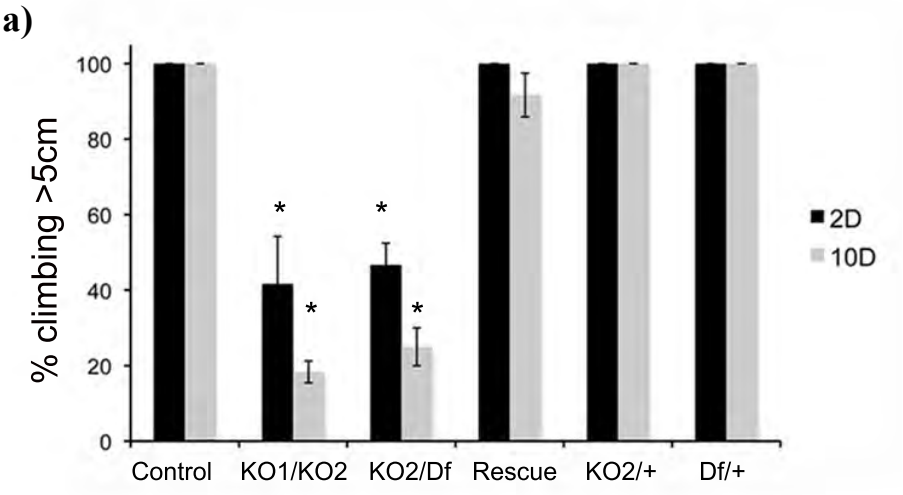
% climbing >5cm
100
80
60
40
20
0
*
*
*
*
2D
10D
Control
KO1/KO2
KO2/Df
Rescue
KO2/+
Df/+

b)

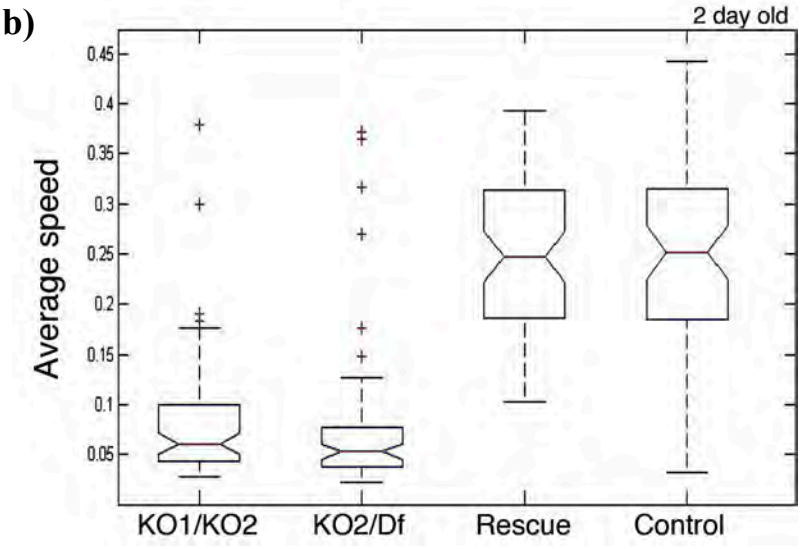
2 day old
Average speed
0.45
0.4
0.35
0.3
0.25
0.2
0.15
0.1
0.05
KO1/KO2
KO2/Df
Rescue
Control

c)

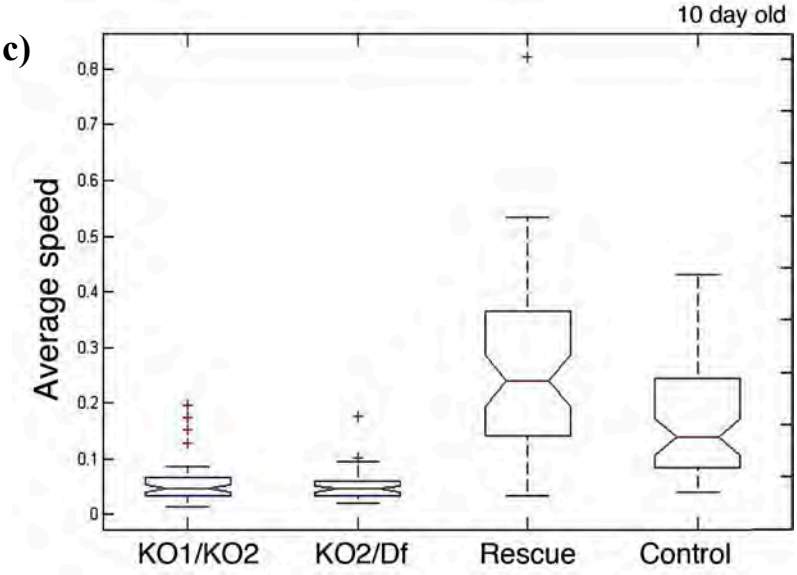
10 day old
Average speed
0.8
0.7
0.6
0.5
0.4
0.3
0.2
0.1
0
KO1/KO2
KO2/Df
Rescue
Control

Figure 14: Age-progressive movement disorder in *miR-1000* mutant

a) Histogram showing climbing assay performed on 2-day (black bars) and 10-day (grey bars) old mutants (KO1/KO2 and KO2/Df), rescue, heterozygous and control flies. Bars show reduced percentage of mutant flies climbing above 5 cm in climbing assay, compared to control and rescue flies. Data represent at least three independent biological replicates. * $p<0.01$ for KO1/KO2 and KO1/Df compared to control at day 2 and day 10.
b) Graph showing reduced average walking speed of mutants (KO1/KO2 and KO2/Df), compared to rescue and control flies in an open field assay at day 2.
c) Graph showing age-progressive reduction in average walking speed of mutants (KO1/KO2 and KO2/Df) in 10-day old flies, compared to age-matched rescue and control flies.

4.3.5 Stress tolerance in *miR-1000* mutants

miR-1000 mutants showed sensitivity to oxidative stress, when flies were fed with 2.5% Hydrogen peroxide (H_2O_2) in sucrose. Survival was scored every 12 hours. *miR-1000* mutant flies died faster than the rescue, heterozygous and control flies (Fig 15a), suggesting increased sensitivity to oxidative stress.

In contrast, *miR-1000* mutants showed resistance to starvation. They withstood food stress better than rescue, heterozygous and control flies, when reared on 1% agar without nutrients (Fig 15b). Mutant survival was almost double that of control flies under starvation stress. They consumed less food, compared to control, when fed food with tracking dye (data not shown). Their low energy consumption due to less movement and reproduction might contribute to this phenotype, but further work would be required to support this conclusion.

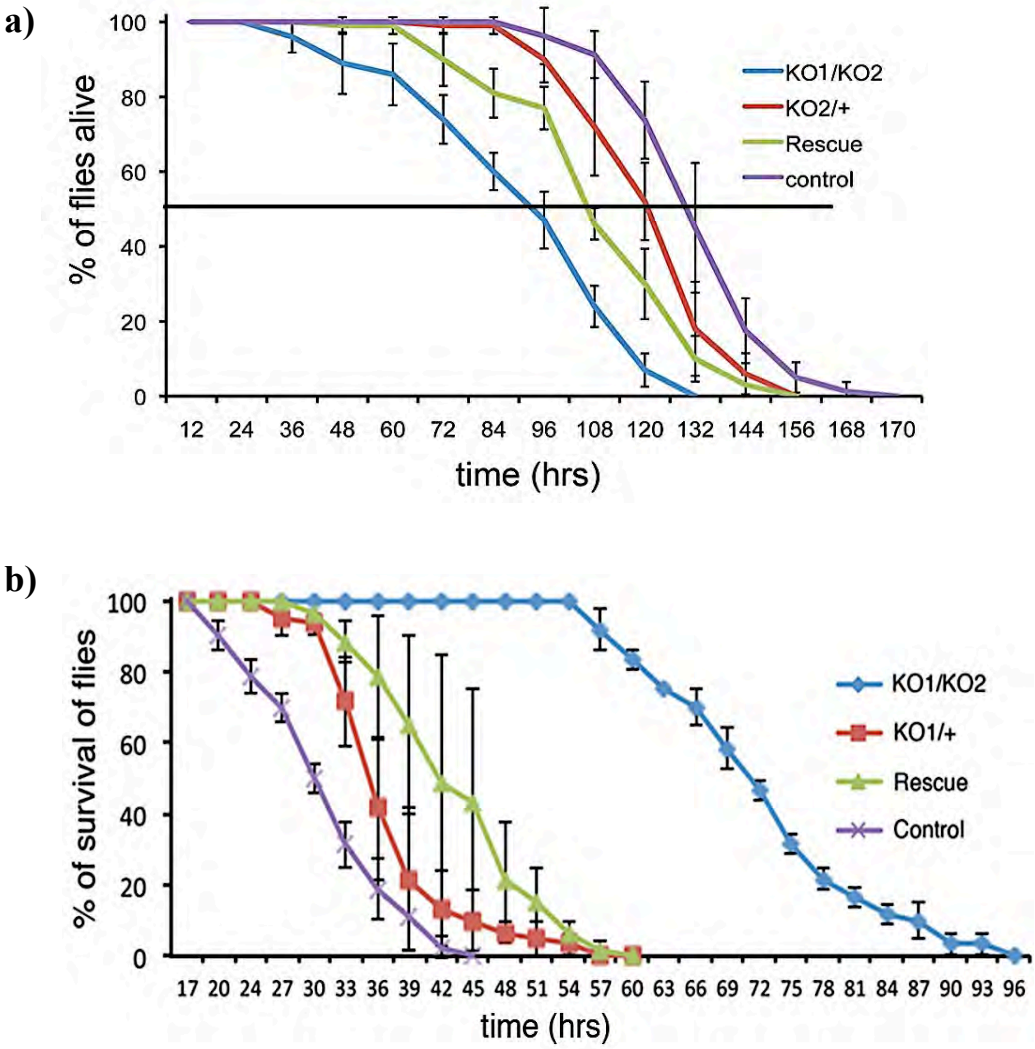

Figure 15: Oxidative stress and starvation stress in *miR-1000* mutant

a) Graph showing survival of flies under oxidative stress. *miR-1000* mutant (KO1/KO2) flies (blue) showed more sensitivity to oxidative stress than rescue (green), heterozygous (red) and control (purple) flies. $p<0.001$ when compared mutant with control, rescue and heterozygous for 50% survival on oxidative stress.

b) Graph showing survival of flies under starvation stress. *miR-1000* mutant (KO1/KO2) flies (blue) showed greater resistance to starvation than rescue (green), heterozygous (red) and control (purple) flies. $p<0.001$ when compared mutant with control, rescue and heterozygous flies.

4.4 Age-progressive neurodegeneration in the brain of *miR-1000* mutants

Because of nervous system specific expression of *miR-1000*, I asked whether reduced lifespan and age-progressive movement disorder in the *miR-1000* mutant might be caused by neurodegeneration in the brain. To check this possibility, I did antibody staining for Caspase3 in adult brains at 2 and 10 day. Caspase 3 antibody marks cells undergoing apoptosis. Increased apoptosis was observed in *miR-1000* mutant at day 2, compared to control and rescue brains (Fig 16a,b). Quantification of Caspase3 positive cells was done using Imaris software (Chapter 2). In 10 days old fly brain, number of apoptotic cells increased more than 10 fold. This was rescued to a considerable level by restored *miR-1000* expression in rescue flies (Fig 16a,b).

Vacuole formation, a characteristic of age-related neurodegeneration, was also observed in mutant brains from 10 days onwards (Fig 16c). Vacuolization is not typically observed in the brains of normal animals until much later in life. Vacuolization often results from death of neurons, caused by continuous exposure to neurotoxicity in the brain.

In conclusion, *miR-1000* mutants displayed features characteristic of *Drosophila* models of neurodegeneration, including reduced lifespan, movement defects and increased apoptosis in the brain. *miR-1000* mutants suffered from early-onset neurodegeneration, showing defects as early as 2 days of age.

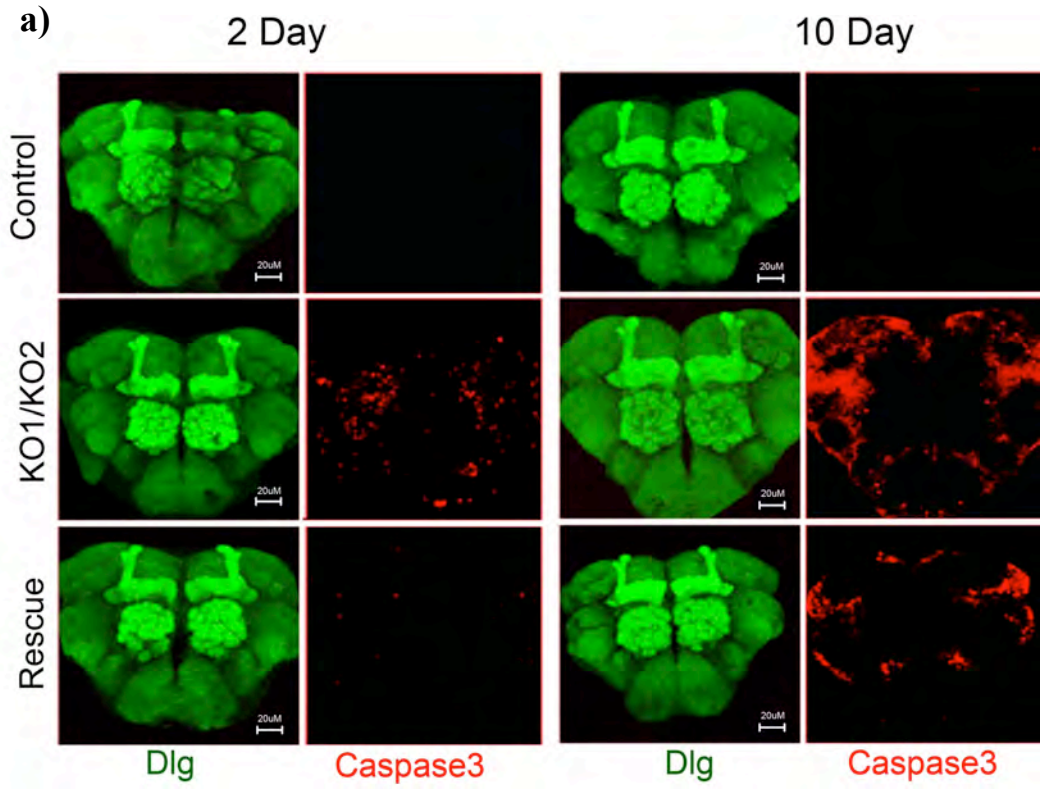
a)
2 Day
10 Day
Control
KO1/KO2
Rescue
Dlg
Caspase3
Dlg
Caspase3

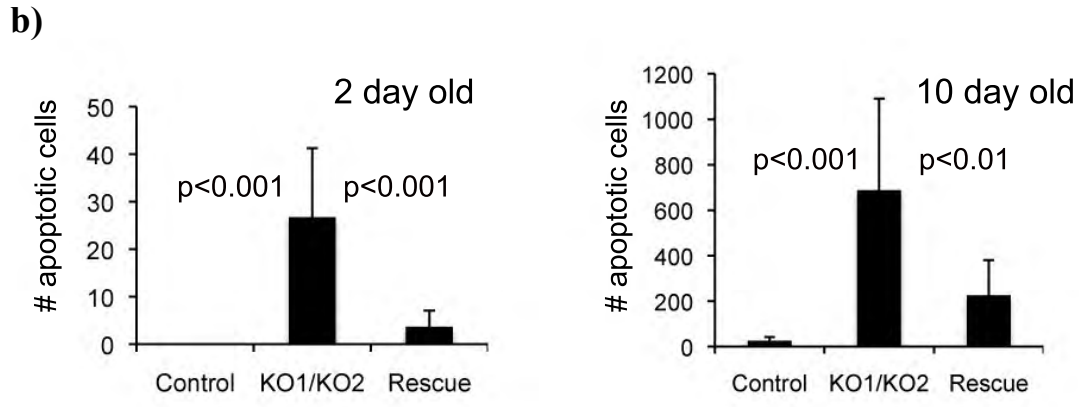
b)
2 day old
apoptotic cells
50
40
30
20
10
0
p<0.001
p<0.001
Control
KO1/KO2
Rescue
10 day old
apoptotic cells
1200
1000
800
600
400
200
0
p<0.001
p<0.01
Control
KO1/KO2
Rescue

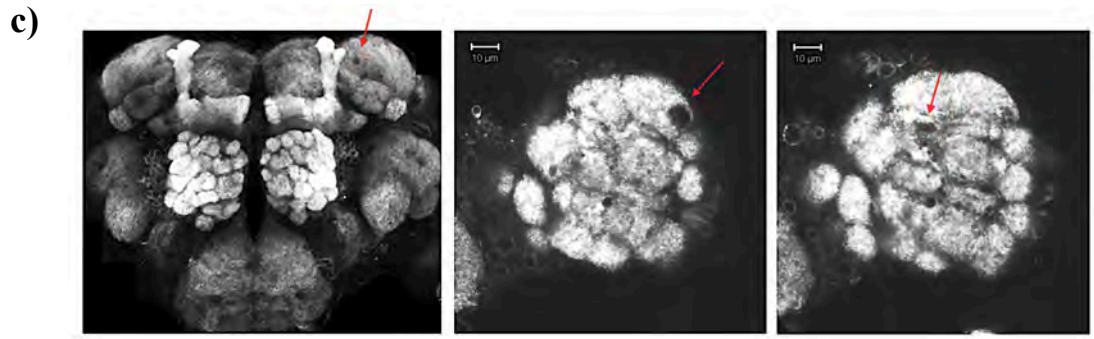
c)

Figure 16: Age-progressive neurodegeneration in *miR-1000* mutant brain

a) Adult brains of the age 2 and 10 day, labeled with antibody against activated Caspase3 (red) to mark apoptotic cells in KO1/KO2, rescue and control brains. Dlg (green), a post-synaptic marker is used to visualize the outline of brain. Images are maximum projections from a stack of optical sections. Scale bar - 20μM.
b) Quantification of Caspase 3 positive cells in brains, shown in a. Histograms show quantification of Caspase3 positive cells in 2 day (left panel) and 10 day (right panel) for KO1/KO2, rescue and control brain. Note that the scales differ for the Y-axis in the 2-day and 10-day samples. n=8 brains each.
c) Confocal microscope images of 10 day old adult brains from *miR-1000* mutant, labeled with Dlg antibody to outline brain tissue. Left panel: overview of brain, showing prominent olfactory lobes and mushroom bodies. Centre and right panels show magnified views of inside part of olfactory lobes of brain with vacuoles. Arrows indicate vacuoles in the brain. Scale bars - 10μM.

4.5 Target search for *miR-1000*

In miRNA mutants, a phenotype generally results from upregulation of one or more target genes, in the absence of miRNA-mediated repression. I took many approaches to find a biologically important target of *miR-1000*.

4.5.1 Prediction of possible targets of *miR-1000*

Targetscan program (http://www.targetscan.org/fly_12/) predicted 377 putative targets of *miR-1000*. To narrow down the number of target genes, I used RNA hybrid (http://bibiserv.techfak.uni-bielefeld.de/rnahybrid/submission.html) program to look for strong *miR-1000* seed matches among all the candidate genes. I considered genes having strong 8-mer seed sites for *miR-1000* targeting. Expression pattern of the predicted target genes was also taken into account. *miR-1000* is a CNS specific miRNA, so during initial screening, I selected target genes, that are known to express in the CNS. I also looked for their function in the nervous system, which might suggest their contribution to phenotypes of the *miR-1000* mutant. Based on these criteria, 7 genes were selected for further analysis.

4.5.2 Target search by RT-qPCR

In miRNA mutants, target genes are often upregulated. I looked for up-regulation of transcript levels by qPCR (Fig 17a). RNA extracted from the brains of mutant, rescue and control was used for qPCR. I looked for genes that showed upregulation in the mutant but returned to almost normal levels in the rescued mutant. Amongst 7 genes analyzed, I found a gene, *VGlut* (Vesicular Glutamate transporter), which showed a 3-4 fold up-regulation in mRNA transcript level that returned by almost half in the rescue flies (Fig 17b). The level of *VGlut* transcript was consistent with the level of *miR-1000* (~50%) restored in the rescue flies (Fig 17b).

4.6 *VGlut* as direct target of *miR-1000*

miRNAs generally bind to specific "seed" sites in the 3'UTR of their target genes. The 3' UTR of the *VGlut* mRNA contained two predicted *miR-1000* sites- one average 7mer site (site 1) and one strong 8mer site (site 2) (Fig 17c). To test whether *VGlut* is a direct target of *miR-1000*, a luciferase reporter carrying the endogenous 3'UTR of *VGlut* was used. In S2 cells, co-expression of *VGlut* 3'UTR luciferase reporter with a *miR-1000* expressing plasmid, caused ~50% reduction in luciferase activity, compared to luciferase control vector (empty vector without *VGlut* 3'UTR). To show that repression of the luciferase reporter was mediated by *miR-1000* sites in the 3'UTR of *VGlut*, I mutated each seed site. When seed site 1 and site 2 were mutated individually, repression was relieved by a modest level, whereas when both sites were mutated simultaneously, repression was completely relieved (Fig 17d).

a)

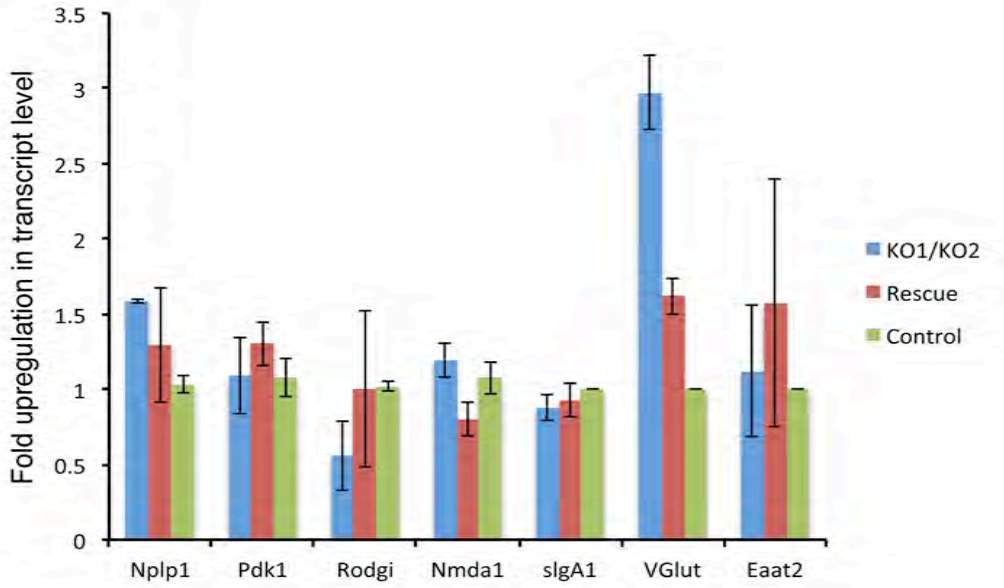
Fold upregulation in transcript level
3.5
3
2.5
2
1.5
1
0.5
0
Nplp1
Pdk1
Rodgi
Nmda1
slgA1
VGlut
Eaat2
KO1/KO2
Rescue
Control

b)

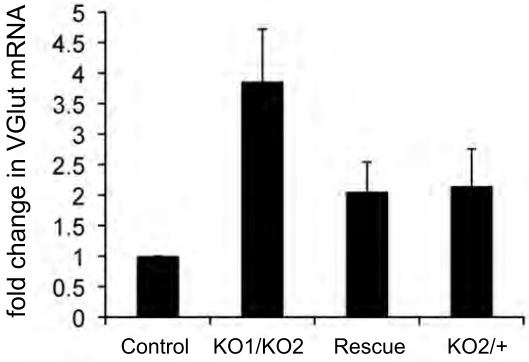
fold change in VGlut mRNA
5
4.5
4
3.5
3
2.5
2
1.5
1
0.5
0
Control
KO1/KO2
Rescue
KO2/+

c)

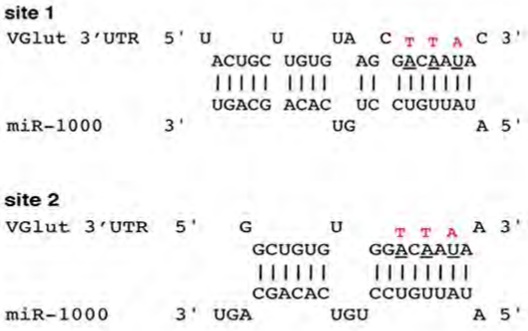
site 1
VGlut 3'UTR 5' U U UA C T T A C 3'
ACUGC UGUG AG GACAAUA
UGACG ACAC UC CUGUUAU
miR-1000 3' UG A 5'
site 2
VGlut 3'UTR 5' G U T T A A 3'
GCUGUG GGACAAUA
CGACAC CCUGUUAU
miR-1000 3' UGA UGU A 5'

d)

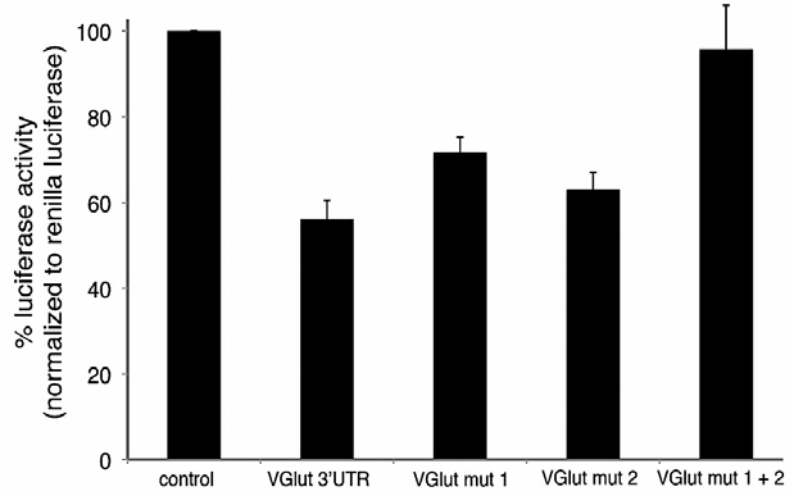
% luciferase activity
(normalized to renilla luciferase)
100
80
60
40
20
0
control
VGlut 3'UTR
VGlut mut 1
VGlut mut 2
VGlut mut 1 + 2

Figure 17: *VGlut* as direct target of *miR-1000*

a) RT-qPCR for predicted target genes, showing transcript levels of gene *Nplp1, Pdk1, Rodgi, NMDA1, slgA1, VGlut, Eaat2* in mutant (KO1/KO2), rescue and control brains. Data were normalized to control brain RNA and endogenous control rp49.
b) RT-qPCR showing *VGlut* transcript levels in RNA isolated from heads of mutant, rescue, heterozygous and control flies. Data was normalized to rp49. Data represent at least 3 independent experiments. $p<0.01$ comparing mutant vs control and rescued mutant.
c) Predicted target sites for *miR-1000* in the *VGlut* 3'UTR. Site 1 is 7-mer and site 2 is 8mer site. Residues mutated for the mutant *VGlut* 3'UTR luciferase reporters used in the luciferase assays are shown in red.
d) Histogram showing regulation of luciferase activity directed by the *VGlut* 3'UTR reporter and the reporter carrying mutations in each *miR-1000* site and combined mutations in both sites. Expression of *miR-1000* reduced luciferase activity in the intact *VGlut* 3'UTR reporter. Regulation was lost when the *miR-1000* sites were mutated. Data represent at least 3 independent experiments. $p<0.001$ comparing *VGlut* 3'UTR reporter with control and mutant reporters.

4.7 Biological functions of Vesicular Glutamate Transporter (*VGlut)*

For transmission of signal from brain to the different parts of body, neurons communicate with each other across a synapse, using chemical neurotransmitters. There are two kinds of neurotransmitters in the brain- Excitatory and Inhibitory, depending on their ability to stimulate or inhibit generation of action potential. Neurotransmitters are generally stored in pre-synaptic neurons inside specialized organelles called synaptic vesicles. The VGlut protein loads an excitatory neurotransmitter, Glutamate into these synaptic vesicles. Glutamate loading into synaptic vesicles by VGlut depends on the action of the vacuolar H^+-ATPase, which generates an electrochemical proton gradient across the synaptic vesicle membrane by hydrolyzing ATP molecules (Bellocchio et al 2000, Disbrow et al 1982, Floor et al 1990, Naito S 1985, Takamori et al 2000). VGlut protein has preferential affinity towards L-glutamate over D-Glutamate (Moriyama & Yamamoto 1995).

VGlut ensures storage of the proper amount of glutamate in the synaptic vesicles and hence, maintains the proper vesicle size (Quantal size) required for the appropriate amount of glutamate release. Overexpressions of VGlut causes excess glutamate release and hence increase in quantal size at the *Drosophila* larval NMJs (Daniels et al 2004).

VGlut is a highly conserved gene, found in all species from flies to human. In mammals, there are three homologous *VGlut* genes- *VGlut-1*, *VGlut-2* and *VGlut-3*, expressed in different parts of the brain. *VGlut1* and *VGlut2* transcripts are more abundant than *VGlut3* in CNS (Liguz-Lecznar & Skangiel-Kramska 2007). In *Drosophila*, there is only one *VGlut (DVGlut),* which is expressed in the brain during all developmental stages and controls all glutamate-mediated neurotransmission.

The expression of *VGluts* in various parts of brain is developmentally regulated and age-dependent. In mouse, *VGlut2* expression is relatively high at birth. *VGlut2* levels increase with age in the cortex (Liguz-Lecznar & Skangiel-Kramska 2007) but decrease by 14-fold in the cerebellum region of the brain after one week post-natally (Boulland et al 2004). Similarly, *VGlut3* increases progressively in the cortex but declines by 5-fold in the cerebellum from P7 (Post-natal day 7) to adulthood (Boulland et al 2004).

In humans, abnormal expression of *VGluts* gives rise to several neurological disorders. Upregulation of *VGlut1* and *VGlut2* levels were observed in the putamen region in brains of Parkinson's patients. However, *VGlut1* levels were found to be at a low level in pre-frontal and temporal cortex of these patients (Kashani et al 2007).

In summary, *VGlut* plays an important role in maintaining glutamatergic signaling in the brain and facilitating reliable transmission of signals from brain to various parts of body. Misregulation of *VGlut* results in neurological disorders.

4.8 Co-expression of *VGlut* and *miR-1000* in nervous system

Expression of *VGlut* and *miR-1000* were detected in the CNS throughout development from embryo to adult. Expression of VGlut transcript in embryos shown by *in-situ* hybridization shares a similar expression pattern with *miR-1000* (Mahr & Aberle 2006) (Fig 18a). During larva stages, *miR-1000* and *VGlut* showed expression in overlapping as well as distinct pattern in different parts of the brain and ventral nerve cord (Fig18b, c). *miR-1000* showed wider expression pattern than *VGlut*, which might indicates its role in regulation of other targets in other parts of the brain.

miR-1000 showed very strong expression in the mushroom bodies during larva and adult stages (Fig 18b,e), indicating possible role of *miR-1000* in memory and learning, which needs to be explored in further detail in future.

Using VGlut antibody, I detected a reciprocal expression pattern between VGlut protein and *miR-1000*. Cells expressing high level of *miR-1000* were observed to have low VGlut protein level and vice-versa (Fig 18d), suggesting modulation of VGlut level by *miR-1000 in vivo*. Similarly, *VGlut* and *miR-1000* also have reciprocal expression in adult eye (Fig 18f),

a)

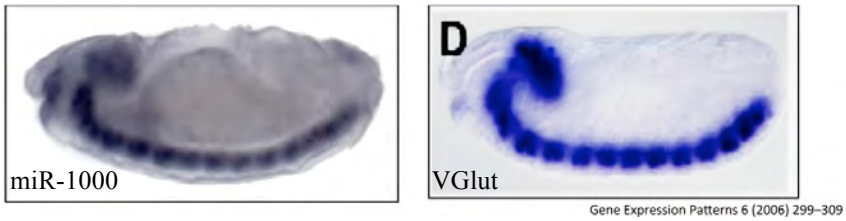
miR-1000
D
VGlut
Gene Expression Patterns 6 (2006) 299–309

b)

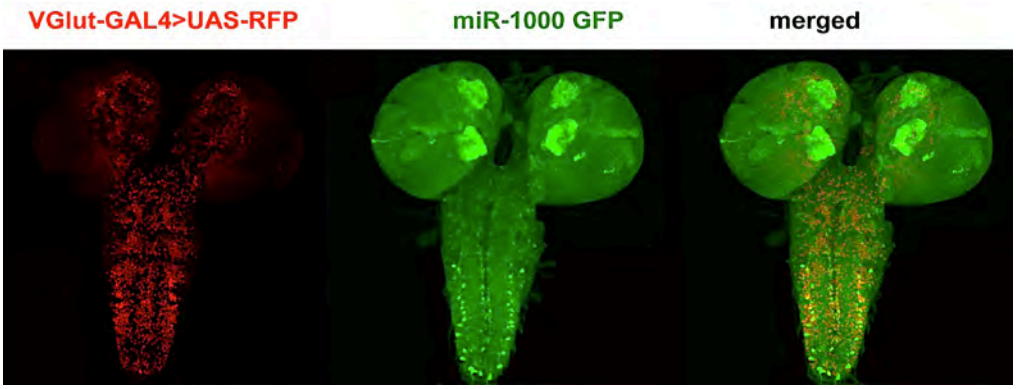
VGlut-GAL4>UAS-RFP
miR-1000 GFP
merged

c)

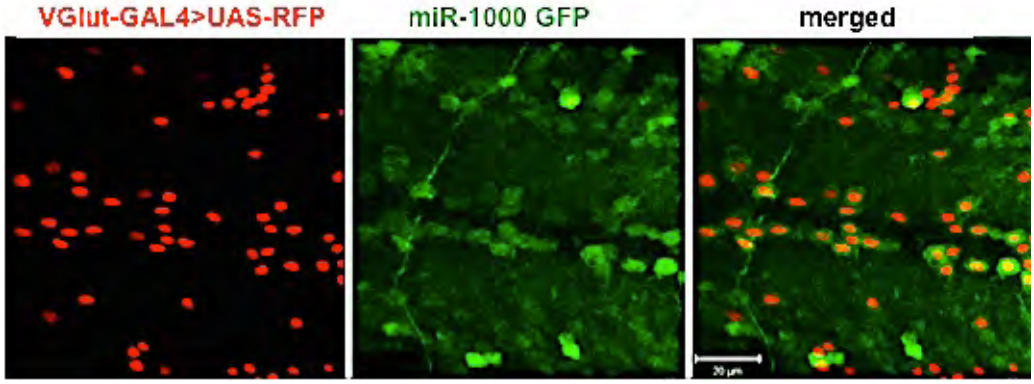
VGlut-GAL4>UAS-RFP
miR-1000 GFP
merged

d)

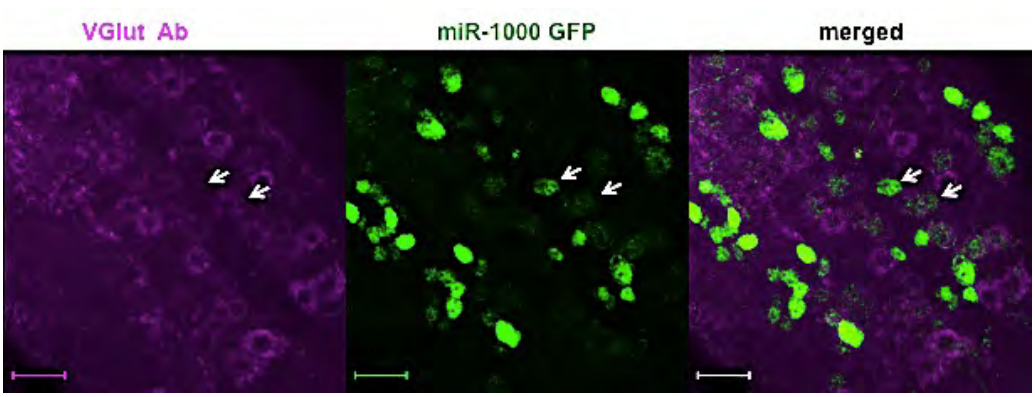
VGlut Ab
miR-1000 GFP
merged

e)

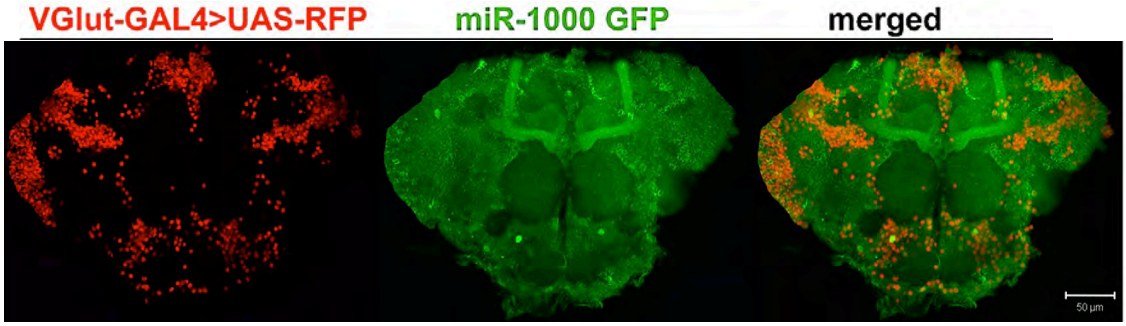
VGlut-GAL4>UAS-RFP
miR-1000 GFP
merged

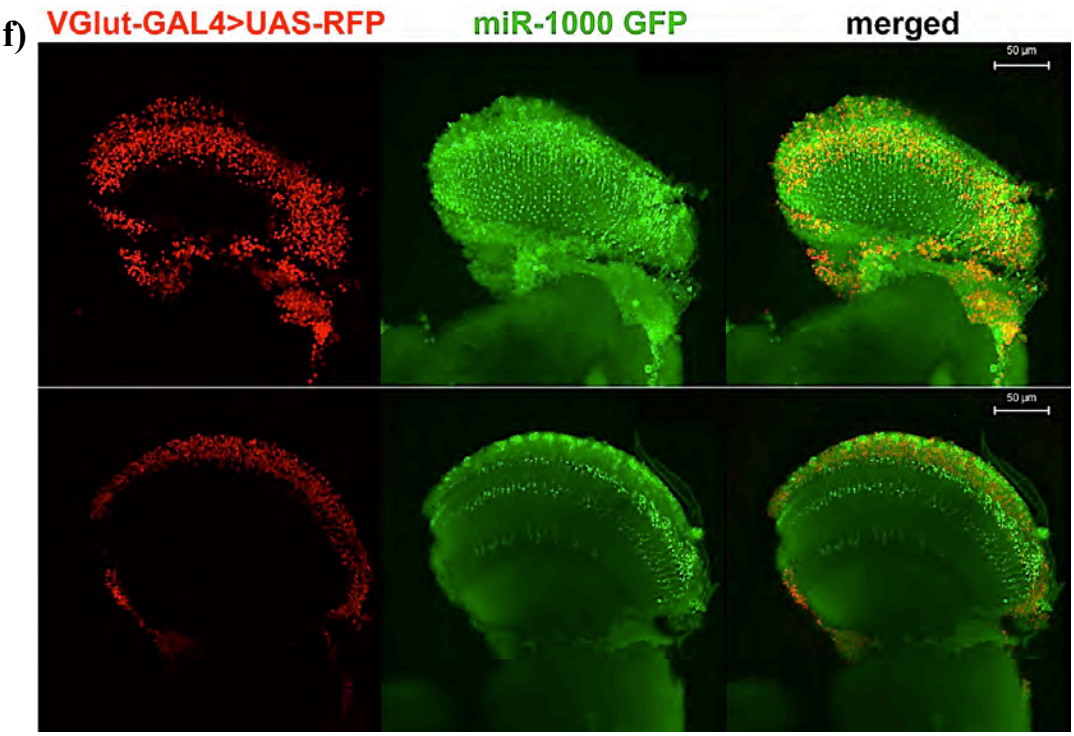

Figure 18: Nervous system specific expression of *VGlut* and *miR-1000* during different developmental stages.

a) *In-situ* hybridization of *miR-1000* (left panel) and *VGlut* (right panel) showing expression in embryonic CNS.
b) *VGlut*-GAL4 driving expression of UAS-RFP (red) and *miR-1000*-GFP (green) showing expression in the larval brain and ventral nerve cord. Image is maximum projection of various confocal sections.
c) Magnified part of larval ventral nerve cord showing expression of *VGlut* (red) and *miR-1000* (green). Note that *VGlut* and *miR-1000* showed overlapping expression in most of the cells, however there are few cells expressing either *VGlut* or *miR-1000*. Scale bar- 20µM
d) Larval ventral nerve cord showing expression of VGlut protein by VGlut antibody (purple) and *miR-1000* expression in green. Arrows indicate reciprocal quantitative expression between *miR-1000* and *VGlut*. Scale bar- 20µM.
e) Adult brain showing expression of *VGlut* (red) and *miR-1000* (green). Mushroom bodies showed strong expression of *miR-1000* but not *VGlut*. Image is maximum projection of various confocal sections. Scale bar- 50µM.
f) Expression of *VGlut* (red) and *miR-1000* (green) in upper layer (upper panel) and middle layer (lower panel) of adult eye. Scale bar- 50µM

4.9 *VGlut* as a target of *miR-1000 in vivo*

If up-regulation of *VGlut* is the cause of the defects observed in the *miR-1000* mutants, then selectively reducing *VGlut* levels in the mutant background should rescue defects of *miR-1000* mutant. To test this hypothesis, two different genetic approaches were used.

4.9.1 Rescue of *miR-1000* phenotypes by removing one copy of *VGlut*

To test whether the *VGlut* is a real target of *miR-1000 in vivo*, one copy of the *VGlut* locus was removed using a chromosomal deletion Df{2L}BSC37 (referred to as Df(VGlut) in Fig19a) in the *miR-1000* mutant background. The climbing ability of *miR-1000* mutant flies improved when *VGlut* was reduced to half by removing one copy of the *VGlut* gene (Fig 19a). I also tested lifespan for *miR-1000* mutant flies along with flies carrying Df (VGlut). Mutant flies with reduced *VGlut* level survived longer than *miR-1000* mutants alone (Fig 19b).

4.9.2 Rescue of *miR-1000* phenotype by knocking down *VGlut* levels in *miR-1000* expressing cells

I introduced a VGlut-UAS-RNAi transgene into the *miR-1000* mutant background to selectively deplete *VGlut* transcript in *miR-1000*-expressing cells. I made use of the *miR-1000-Gal4* allele (refer to as KO-GAL4 in Fig 19c) for this purpose. The *miR-1000* mutants with reduced *VGlut* levels performed better in the climbing assay (Fig 19c) and also extended the lifespan of the *miR-1000* mutants (Fig 19d).

The results of both experiments, using chromosomal deletion or *VGlut*-RNAi to reduce *VGlut* levels, are consistent with *VGlut* overexpression being a cause of movement disorder and reduced lifespan in *miR-1000* mutants.

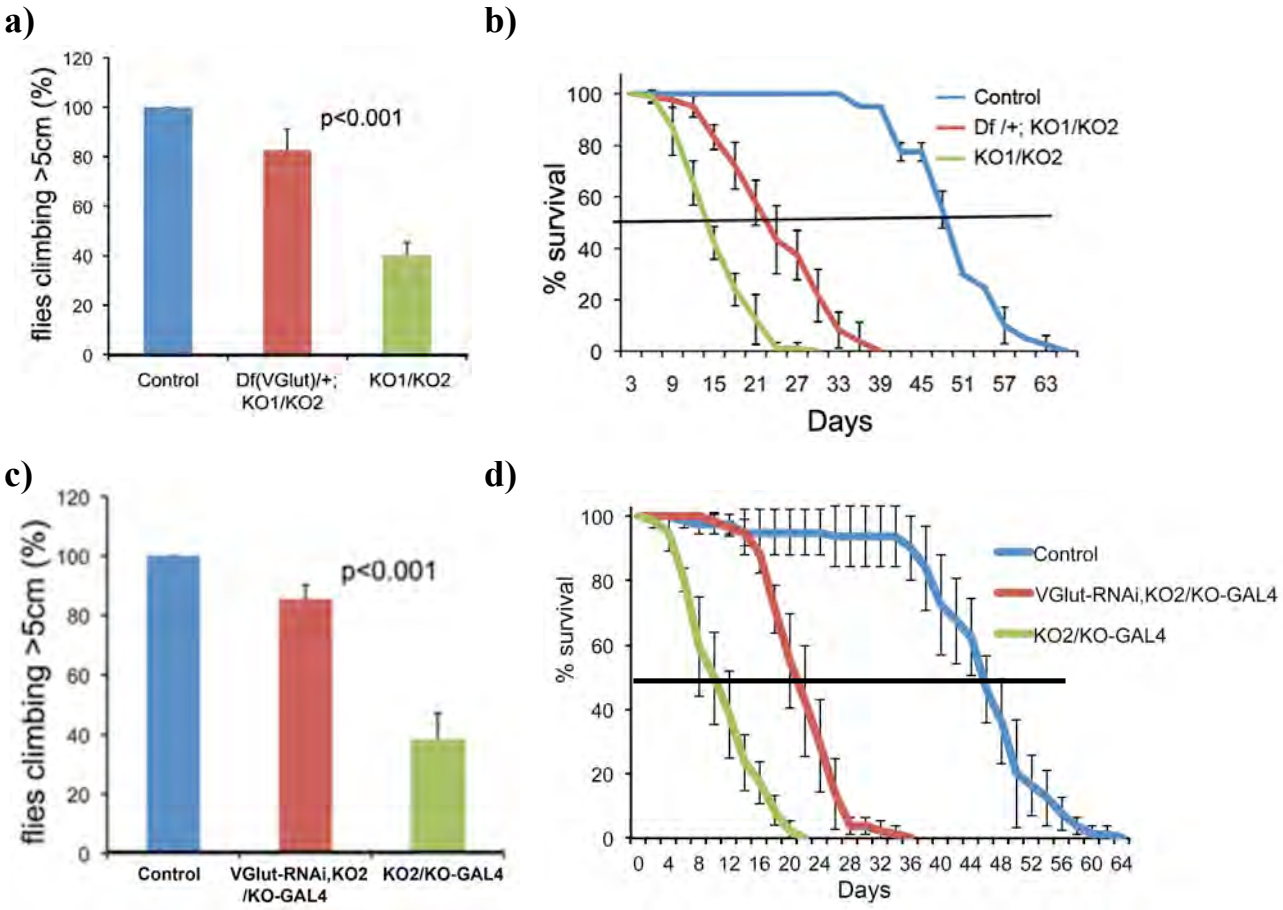

Figure 19: Confirmation of *VGlut* as a target of *miR-1000 in vivo*

a) Histogram showing climbing performance of *miR-1000* mutant (KO1/KO2, green), flies with the same mutant carrying a deletion that eliminates one copy of the *VGlut* gene (Df(VGlut)/+; KO1/KO2, red) and control (blue) flies. Data represent at least three independent experiments. $p<0.001$ comparing KO1/KO2 with Df(VGlut)/+;KO1/KO2.

b) Graph showing life span of flies used in Fig 19a. Data represent at least three independent experiments. $p<0.001$ comparing median survival of KO1/KO2 with Df(VGlut)/+; KO1/KO2.

c) Histogram comparing climbing ability of trans-allelic *miR-1000* mutant with the *miR-1000*-GAL4 (KO2/KO-Gal4, green) with the same mutants carrying a VGlut-UAS-RNAi transgene to deplete *VGlut* mRNA in the miRNA expressing cells (*VGlut*-RNAi, KO2/KO-Gal4, red). Data represent at least three independent experiments. $p< 0.001$, comparing KO2/KO-Gal4 with *VGlut*-RNAi, KO2/KO-Gal4.

d) Graph showing life span of flies used in Fig 19c. Data represent at least three independent experiments. $p<0.001$ comparing median survival of KO2/KO-Gal4 with *VGlut*-RNAi,KO2/KO-Gal4 flies.

4.10 Excess glutamate release in *miR-1000* mutants

Glutamate is the most abundant excitatory neurotransmitter in the brain, responsible for majority of excitatory signaling. Approximately 90% of brain synapses are glutamatergic. Glutamate is involved in a variety of processes that regulate brain development, including cell survival and differentiation; formation and removal of synapses; cognition, learning and memory. The optimal amount of extracellular glutamate levels is very important for normal synaptic neurotransmission. Excessive extracellular levels of glutamate contribute to neurological diseases, including seizures, stroke, traumatic brain injury, ALS (Amyotropic Lateral Sclerosis), Alzheimer's disease, and Huntington's disease (Mattson 2003, Olney 2003).

In *miR-1000* mutants, *VGlut* levels was observed to be high, which might result in release of extra glutamate at synapses. To investigate this possibility, electrophysiological recording of spontaneous synaptic activity at the NMJs was performed. *Drosophila* NMJ are glutamatergic and *miR-1000* is expressed in larval NMJs (Fig 7b). I recorded synaptic activity from larval muscle 6, which is known to have big synaptic boutons, making synaptic recordings easier to measure. All recordings were done from muscle 6 of either segment 3 or 4 of larva. Neuronal connections to the brain were cut to eliminate responses evoked by presynaptic action potentials.

Spontaneous miniature excitatory junction potentials (mEJPs) were used as a measure of synaptic transmission in larval NMJs. Peaks of mEJPs were observed to be bigger in *miR-1000* mutants (Fig 20a) compared to control and rescue. Increase in amplitude of mEJPs (Fig 20b,c) as well increased frequency (Fig 20d) was observed in *miR-1000 mutants*, which was rescued to a significant degree by restoring *miR-1000* levels in rescue. This indicated that there is increased glutamatergic signaling in

the NMJs. *VGlut* and *miR-1000* are not expressed in the muscle, thus indicating that these effects were due to excess release of glutamate from presynaptic motor neurons in the *miR-1000* mutants.

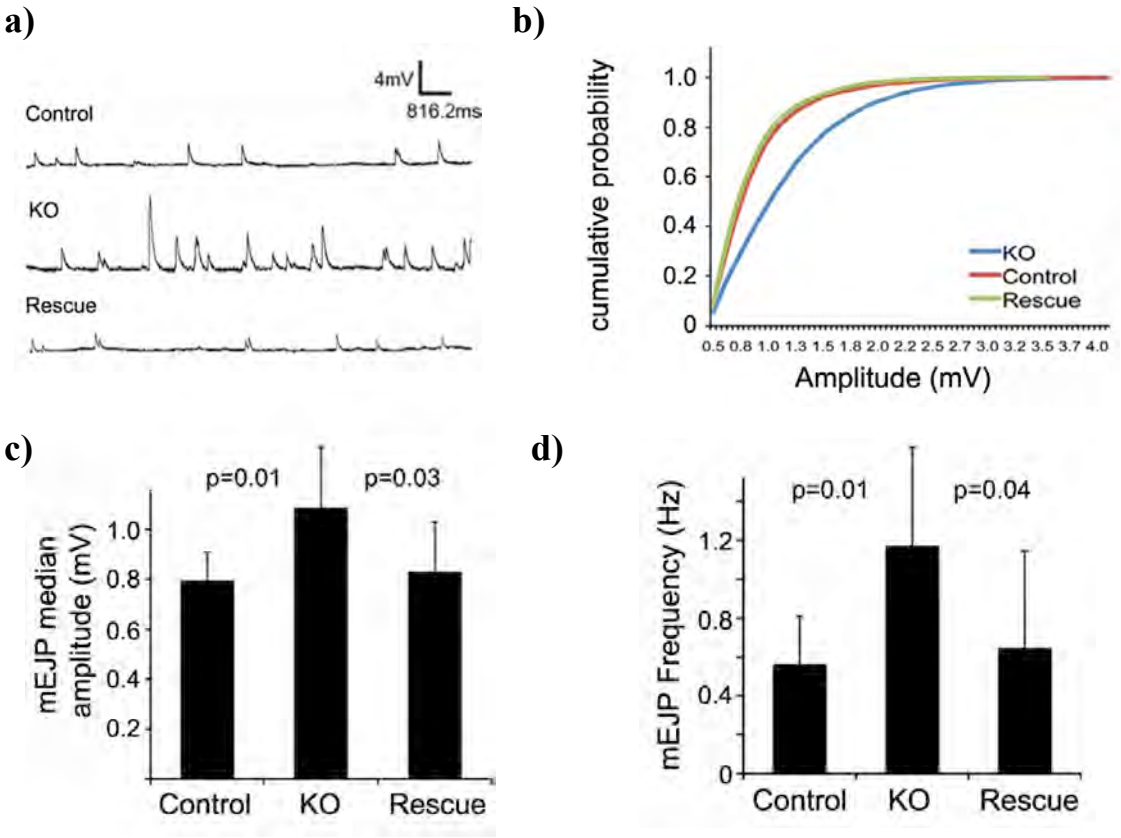

Figure 20: Excess glutamate release in *miR-1000* mutants

a) Representative traces of spontaneous mEJPs at the NMJ. Recordings were made from larval muscle 6. For panels a-d KO indicates flies homozygous for the *mini-white* excised deletion allele (KO1). Rescue indicates flies homozygous for the *miR-1000* RMCE rescue allele.

b) Cumulative probability distribution of mEJP amplitudes for *miR-1000* mutant (blue), rescue (green) and control (red).

c) Histogram showing median amplitude of mEJPs in control, mutant and rescue. mEJP was significantly higher in the mutant compared to control (p=0.01) and significantly rescued (p=0.03).

d) Histogram showing frequency of mEJPs in control, mutant and Rescue. mEJP frequency was higher in the mutant (p=0.01) and significantly rescued (p=0.04).

4.11 Glutamatergic signaling and its associated excitotoxicity

Synaptic neurotransmission is a highly regulated process, initiated by arrival of an action potential at the presynaptic neuronal surface. It is followed by calcium signaling mediated fusion of synaptic vesicles with the membrane of pre-synaptic neuron and subsequent release of synaptic vesicle's contents into synaptic cleft. Synaptic vesicles generally undergo endocytosis-mediated recycling, in which they are refilled with neurotransmitters and reused (Fig 21).

Excitatory glutamatergic signaling consists of following components:

4.11.1 Vesicular Glutamate Transporter (*VGlut)*

The VGlut protein loads Glutamate into synaptic vesicles inside pre-synaptic neurons as mentioned before.

4.11.2 Glutamate Receptors

Glutamate exerts its signaling function by binding to and activating specific glutamate receptors that are present on the membrane of post-synaptic neurons. There are two major kinds of glutamate receptors.

1. Ionotropic Glutamate receptors (iGluR): Excitatory synaptic neurotransmission in the brain is mostly mediated by ionotropic glutamate receptors. Ionotropic receptors are ion channels receptors, which get activated by binding of the glutamate to an ion channel pore. The three classes of ionotropic receptors are called NMDA, AMPA, and Kainate receptors (KR).

a) **NMDA receptors:** NMDA receptors derived their name because of their activation by NMDA (*N*-methyl-D-aspartate). They can be activated by glutamate and aspartate also. NMDA receptors have higher affinity for

Glutamate (Chen et al 2005a) and function as both ligand-gated and voltage gated channels. Their activation requires binding of glutamate and an additional co-activator such as glycine or d-serine (Wafford et al 1995, Wolosker et al 1997). NMDA receptors allow entry of Ca^{2+} and Na^{+} into the cell and K^{+} out of the cell. Mg^{2+} ions block the channels at its resting membrane potential. Binding of glutamate to the channel and subsequent depolarization of NMDA bearing post-synaptic membrane by AMPA or Kainate receptors, removes blockage by Mg2+ ions. The NMDA receptors exist as a heterodimer of two glutamate binding subunits (GluNR). This heterodimer consists of two basic GluNR1 and two subunits of various forms of GluNR2 (Ryan et al 2009). NMDA receptors are widely studied as a therapeutic target for a variety of neurological disorders including Schizophrenia, Parkinson's, Alzheimer's, and Huntington's diseases (Cull-Candy et al 2001).

b) AMPA receptors: AMPA receptors derived their name from an artificial glutamate analog, AMPA (α-amino-3-hydroxy-5-methyl-4-isoxazolepropionic acid), which activate these receptors. AMPA receptors are non-NMDA type receptors, which get activated by binding to L-Glutamate but their affinity for Glutamate is much lower than that of NMDA receptors (Dingledine et al 1999). AMPA receptors exist as transmembrane heterotetrameric receptors, consisting of GluR2 subunit with any of GluR1, GluR3 and GluR4 subunits (Kim et al 2001, Mayer 2011). The GluR2 subunit of AMPA receptor controls the permeability of calcium, sodium and potassium ions. The presence of a GluR2 subunit makes the channel impermeable to calcium ions, by converting adenosine to inosine (A-to-I) in its mRNA by an enzyme called as adenosine

deaminase acting on RNA 2 (ADAR2). Failure of A-to-I conversion affects properties of AMPA receptor and makes them permeable to calcium ions, which leads to induction of fatal epilepsy in mice (Brusa et al 1995, Feldmeyer et al 1999). Inefficient GluR2 editing causes molecular dysfunction found in the motor neurons of sporadic ALS patients (Kawahara et al 2004). Impermeability to calcium ions makes AMPA receptors distinguishable from calcium permeable NMDA receptors. AMPA receptors open and close quickly, and are thus responsible for most of the fast excitatory synaptic transmission (Tzschentke 2002). Once open, they undergo very fast desensitization and then rapidly close the pore.

c) **Kainate receptors (KR):** Kainate-type glutamate receptors are expressed throughout the nervous system, though at a much lower level than AMPA and NMDA receptors. Kainate receptors are present on the pre-synaptic as well as post-synaptic surface (Huettner 2003). On pre-synaptic surface, these receptors acts as modulators of excitatory and inhibitory transmission, neuronal excitability, synaptic development and various other aspects of brain functions (Contractor et al 2011). However, on the post-synaptic surface, they are involved in excitatory synaptic transmission, similar to AMPA and NMDA receptors. They exist as tetramers, consisting of combination of five subunits (GluR5, GluR6, GluR7, KA1 and KA2). Ion channels formed by kainate receptors are permeable to sodium and potassium ions with very low permeability for calcium ions. Kainate receptors are attractive targets of therapeutics because of their modulatory effect on synaptic activity. They have been implicated in human diseases like epilepsy and migraine (Vincent & Mulle 2009).

2. Metabotropic receptors (mGluR): mGluR receptors belong to a family of G protein-coupled receptors (GPCRs), consisting of seven transmembrane domains, coupled to a GTP binding protein (G-proteins). Unlike ionotropic receptors, they do not form ion channels; instead they activate biochemical signaling, leading to the modification of other proteins or ion channel receptors. mGluRs have been shown to be involved in synaptic plasticity, neurotoxicity and neuroprotection by modulating other receptors, including NMDAR (Siliprandi et al 1992). mGluR receptors have the highest affinity for glutamate and exist both on the pre-synaptic and post-synaptic surface of neurons. There are eight different kinds of mGluR receptors known in mammals, which are divided into three categories, based on sequence similarity, signal transduction and pharmacology (Conn & Pin 1997).

Group I mGluR: This group includes mGluR1 and mGluR5 that are mainly present on the post-synaptic surface of neurons and are positively coupled to the downstream effector phospholipaseC. mGluRs of this group are activated by 3,5-dihydroxyphenylglycine (DHPG) (Shigemoto et al 1997). These receptors increase activity of NMDA receptors.

Group II mGluR: This group includes mGluR2 and mGluR3, which are mostly present on the pre-synaptic surface and are coupled negatively to enzyme adenylate cyclase (AC) activity. Group II mGluRs are activated by 2-(2,3-dicarboxycyclopropyl) glycine (DCG-IV). These receptors decrease activity of NMDA receptors.

Group III mGluR: This group includes mGluR4, mGluR6, mGluR7 and mGluR8, which are mainly present on the pre-synaptic surface and are coupled negatively to

enzyme adenylate cyclase (AC) activity. These receptors are activated by 2-amino-4-phosphonobutyrate (L-AP4). These receptors also reduce activity of NMDA receptors.

The mGluRs are well-studied receptors due to their widespread expression and function in the CNS. They have been shown to be involved in neurological disorders including spinal cord injury, ischemia, epilepsy, multiple sclerosis, ALS, oxidative stress and diabetes (Spillson & Russell 2003). mGluRs are also reported to contribute to motor dysfunctions in ALS, Huntington's disease, Parkinson's disease and cerebellar ataxia (Conn & Pin 1997). mGluRs have been observed to regulate ROS (reactive oxygen species) production and associated oxidative stress. The mechanism of action of mGluR involves activation of the phosphatidylinositol 3-kinase (PI3K) and MAPK signaling pathways, which in turn, leads to decreased ROS concentration and ultimately a decrease in oxidative stress and programmed cell death (D'Onofrio et al 2001, Iacovelli et al 2004), thus playing a neuro-protective role.

In *Drosophila*, there is only one metabotropic receptor, *DmGluRA*, which has high homology to the mammalian group II mGluRs.

In addition to the above-mentioned receptors, there are distinct types of glutamate receptors that are expressed in *Drosophila* somatic muscles and are excluded from the CNS (Currie et al 1995). These receptors include two closely linked genes, *GluRIIA* and *GluRIIB*. The *Drosophila* GluRII glutamate receptors share ~26-28% sequence similarity with AMPA and Kainate receptors of the ionotropic glutamate receptor family (Schuster et al 1991).

4.11.3 Excitatory Amino Acid Transporters (EAATs)

The EAATs (Excitatory Amino Acid Transporters) are Na^+ dependent high affinity glutamate transporters, localized to the plasma membrane of glia as well as neurons. These transporters are called glutamate "scavengers". They remove excess glutamate from the synaptic cleft after synaptic transmission has taken place. EAATs, present on the surface of glial or astroglial cells, remove glutamate by a process called "glutamate uptake". Astroglial cells convert glutamate to glutamine by an enzyme, Glutamine synthetase. Glutamine is released from astroglial cells into the extracellular space and then taken up by pre-synaptic neurons, where it is recycled into Glutamate by an enzyme, glutaminase and repackaged into synaptic vesicles by VGluts. This process is referred to as the glutamate-glutamine cycle (Bak et al 2006, Daikhin & Yudkoff 2000) (Fig 21).

There are five EAATs known in mammals, with differential CNS specific expressions. EAAT1 and EAAT2 are primarily located on the membrane of glial cells, EAAT3 and 4 are found on the surface of neurons (Chen et al 2002, Furuta et al 1997, Schmitt et al 2002) and EAAT5 expression is limited to very few neurons and cells of the retina (Eliasof et al 1998). The EAAT2 is considered as primary transporter involved in clearing glutamate from the extracellular space (Koch et al 1999). Loss of the EAAT2 is suspected to be associated with Alzeimer's disease, Huntington's disease, ALS etc (Yi & Hazell 2006).

There are two EAATs in *Drosophila*- EAAT1 and EAAT2. *Drosophila* EAAT1 has 41% and 35% amino acid identity to human EAAT1 and EAAT2 respectively (Besson et al 1999). EAAT1 is the only transporter in flies with high-affinity for glutamate whereas EAAT2 acts as high-affinity transporter for taurine and aspartate (Besson et al 2005, Besson et al 2000).

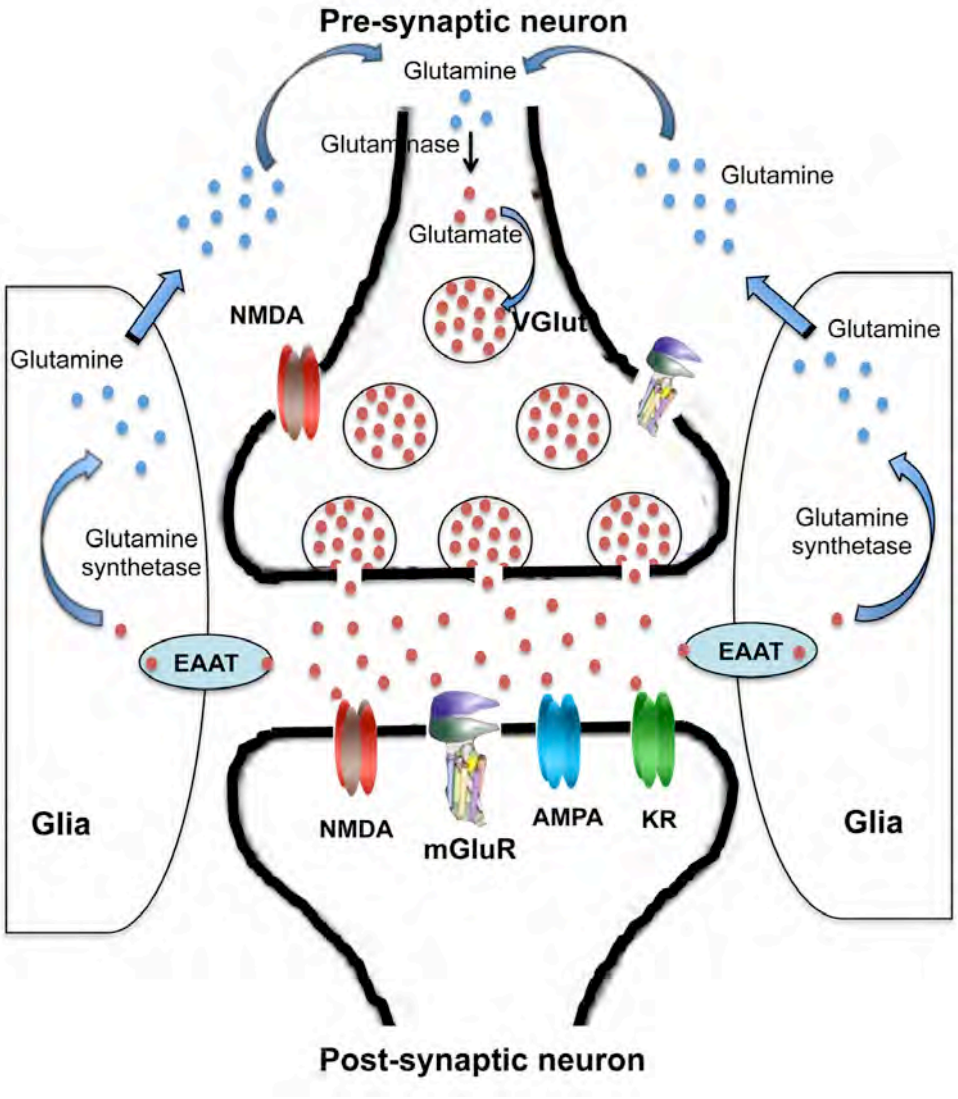

Figure 21: Excitatory glutamatergic signaling in the nervous system

Diagram showing excitatory glutamatergic signaling in the brain. Excitatory neurotransmitter, Glutamate (red dots) is loaded into synaptic vesicles (circle surrounding red dots) by VGlut in pre-synaptic neurons. On the membrane of post-synaptic neuron, metabotropic glutamate receptor (mGluR) and ionotropic receptors (iGluR-NMDA, AMPA and KR) are shown as heterodimers. Excitatory Amino Acid Transporters (EAATs, in blue circle) present on the glial surface perform glutamate uptake from synaptic cleft and convert it to glutamine by glutamine synthetase enzyme. Glutamine is recycled back to glutamate by glutaminase enzyme in pre-synaptic neurons.

4.11.4 Glutamate excitotoxicity

Synaptic neuro-transmission occurs when Glutamate activates downstream glutamate receptors, which in turn activate downstream signaling. Excess glutamate in extracellular space is not deleterious if it does not overactivate glutamate receptors and cleared up by EAATs. Glutamate receptors, when continuously overactivated by excess glutamate cause death of neurons, a process known as neuronal "excitotoxicity" (Olney 1969). Excess glutamate in the extracellular space either results from overproduction and subsequent release of glutamate into synaptic cleft or inability of EAATs to uptake glutamate into surrounding glial cells for recycling.

4.12 Glutamate excitotoxicity causing defects in *miR-1000* mutants

In *miR-1000* mutants, excess glutamate was observed. Next, I wanted to ask whether glutamate mediated excitoxicity is a cause of the mutant phenotypes in *miR-1000* mutant and whether mutant phenotypes can be rescued by preventing overactivation of glutamate receptors.

4.12.1 Rescue of *miR-1000* phenotypes by blocking glutamate receptors with drug

To investigate the possibility that *miR-1000* mutant defects are due to excess glutamate release and overactivation to glutamate receptors, I first made use of a drug memantine, a glutamate receptor antagonist used to treat Alzheimer's disease (Reisberg et al 2003). Flies were fed on food containing 0.01mM memantine and climbing performance was measured after one day of drug treatment. Drug treated mutants showed a significant improvement compared to untreated mutant controls in the climbing assay (Fig 22a).

4.12.2 Rescue of *miR-1000* phenotypes by blocking glutamate receptors *in vivo*

Next, I tested the effects of reducing expression of various glutamate receptors *in vivo* in *miR-1000* mutant background. First, to rule out effects from muscles, I reduced activity of the muscle specific glutamate receptors encoded by the *GluRIIA* and *GluRIIB* genes using a chromosomal deletion Df{2L}Exel8016. Reduction of *GluRIIA* and *GluRIIB* by eliminating one copy of both genes in *miR-1000* mutant had no effect on the climbing capacity of mutant flies (Fig 22b).

Then, I reduced levels of glutamate receptors known to be expressed in the brain. Reduced expression of the glutamate ionotropic AMPA receptor encoded by

the *GluRI* locus improved climbing ability of *miR-1000* mutants. The *miR-1000* mutants showed modest improvement in climbing by reducing levels of *GluR1*, with *GluR1* mutant in one copy (KO1/KO2, *GluR1*) and significant improvement with two mutant GluR1 copies (KO2, *GluR1*/KO2, *GluR1*). Heterozygous control (KO2, *GluR1*/+) and *GluR1* homozygous mutants performed normally in the climbing assay (Fig 22c). Although reduced *GluR1* levels were effective in suppressing the climbing defect, this had little effect on mutant lifespan (Fig 22d), which might be due to fast and transient effect of AMPA receptors.

In contrast, *miR-1000* mutants carrying a mutation in the metabotropic glutamate receptor encoded by the *mGluRA* showed a clear improvement in the climbing ability (Fig 22e) as well as a significant increase in lifespan (Fig 22f) of mutant flies. Similar results were obtained using two independent RNAi transgenes to deplete *mGluRA* in *mGluRA* expressing cells in the *miR-1000* mutant background. Both RNAi transgenes showed better results for climbing as well as in longevity of the *miR-1000* mutant, with reduced level of *mGluRA* (Fig 22g, h). *mGluRA*-RNAi transgenes used here had leaky expression and rescued climbing defects as well as lifespan significantly without driving with GAL4. Rescue of mutant defects was further improved by driving *mGluRA*-RNAi transgenes in the *mGluRA* producing cells using mGluRA-GAL4.

These findings implicated excess glutamatergic signaling as the cause of movement disorder and reduced lifespan of *miR-1000* mutants. Different glutamate receptors appeared to contribute to different extents of glutamate excitotoxicity, with *mGluRA* playing a major role in mediating excitotoxicity.

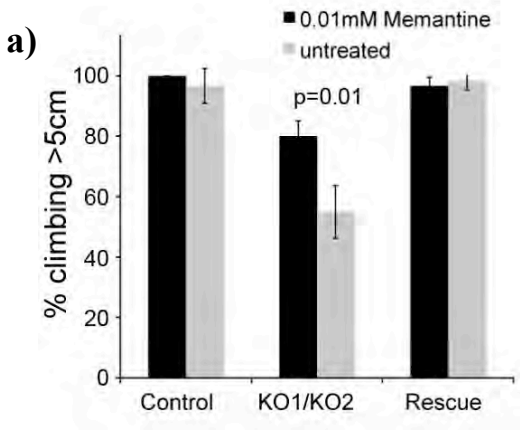
a)
0.01mM Memantine
untreated
p=0.01
% climbing >5cm
Control
KO1/KO2
Rescue

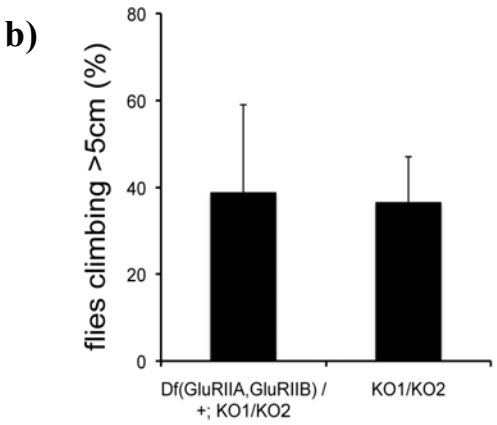
b)
flies climbing >5cm (%)
Df(GluRIIA,GluRIIB) / +; KO1/KO2
KO1/KO2

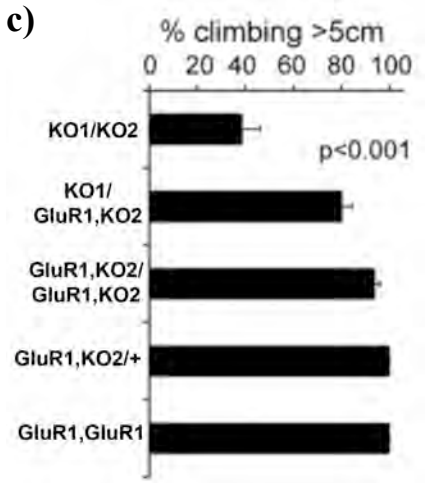
c)
% climbing >5cm
KO1/KO2
p<0.001
KO1/ GluR1,KO2
GluR1,KO2/ GluR1,KO2
GluR1,KO2/+
GluR1,GluR1

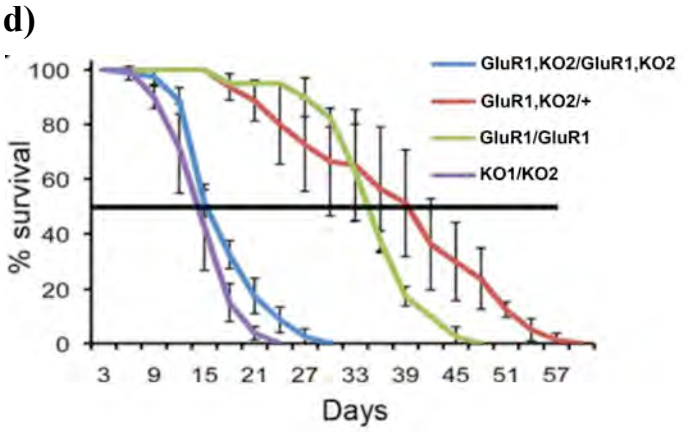
d)
GluR1,KO2/GluR1,KO2
GluR1,KO2/+
GluR1/GluR1
KO1/KO2
% survival
Days

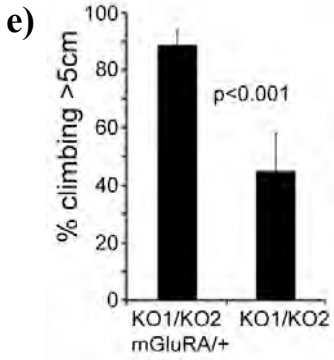
e)
% climbing >5cm
p<0.001
KO1/KO2
KO1/KO2 mGluRA/+

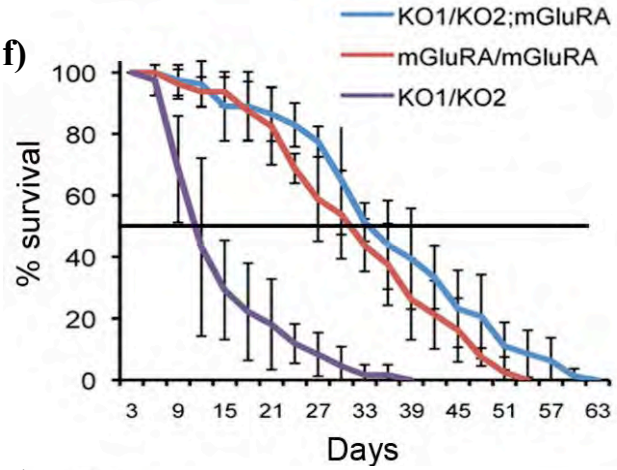
f)
KO1/KO2;mGluRA
mGluRA/mGluRA
KO1/KO2
% survival
Days

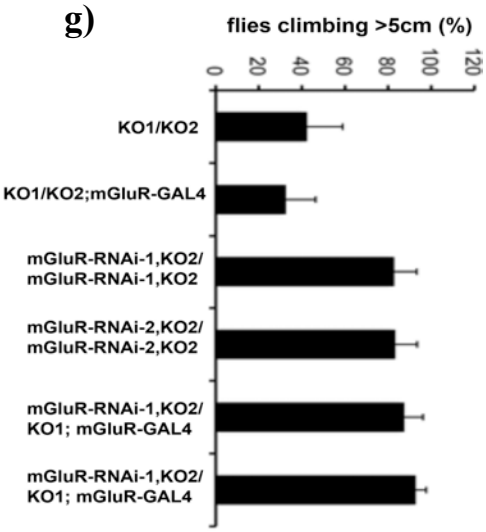
g)
flies climbing >5cm (%)
KO1/KO2
KO1/KO2;mGluR-GAL4
mGluR-RNAi-1,KO2/ mGluR-RNAi-1,KO2
mGluR-RNAi-2,KO2/ mGluR-RNAi-2,KO2
mGluR-RNAi-1,KO2/ KO1; mGluR-GAL4
mGluR-RNAi-1,KO2/ KO1; mGluR-GAL4

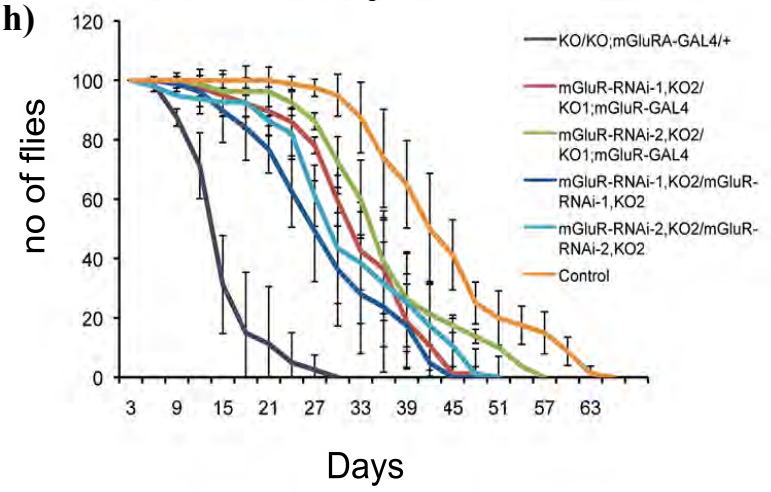
h)
KO/KO;mGluRA-GAL4/+
mGluR-RNAi-1,KO2/ KO1;mGluR-GAL4
mGluR-RNAi-2,KO2/ KO1;mGluR-GAL4
mGluR-RNAi-1,KO2/mGluR-RNAi-1,KO2
mGluR-RNAi-2,KO2/mGluR-RNAi-2,KO2
Control
no of flies
Days

Figure 22: Rescue of *miR-1000* phenotypes by manipulating glutamate receptors

a) Climbing assay performed on *miR-1000* mutant and control flies fed for one day on food containing 0.01mM Memantine (black bars) or with food lacking drug (grey bars). p=0.01 treated vs untreated *miR-1000* mutant.
b) Climbing assay on mutant flies (KO1/KO2) and mutant flies carrying one copy of a chromosomal deletion, Df(GluRIIA,GluRIIB). Data represent average of at least three independent experiments. p-value=0.87
c) Climbing assay performed on *miR-1000* mutant flies with reduced expression of the GluR1 receptor. The $GluR1^{f05411}$ mutant was recombined onto the *miR-1000* KO2 chromosome (KO2,*GluR1*). Flies carrying KO2, *GluR1*/KO1 showed improved climbing ability ($p<0.001$). This was further improved in the KO2, *GluR1* homozygous flies ($p<0.001$). Data represent average of at least three independent experiments.
d) Graph showing longevity of adult flies of indicated genotypes. Median survival of KO1/KO2 with KO2,*GluR1*/KO2,*GluR1* was not significantly different (p=0.1). Data represent average of at least 3 independent experiments.
e) Climbing assay performed on *miR-1000* mutant flies (KO1/KO2) and mutant flies with reduced expression of the *mGluRA*. KO1/KO2; *mGluRA*/+ indicates *miR-1000* mutant flies carrying one copy of a *mGluRA* mutation ($mGluRA^{MI02169}$). Data represent average of at least three independent experiments; $p<0.001$, comparing KO1/KO2 with KO1/KO2; *mGluRA*/+.
f) Graph showing lifespan of flies of indicated genotypes. $p<0.001$ comparing median survival of KO1/KO2 with KO1/KO2; *mGluRA*. Data represent average of 4 independent experiments.
g) Climbing assay performed on flies expressing two independent *mGluR*-RNAi in mGluRA expressing cells in *miR-1000* mutant background. The *mGluR*-Gal4 is a Gal4 insertion at the *mGluRA* locus. Two independent UAS-mGluR-RNAi transgenes were recombined onto the KO2 chromosome. In both cases, considerable rescue of the KO2 mutant phenotype was observed due to leaky RNAi transgenes. Addition of Gal4 provided a further modest improvement in the climbing performance. $p<0.001$ when comparing KO1/KO2;*mGluR*-GAL4 with KO2,$mGluR^{RNAi}$-1/KO1;*mGluR*-GAL4 and KO2,$mGluR^{RNAi}$-2/KO1;*mGluR*-GAL4. p-value=0.006 and p=0.005 when comparing KO1/KO2 with KO2,$mGluR^{RNAi}$-1 and KO2,$mGluR^{RNAi}$ -2 respectively.
h) Lifespan of adult flies of indicated genotypes. $p<0.001$ when comparing KO1/KO2;*mGluR*-GAL4/+ with *mGluR*-RNAi-1,KO2/ *mGluR*-RNAi-1,KO2, *mGluR*-RNAi-2,KO2/*mGluR*-RNAi-2,KO2, *mGluR*-RNAi-1,KO2/KO1; *mGluR*-GAL4, *mGluR*-RNAi-2,KO2/KO1;*mGluR*-GAL4 and Control for 50% survival.

4.13 Glutamate excitotoxicity causing neurodegeneration in *miR-1000* mutants

4.13.1 Reduction of apoptosis in the mutant brains by reducing level of glutamate receptors

To verify that the neurodegeneration observed in the *miR-1000* mutants was indeed due to glutamate excitotoxicity, I examined cell death using Caspase3 antibody in the brains of *miR-1000* mutants, with reduced levels of *mGluR* and *GluR1* receptors. I observed a significant reduction in cell death in the brains of *miR-1000* mutants, in which levels of glutamate receptors were reduced (Fig 23a).

4.13.2 Rescue of *miR-1000* mutant climbing defect by blocking apoptosis in glutamate receptor cells

To test whether death of glutamate receptor expressing cells contributes to the defects of *miR-1000* mutant, I blocked apoptosis in *mGluRA* producing cells, by overexpression of anti-apoptotic gene, *Drosophila* Inhibitor of Apoptosis1 (*DIAP1*). Climbing performance of the *miR-1000* mutants expressing UAS-DIAP1 in *mGluRA* cells improved significantly, compared to the *miR-1000* mutants (Fig 23b). This observation indicated that death of *mGluRA*-expressing cells contributes to the defects in the *miR-1000* mutant.

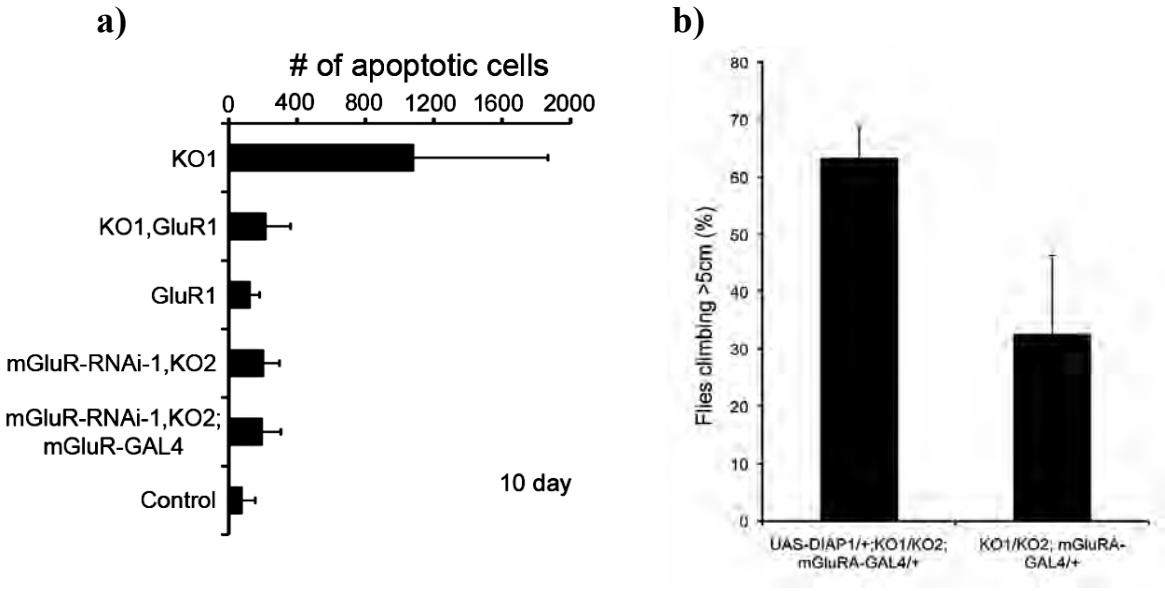

Figure 23: Glutamate excitotoxicity causing neurodegeneration in the *miR-1000* mutants

a) Quantification of apoptotic cells in 10 day-old brains of the indicated genotypes. p≤0.001 comparing KO1/KO1 with KO1,*GluR1* homozygous flies, *mGluR*-RNAi-1,KO2 homozygous flies and *mGluR*-RNAi-1,KO2; *mGluR*-GAL4. control n=10 brains; n≥14 other genotypes.
b) Climbing assay performed on flies expressing UAS-DIAP1 driven by *mGluR*-GAL4 in *miR-1000* mutant allelic combination (KO1/KO2). p=0.006 when comparing KO1/KO2;*mGluR*-GAL4 with UAS-DIAP1/+; KO1/KO2;*mGluR*-GAL4.

4.14 Functional conservation of *VGlut* regulation in mammals

Mammals have three genes encoding vesicular glutamate transporters- *VGlut1, VGlut2, VGlut3*, whereas *Drosophila* has a single *VGlut* gene.

4.14.1 Conservation of seed sequence of *miR-1000*

In light of the importance of *VGlut* regulation, I asked whether the miRNA-mediated regulation of *VGlut* might be conserved across phyla. *miR-1000* is not present in mammals, but I identified a seed-similar miRNA, *miR-137* in human, which is conserved among all species from flies to human (Fig 24a) (Ibanez-Ventoso et al 2008). 5 nucleotide bases (Shown in blue, Fig 24a) among 7-mer seed site matched between *Drosophila miR-1000 (Dme-miR-1000), miR-137 (Dme-miR-137*) and human *miR-137* (*Hsa-miR-137*). *Drosophila miR-137* is shorter by 1 residue at the 5' end, which might affect target site preference in fly and human.

4.14.2 Human *VGlut2* as a direct target of *miR-137*

To determine whether transcripts of any of the human *VGlut* genes are regulated by *miR-137*, I looked for predicted miRNA binding sites in the 3'UTR of human *VGlut1, VGlut2* and *VGlut3*. I found a predicted target site for human *miR-137* in the 3' UTR of the human *VGlut2* transcript (Fig 24b). Next, I performed a luciferase reporter assay using *Hsa-VGlut2* 3'UTR by expressing either *hsa-miR-137* or *dme-miR-1000*. Luciferase reporter assays showed that the human *VGlut2* 3'UTR subjected to direct regulation by human *miR-137* as well as by *Drosophila miR-1000* (Fig 24c). This repression was relieved after mutating the predicted seed match in the human *VGlut2* 3'UTR. Therefore, miRNA-mediated regulation of *VGlut* appears to be conserved in humans.

a)

```
Dme-miR-137      GAUGCACAUAAGAGUUCGUUAU- 5′
Hsa-miR-137      GAUGCGCAUAAGAAUUCGUUAUU 5′
Dme-miR-1000       UGACGACACUGUCCUGUUAUA 5′
```

b)

```
Hsa VGlut2   5'     AACAUUUGUGUACCAAGCAAUAA..
                                  |||||||
Hsa-miR-137  3'     GAUGCGCAUAAGAAUUCGUUAUU
Dme-miR-1000          UGACGACACUGUCCUGUUAUA
```

c)

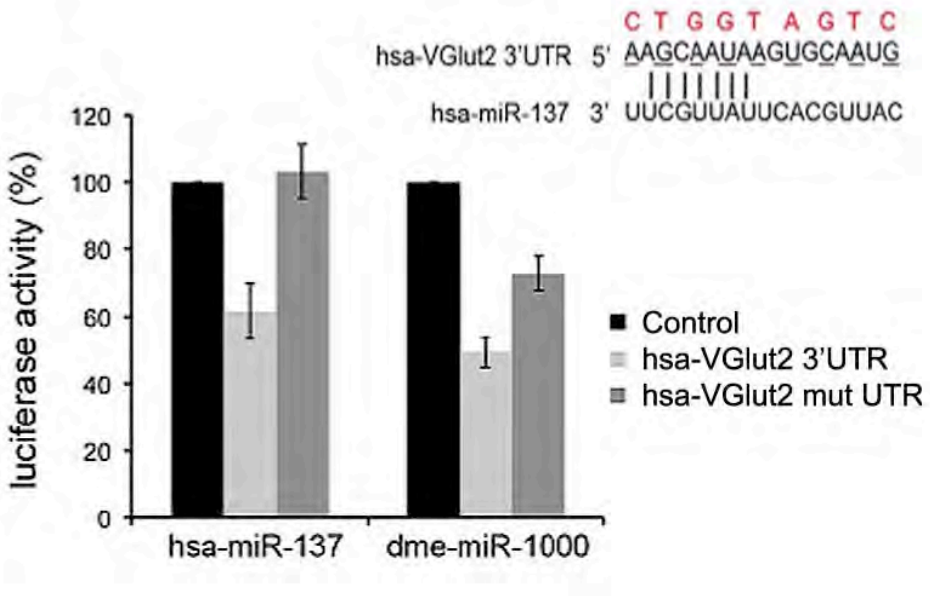

Figure 24: Conservation of *VGlut* regulation by miRNA in mammals

a) Alignment of *miR-1000* with human and *Drosophila miR-137*. miRNA sequences are shown with the 5' end to the right to facilitate alignment with the target sites shown in b. Seed sequences are highlighted in blue. Orange indicates sequence differences between human and *Drosophila miR-137*, which are expected to have limited impact on target selection.

b) Predicted target site of human *miR-137* in the 3'UTR of human *VGlut2* transcript (Slc17a6). Vertical lines show pairing between human *VGlut2* and *miR-137*. *Drosophila miR-1000* is shown below for comparison with seed pairing (in blue).

c) Luciferase activity of a reporter containing the human *VGlut2* 3'UTR. Expression of human *miR-137* or fly *miR-1000* reduced activity of the intact reporter. Regulation was lost when the *miR-137* site was mutated, as shown in red (residues outside seed sequence were mutated to prevent strong binding at the 3' end). Data represent 3 independent experiments. $p<0.001$ comparing the intact *VGlut2* 3'UTR reporter and control following miRNAs expression. $p<0.001$ comparing intact and mutated *VGlut2* 3'UTR reporter with each miRNA.

4.15 *VGlut* Regulation by *miR-137/miR-1000* family in *Drosophila*

After finding functional conservation of *VGlut* regulation by *dme-miR-1000* and seed similar *miR-137*, I wanted to check whether *Drosophila miR-137* might also regulate *VGlut*. I found *VGlut* as one of the predicted targets of *miR-137,* using Targetscan. The *VGlut* 3'UTR had one weak 7-mer site for *miR-137* and two sites for *miR-1000* (Fig 25a). I obtained a *miR-137* mutant from the knockout mutant collection in our lab and checked the level of *VGlut* transcript by qPCR. *VGlut* level was found to be upregulated by 2-fold in the *miR-137* mutant, less than the 3-4 fold upregulation in the *miR-1000* mutant (Fig 25b). Approximately 50% of *miR-137* mutant flies showed climbing defect, when made to climb above 5cm in 1 minute (Fig 25c). This defect was less severe than that of *miR-1000* mutants, where 50% of flies could not climb above 5cm in 5 minutes. I checked levels of *miR-137* and *miR-1000* in both *miR-137* and *miR-1000* mutants. I found that level of *miR-137* remained unaffected in *miR-1000* mutant, whereas *miR-1000* level was upregulated by 2 fold in *miR-137* mutant (Fig 25d). Double mutants lacking *miR-137* and *miR-1000* could not survive, suggesting importance of miRNA-mediated regulation of *VGlut*.

In summary, these results suggest that *miR-137* and *miR-1000* both repress *VGlut* expression in *Drosophila* but with different strength (Fig 25e). In addition, *miR-137* represses *miR-1000* expression to allow optimal level of *VGlut* expression and lack of regulation of *VGlut* in absence of both miRNAs is deleterious for the organism.

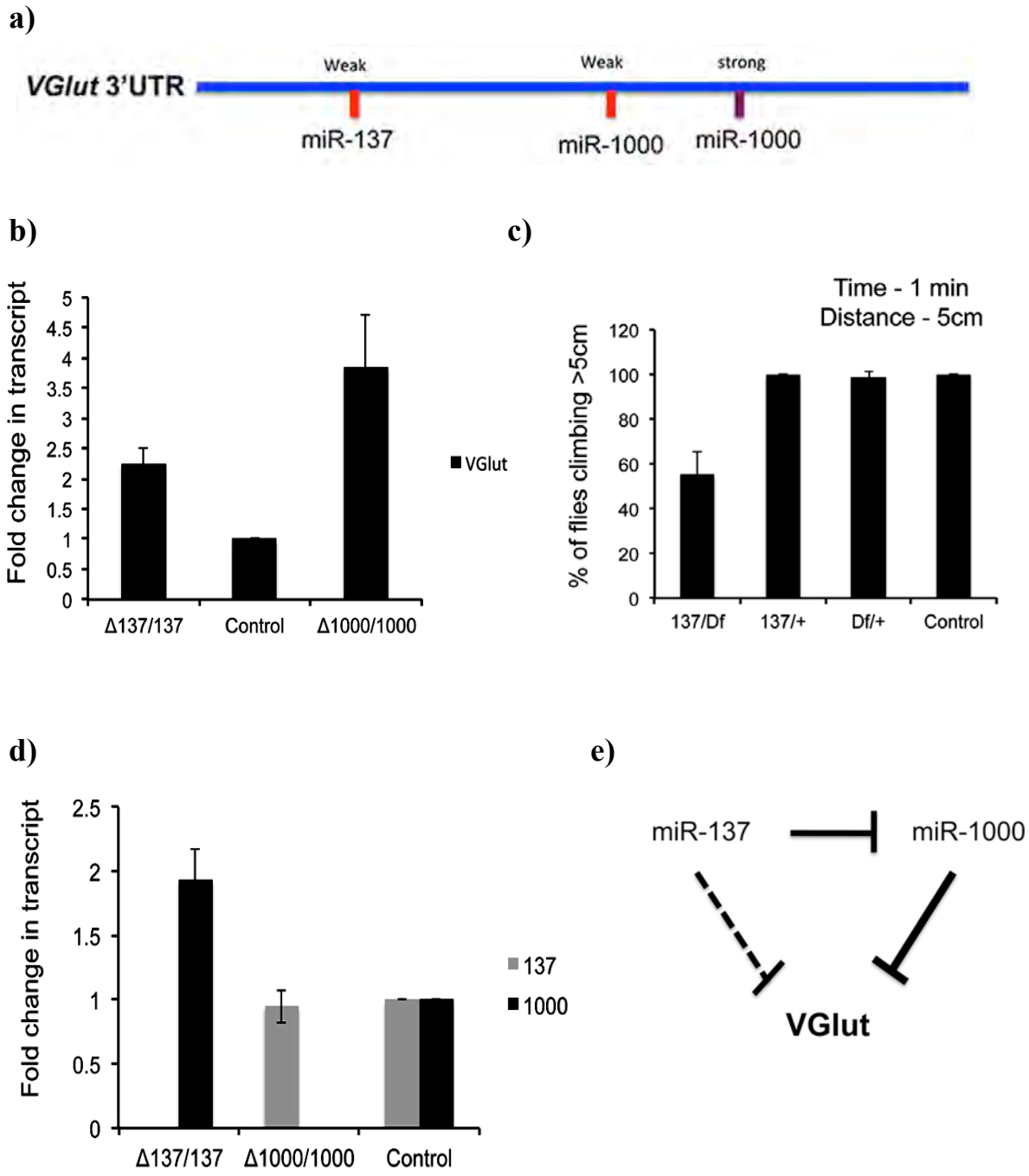

Figure 25: *VGlut* regulation by *miR-137/miR-1000* in *Drosophila*

a) Structure of *VGlut* 3'UTR, showing one weak site for *miR-137* (red) and one weak (red) and one strong (purple) site for *miR-1000*.
b) RT-qPCR showing upregulation of *VGlut* transcript in *miR-137* and *miR-1000* mutants. Data were normalized to wild type head RNA and rp49. Data represent results from three biological samples.

c) Climbing assay showing impaired climbing of trans-allelic (*miR-137*/Df) combination of *miR-137* mutant with a chromosomal deletion, Df(2R)BSC888. Heterozygous mutant and Df/+ were taken as additional controls.
d) miRNA qPCR for *miR-137* and *miR-1000*, showing upregulation of *miR-1000* in *miR-137* mutant. Data were normalized to control brain RNA and endogenous controls, U14 and U27.
e) Hypothesis of *VGlut* regulation in *Drosophila*, where *miR-137* and *miR-1000* display different strength of *VGlut* repression. The *miR-137* represses *miR-1000* to keep strong repression of *VGlut* by *miR-1000* under control.

4.16 DISCUSSION

In this study, I showed that two nervous system specific miRNAs, *miR-1000* and *miR-137* play a neuroprotective role by regulating the expression of the *VGlut*, overexpression of which causes early-onset neurodegeneration in the brain.

miR-1000 is expressed in the nervous system throughout different stages of development and its expression decreases with age. In constrast, no downregulation was observed for *miR-137* with age. In the context of the observed age-related downregulation of *miR-1000*, it is interesting that human *miR-138*, which is predicted to target human *VGlut1*, also shows a 2-fold downregulation with age (Noren Hooten et al 2010). Changes in expression levels of these miRNAs with age might reflect differential requirements of glutamatergic activity in the brain.

Lack of *miR-1000* causes early-onset neurodegeneration and vacuolization in the brain, resulting in movement disabilities and reduced lifespan. Similarly, loss of *miR-137* also caused impaired mobility in flies. Together, *miR-1000/miR-137* regulate *VGlut* (vesicular glutamate transporter), a protein responsible for loading glutamate into synaptic vesicles and thus controlling synaptic glutamate release. Failure in this regulation leads to excess glutamate release and yields excitotoxicity. Excitotoxicity caused by upregulation of *VGlut* has previously been shown by Gal4-directed overexpression of *VGlut* (Daniels et al 2011). The amount of Glutamate is critical for proper neurotransmission in brain and thus, *VGlut* regulation by miRNAs is of paramount importance in synaptic transmission across neurons. Single nucleotide polymorphisms (SNPs) affecting *VGlut* miRNA target sites could lead to low-level constitutive overexpression of the *VGlut*. Similarly, mutations affecting expression of

these miRNAs might lead to elevated *VGlut* expression. Schizophrenia patients have been observed to have SNPs in *miR-137* locus in human (Cummings et al 2012). Therefore, miRNA mediated regulation makes *VGlut* genes possible risk factors in neurodegenerative diseases and a therapeutic target.

I also showed that the *miR-1000* is expressed in NMJs. The *miR-1000* mutants also showed excess glutamatergic transmission in electrophysiology on NMJs indicated by bigger spontaneous peaks of excitatory glutamatergic signal with increased amplitude and frequency. Presence of excess glutamate in NMJs might also be the cause of sterility observed in *miR-1000* mutants. Sterility observed in females was due to their inability to lay eggs. Egg laying is facilitated by NMJs present on ovarian muscle wall and it is possible that *miR-1000* mutant females could not lay eggs because of affected NMJs in the presence of excessive glutamatergic signaling.

I also showed that *VGlut*-mediated excitotoxicity can be prevented by blocking ionotropic receptor *GluR1* and metabotropic receptor *mGluRA,* both using glutamate receptor antagonist drug and by genetic methods *in vivo*. However, rescue of defects in *miR-1000* mutants was greater with reduction in *mGluRA* than *GluR1*. This might be due to the differential activities of these receptors. The AMPA receptor, *GluR1* are known to exhibit a fast but short lasting effect, therefore it managed to rescue the climbing of mutant flies at 2 day of age but could not rescue long term effects on longevity. On the other hand, metabotropic receptor, *mGluRA* is known for long lasting effects on synaptic neurotransmission and its knockdown accordingly resulted in rescue of climbing as well as life span defects. In addition, metabotropic receptors also have modulatory effects on other receptors including NMDA receptors.

It might also be possible that rescue of *miR-1000* mutant defects was combined effects from *mGluR* and its modulatory influence on other receptors.

Glutamate mediated excitotoxicity is also known to cause increase in ROS (Reactive Oxygen Species), which result in oxidative stress mediated damage to the brain (Sagara & Schubert 1998). The *miR-1000* mutant flies might also have increased ROS in their brain. Consistent with this, they showed increased sensitivity to oxidative stress and died faster, when exposed to source of ROS (i.e. H_2O_2).

Some recent reports have shown involvement of glutamate transporters in metabolism (Gammelsaeter et al 2011, Wu et al 2012). The *miR-1000* mutant showed starvation resistance and abnormal feeding behavior, which might also be contributed by excess glutamatergic signaling, however this link needs to be explored in future. There is also a possibility that the starvation resistance phenotype of *miR-1000* resulted from misregulation of some other target gene(s).

I also showed conservation of *VGlut* regulation by miRNAs in vertebrates, by showing *miR-137*- mediated repression of human *VGlut2*. Interestingly, elevated levels of *VGlut* have been associated with excitotoxicity in vertebrate animal models of epilepsy and traumatic brain injury. The GAERS rat epilepsy model shows elevated levels of *VGlut2*, but not of *VGlut1* (Touret et al 2007). Similarly, in the model of stroke, ischemic injury was found to result in elevated expression of *VGlut1*, but not of *VGlut2* (Kim et al 2005). *VGlut1* levels are also regulated by long term methamphetamine treatment (Mark et al 2007), likely contributing to the excitotoxic consequences of methamphetamine abuse. *VGlut1* levels have also been reported to

increase in rat brains following antidepressant treatment (Tordera et al 2005). Knockdown of *VGlut1* in mice is embryonic lethal and had reduced amplitude of spontaneous excitatory responses (Wojcik et al 2004). All these evidences indicate importance of *VGlut* regulation in the brain.

In conclusion, appropriate *VGlut* levels are important for glutamatergic synaptic neurotransmission in the brain and its misregulation leads to neurological diseases. *miR-1000/miR-137* mediated regulation sheds new light on how *VGlut* levels are maintained in organisms under different conditions of neuronal activities to facilitate normal neurotransmission without causing neuronal toxicity.

CHAPTER 5: CHARACTERIZATION OF *miR-965*

5.1 RESULTS: Expression analysis of *miR-965*

No *miR-965* expression was detected in embryos using *in-situ* hybridization. *miR-965*-GFP and *miR-965*-GAL4 could not be used for expression analysis of *miR-965* because insertion of GFP and GAL4 into the *miR-965* locus interfered with its host gene, *kismet* (see 5.4 below). The *miR-965* GFP sensor was used for tissue-specific expression pattern studies.

During larval stage, *miR-965* expression was detected in the brain (Fig 4e) and in mid-pupal to late-pupal stage, *miR-965* showed expression in the histoblast nests.

5.1.1 Histoblast nests and their specification

Histoblast nests (group of histoblast cells) are the precursor cells of adult abdominal segments, which are specified during embryogenesis (Roseland & Schneiderman 1979, Simcox et al 1991). They remain quiescent from embryo till end of the larval stage. During larval stage, they appear as a group of small diploid cells, which are easily distinguishable from surrounding big polyploidy larval epithelial cells (LECs). At the onset of pupal stage during metamorphosis, histoblast nests proliferate under the influence of Ecdysone hormone to replace LECs and eventually differentiate into adult abdominal epithelium (Madhavan & Schneidermann 1977, Ninov et al 2007, Ninov et al 2009).

The adult abdomen in *Drosophila* is made up of ten segments (A1-A10). First seven segments, A1-A7 are formed from histoblast nests and remaining three segments, A8-A10, are derived from genital discs. Each adult abdominal segment is

generated from four pairs of histoblast nests (Madhavan & Schneidermann 1977, Roseland & Schneiderman 1979) (Fig 26a):

1. The anterior and posterior dorsal pairs of histoblast nests give rise to anterior and posterior parts of dorsal surface called as "tergite" of adult abdominal segment. Each anterior dorsal nest consists of approximately 12-17 cells and posterior nest is composed of approximately 5-8 cells.
2. The ventral pair of histoblast nests give rise to the ventral area called sternites and a membranous ventro-lateral part called pleurites. Each ventral histoblast nest is composed of approximately 11-14 cells.
3. The spiracular pair of histoblast nests forms the spiracle and the surrounding pleurite tissues. Each spiracle histoblast nest has approximately three cells.

5.1.2 Histoblast development during morphogenesis

The development of the adult abdominal epidermis is characterized by mainly three kinds of morphogenetic processes occurring in the histoblast nests and LECs (Madhavan & Madhavan 1980).

1. **Division phase**: Histoblast cells remain arrested in G2 phase during larval stage. They then enter a proliferative stage at the onset of pupal stage by ecdysone-dependent *string/Cdc25 phosphatase* transcription, marked by rapid mitotic division (Fig 26b). Histoblast cells increase in number without undergoing any increase in size (Ninov et al 2009). Dorsal and ventral histoblast nests follow the same pattern of mitotic divisions, taking place every 2-3hrs. There are four peaks of synchronous mitotic division at 2-3hrs, 4-6hrs, 7-8.5hrs and 12hrs after pupa formation (APF), during which a doubling in cell number takes place. Cell division continues in dorsal and ventral nests until about 40hrs APF. Late

divisions are slower and are accompanied by a slight increase in cell size. At the end of the division phase, anterior and posterior nests contain ~1100 histoblast cells.

2. **Growth phase:** This phase is marked by slower proliferation with growth and coordinated spreading of the histoblast nests, which depends on *epidermal growth factor receptor (EGFR)* and *insulin receptor/PI3K*-mediated signaling (Fig 26c) (Ninov et al 2009). Spreading of histoblast nests during this phase is accompanied by programmed cell death (apoptosis) due to caspase activation at the LEC/histoblast boundary and subsequent replacement of LECs (Nakajima et al 2011). Histoblast nest spreading and fusion follows a strict temporal and spatial pattern. The pattern of histoblast nest spreading is identical within each segment. In each segment, anterior and posterior dorsal nests remain distinct, separated by 2-3 rows of LECs until 12hrs APF. At 15hrs APF, histoblast nests start to enlarge (Fig 26d, left panel). At 18hrs APF, anterior and posterior histoblast nests start to come closer (Fig 26d, second panel) and by 28hrs APF, all nests of each segment fuse with each other (Fig 26d, third panel). From 28hrs till 36hrs APF, dorsal and ventral nests from both sides of the segment start spreading towards each other. At 47hrs APF, the histoblast nests meet at the dorsal midline and the whole abdomen is covered with adult epithelium cells (Fig 26d, right panel) (Madhavan & Madhavan 1980).

   LECs play a very important role during the development of histoblasts. Programmed cell death and replacement of LECs should be controlled accurately in order to form proper adult epithelium. Controlled cell death of LECs also helps in smooth migration of histoblast nests. Certain LECs behave differently than

others. For example, rows of LECs that degenerate last during fusion of histoblast nests are more resistant to apoptosis during histoblast migration. These rows of LECs play an important role in maintaining boundaries between segments, by keeping histoblast nests at an equal distance from each other (Madhavan & Madhavan 1980).

3. Differentiation phase: Histoblast cells differentiate into adult cuticular structures, immediately after they cover the entire surface of each segment. Each segment from A1-A7 has a dorsal hard cuticular surface, the tergite, which is covered with small bristles, with a posterior row of longer bristles. The inter-segmental membrane, a soft flexible cuticle, derived from the posterior dorsal nest, connects tergites in adjacent segments. The Inter-segmental membrane does not have bristles and is usually beneath the tergites at the junction of two segments. Ventral nests form a small-bristle bearing plate, sternite and a bristle-free region, pleura, which separates ventral sternite from the dorsal tergites. All abdominal segments follow this pattern except first segment, A1, which lacks posterior row of big bristles dorsally and a sternite ventrally and male A7 segment, which lacks both a sternite and a tergite.

a) **Embryonic histoblasts** **adult abdominal segments**

b) **Division phase of histoblast development (divisions without growth)**

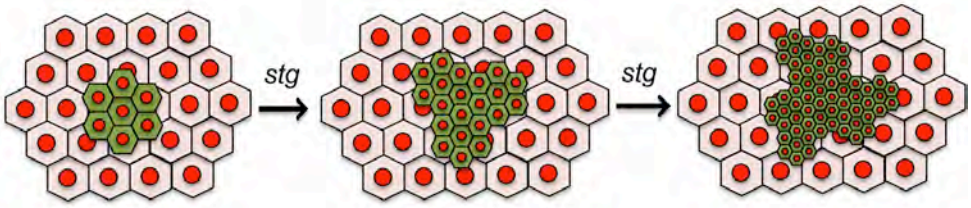

c) **Growth phase of histoblast development (divisions with growth)**

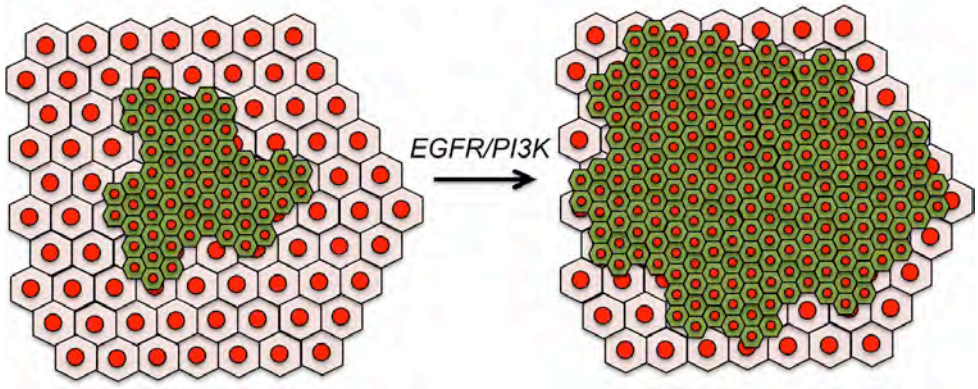

d)

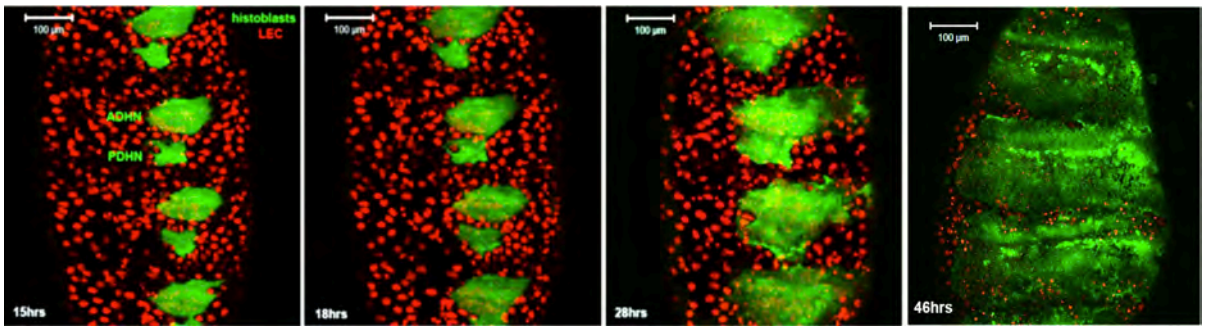

Figure 26: Development of histoblasts in *Drosophila melanogaster*

a) Schematic showing early embryo with anterior-posterior dorsal histoblast nests (red), ventral nest (green) and spiracular nest (blue), specified during embryogenesis and give rise to respective dorsal tergite (red), ventral sternite (green) and spiracles (blue) of adult abdominal segments.
b) Schematic showing early rapid division phase of histoblast development with increased number of cells with no increase in size of cells during early pupariation. This phase is controlled by the *string (stg)* gene. Histoblast cells (small cells) are shown in green and larval epidermal cells (LECs, big cells) are shown in pink.
c) Schematic showing growth phase of histoblast development from 15hrs APF, marked by cell divisions with growth in size of the cells. This phase is controlled by *EGFR* and *PI3K*.
d) Images showing different stages of spreading of histoblast nests from 15hrs, 18hrs, 28hrs and 46hrs APF (from left to right). LECs can be seen as big red nuclei marked by histone RFP and histoblast nests are marked by GFP. ADHN in left panel represents anterior dorsal histoblast nest and PDHN represents posterior dorsal histoblast nest. Scale bars - 100μM.

5.1.3 *miR-965* expression in histoblast nests and LECs

Using *miR-965*-GFP sensor, no expression of *miR-965* could be detected during division phase of histoblasts from 0hrs to 8hrs APF. During growth phase, the sensor showed expression of *miR-965* in the histoblast nests and in only one row of LECs (Fig 27b), which was not observed with the control sensor (Fig 27a).

Sensor GFP was strongly repressed at the periphery of the dorsal nests, which are in direct contact of surrounding LECs, indicating strong expression of *miR-965* at the periphery and moderate expression inside the nest (Fig 27b,c).

The *miR-965* also expressed strongly in one row of LECs, present between two adjacent histoblast nests (Fig 27b,c). The *miR-965* expressing row of LECs was observed to be the most anterior row of cells in each segment, when co-expressed with *hh*-DsRed (*hedgehog*-DsRed). *hh* is expressed in the posterior dorsal nest, which eventually give rise to the dorsal part of each abdominal segment (Fig 27d) (Struhl et al 1997). Time-lapse images of the *miR-965* GFP sensor showed that the *miR-965* expressing row of LECs is the last row of cells to undergo programmed cell death (Fig 27e). Thus, these LECs help in maintaining the boundary between adjacent histoblast nests during spreading.

a)

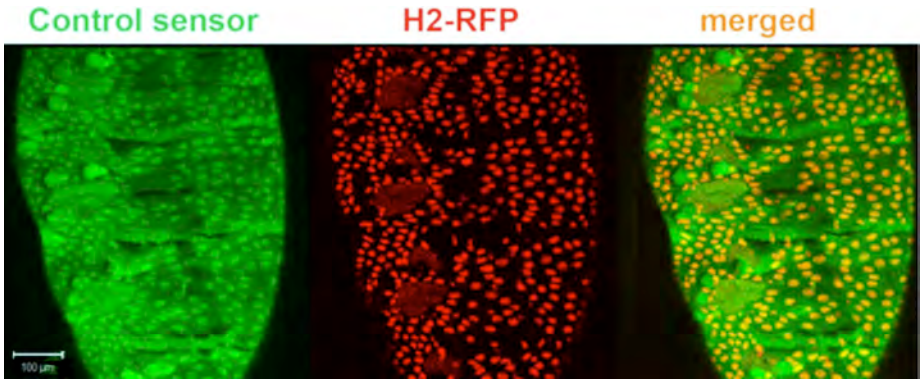
Control sensor
H2-RFP
merged

b)

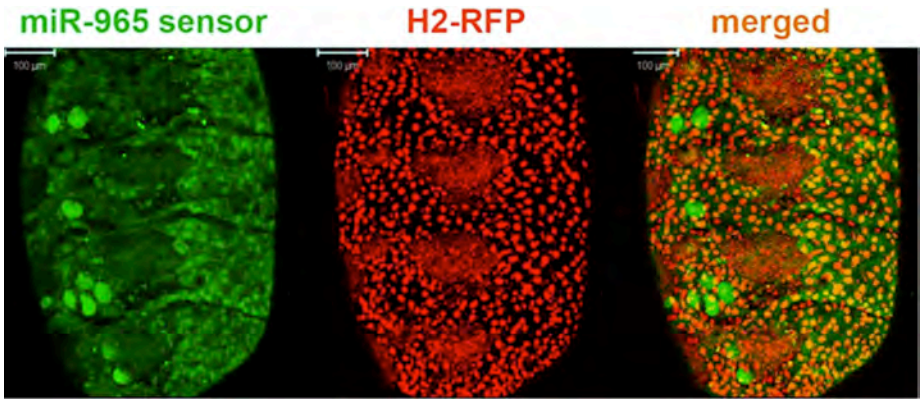
miR-965 sensor
H2-RFP
merged

c)

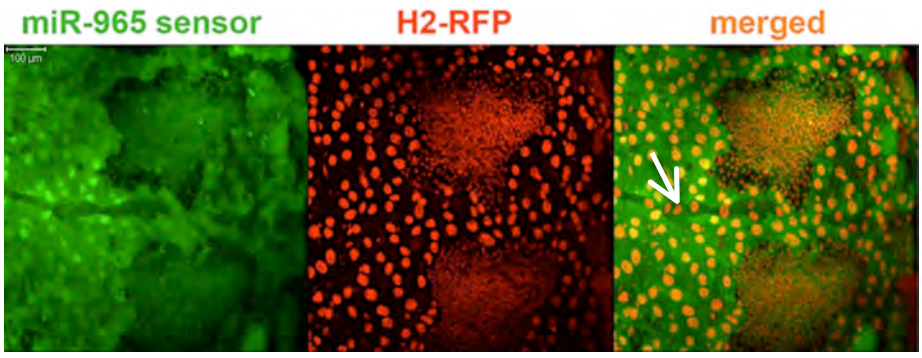
miR-965 sensor
H2-RFP
merged

d)

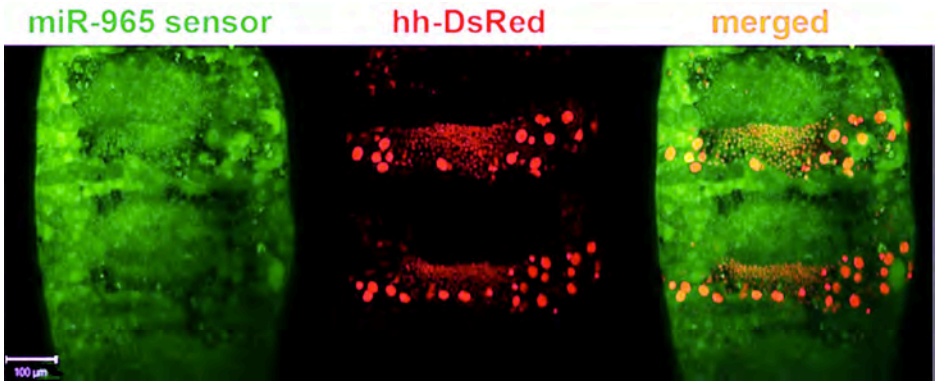
miR-965 sensor
hh-DsRed
merged

e)

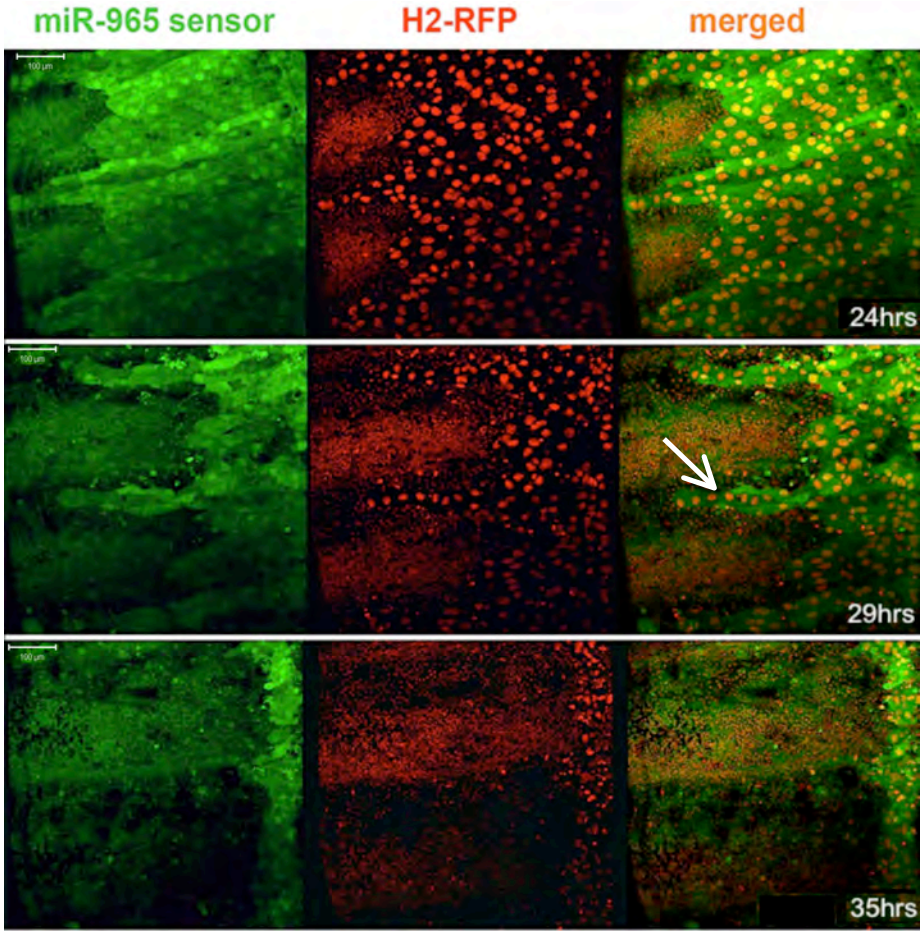

Figure 27: Expression of *miR-965* in Histoblast nest and LECs.

a) Control GFP sensor showing ubiquitous expression of GFP in the dorsal histoblast nests (small nuclei) and surrounding LECs (big nuclei) in pupa at 18hrs APF. H2-RFP (red, 27a-c,e) marks histoblasts and LECs nuclei. Scale bars -100µM.

b) *miR-965* GFP sensor showing *miR-965* expression (lack of GFP) in the dorsal histoblast nests and one row of LECs between adjacent nests in pupa at 24hrs APF. Scale bars - 100µM.

c) Magnified view of fused dorsal histoblast nest at 21hrs APF, showing *miR-965* GFP sensor expression at the periphery of fused anterior-posterior dorsal histoblast nests and row of LECs between two histoblast nests (shown by arrow). Scale bars - 100µM.

d) *miR-965* GFP sensor showing expression in the most anterior row of LECs, immediately below posterior *hh (hedgehog)* expression domain (red) in each abdominal segment. Scale bars - 100µM.

e) Time-lapse images of *miR-965* GFP sensor at 24hrs, 29hrs and 35hrs APF, showing expression of *miR-965* in histoblasts and a row of LECs. Note that *miR-965* expressing row of LECs is the last row (shown by arrow) to degenerate during growth and migration phase of histoblast development. Scale bars-100µM.

5.2 Generation and validation of *miR-965* mutants and Rescue flies

A *miR-965* deletion mutant (KO1) and a *miR-965* RMCE (KO2) mutant were generated as described in Chapter 3. *miR-965* is located in the first intron of the *kismet* gene, with the same direction of transcription (Fig 28a). 4055bp left homology and 4438bp right homology arms were used to generate deletion of 153bp region, containing *miRNA-965* hairpin (Chapter 2). Deletion of the miRNA in both mutants was confirmed using miRNA qPCR (Fig 28b). The *mini-white* marker flanked by loxP sites in the *miR-965* allele was excised by CRE mediated recombination, leaving a single LoxP site in the *kismet* intron. Genetic complementation tests were done to confirm that *kismet* function was not compromised in the *mini-white*–excised *miR-965* mutants. Production of intact *kismet* transcript was confirmed by RT-qPCR (Fig 28c).

For *miR-965* rescue, two different kinds of transgenic flies were made. First, a genomic rescue was generated by cloning 336bp of *kismet* upstream regulatory genomic DNA with 7754bp of the *miR-965* containing *kismet* intronic fragment. For the control rescue, the same genomic fragments were introduced into flies, lacking *miRNA-965* hairpin. Another *miR-965* rescue was made by replacing mini-white marker with 158bp *miR-965* hairpin in the *miR-965* RMCE mutant. Both rescue transgenes restored almost normal levels of *miR-965* (Fig 28b).

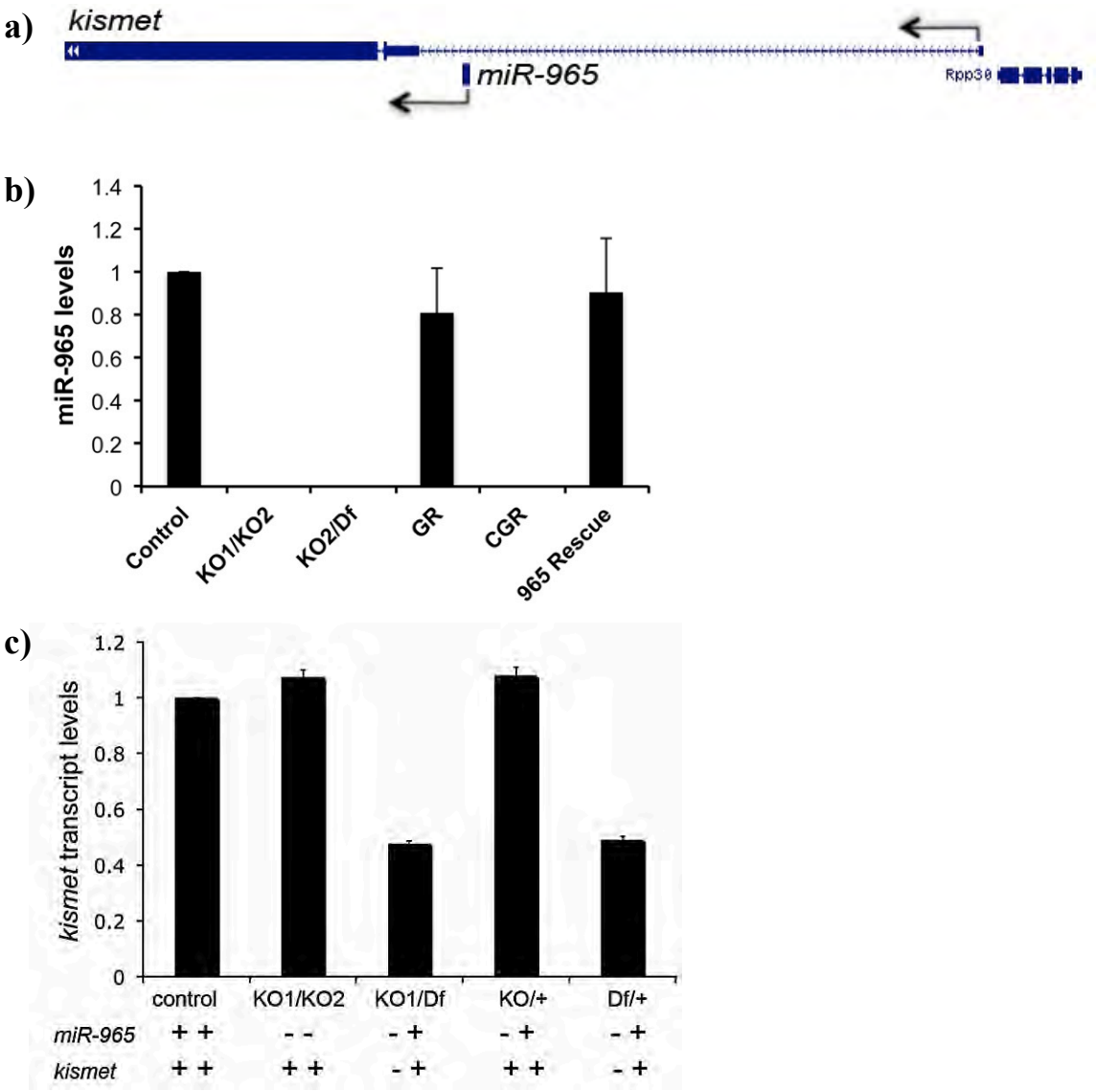

Figure 28: Generation and confirmation of *miR-965* mutants and rescue

a) Genomic locus of *miR-965* showing location of *miR-965* in the first intron of *kismet* gene, with same direction of transcription (shown by arrow). Thick lines represent *kismet* exons and thin line indicates first intron.
b) Confirmation of *miR-965* level by miRNA qPCR in *miR-965* mutant trans-allelic combination (KO1/KO2, KO2/Df), genomic rescue (GR), control genomic rescue (CGR) lacking *miR-965* hairpin and RMCE *miR-965* rescue. Data were normalized to U14 and U27 and three biological samples were used.
c) Confirmation of *kismet* transcript level by RT-qPCR in *miR-965* mutants (KO1/KO2, KO2/Df) and heterozygous controls. No disruption in the *kismet* transcript was observed. Copy number of *miR-965* and *kismet* is mentioned for indicated genotypes. Data were normalized to rp49 and three biological samples were used.

5.3 Phenotypic analysis of *miR-965* mutants

Phenotypic analyses were done, using *miR-965* mutant flies carrying two independently generated alleles (KO1 or KO2) or an allele in trans to a chromosomal deletion, Df(2L)Exel7002 (refer as Df), removing *miR-965* locus (KO1/Df or KO2/Df). Initial viability screening was done with the deletion mutant allele (KO1) and its trans-heterozygous combination with Df(2L)Exel7002 (KO1/Df). Phenotypes observed in both homozygous and trans-heterozygous mutants were later validated using rescued mutant flies to confirm lack of *miR-965* as the cause of the mutant defects.

5.3.1 Viability/ survival of *miR-965* mutants

Viability from embryo to larva (embryo hatching), from larva to pupa (pupariation) and from pupa to adult (adult eclosion) was analyzed, using *miR-965* deletion mutant allele in homozygous condition (KO1/KO1) and trans-allelic combination with Df (KO1/Df). KO1/Df was used for confirmation of mutant phenotypes and for excluding any background effect originated from homologous recombination during *miR-965* mutant generation. No defect was observed during embryo hatching of *miR-965* mutants in either homozygous or trans-allelic combination with Df (Fig 29a). Low pupariation and low adult eclosion was observed in animals homozygous for mutant allele, however these defects were not reproducible in trans-allelic combination (Fig 29a), thus, considered as background effects of *miR-965* homozygous mutant.

5.3.2 Lifespan of *miR-965* mutants

Lifespan of *miR-965* adult mutant flies was scored for both male and females separately by rearing 20 flies in each vial and putting on new food every 2nd or 3rd day. The homozygous mutant (KO1/KO1) showed reduced survival in both sexes, however, this effect was again not reproducible by trans-allelic combination with Df (KO1/Df) (Fig 29b,c), thus reduced survival of *miR-965* mutants could not be attributed to lack of *miR-965* in flies.

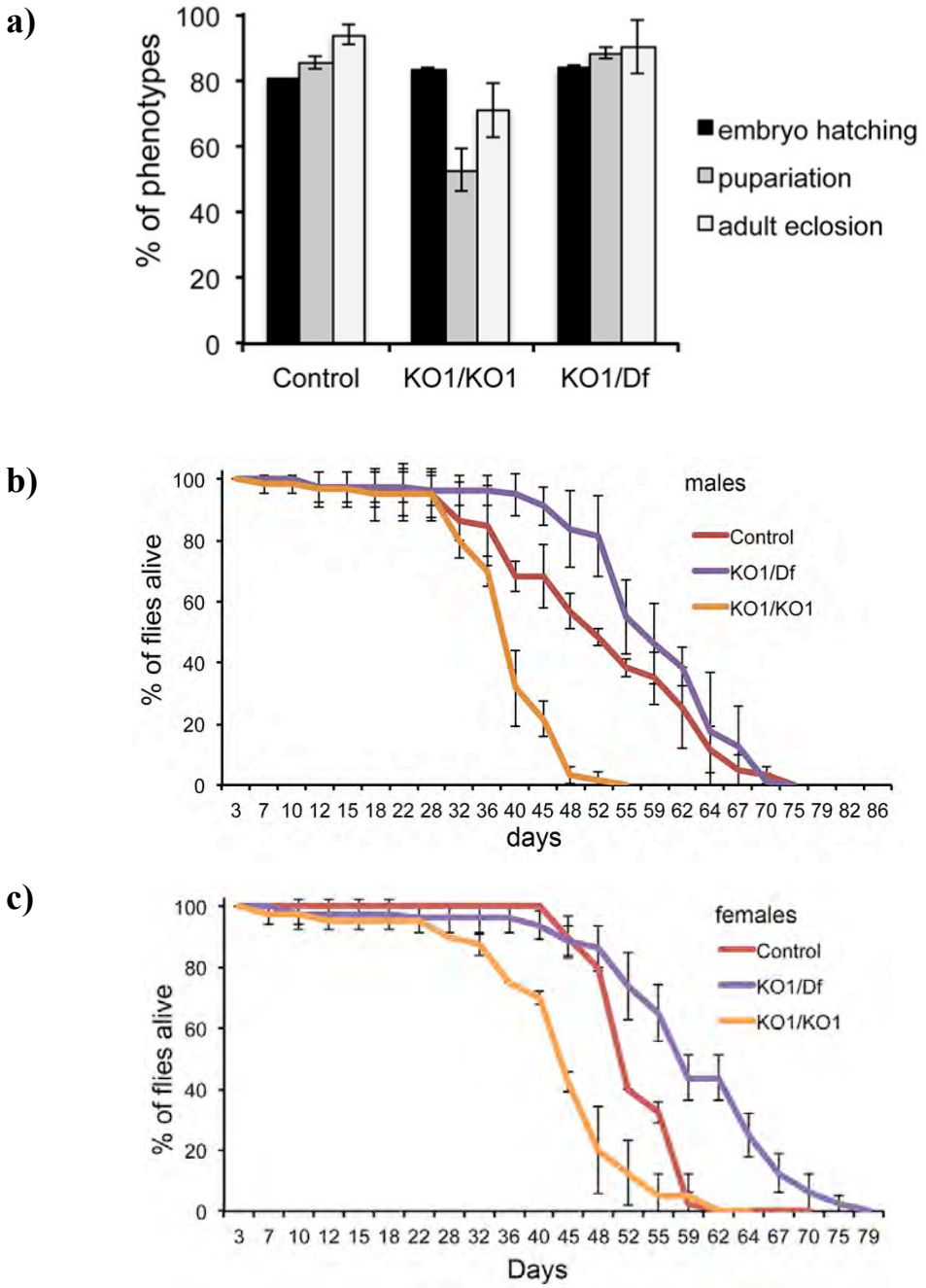

Figure 29: Viability of *miR-965* mutants

a) Embryo hatching (black bars), pupariation (grey bars) and adult eclosion (white bars) of *miR-965* homozygous mutant (KO1/KO1) and trans-allelic mutant (KO1/Df) . Data represent average of three biological replicates.
b) Graph showing longivity for male and c) female *miR-965* mutants (KO1/KO1 and KO1/Df). Data represent average of three biological replicates.

5.3.3 Adult abdominal segmentation defect in *miR-965* mutants

miR-965 mutants in all trans-allelic combination (KO1/KO2, KO1/Df or KO2/Df) showed abnormal adult segmentation in approximately 30-50% of adult flies (Fig 30a,b). Generally, adult segments are arranged in a highly organized pattern with defined compartments and inter-segmental boundaries, but in *miR-965* mutant, their organization was disrupted. Deformed segmentation was observed both in males and females with similar penetrance. Heterozygous flies (KO1/+, KO2/+ and Df/+) flies also showed deformed adult segments, however this penetrance was much lower (2-4%) than *miR-965* mutant flies (Fig 30b). This defect was rescued by expressing *miR-965*, thus confirming lack of *miR-965* as the cause of adult segmentation defects.

Three different approaches were taken for rescue of the segmentation defect in *miR-965* mutants. First, The RMCE *miR-965* rescue flies were used. These flies rescued segmentation defects of *miR-965* mutant almost completely. Second, the genomic rescue of *miR-965* (GR), containing *miR-965* hairpin with its endogenous regulatory portion was used to significantly reduce the penetrance of flies with abnormal segmentation. In contrast, control genomic rescue (CGR) containing only regulatory portion, without the *miR-965* hairpin could not rescue the *miR-965* mutant defects (Fig 30b), thus indicating that *miR-965* is crucial for proper segment formation in adult flies. Third, a leaky *miR-965-UAS* was used for the rescue of segmentation defect in mutant flies (Fig 30b), but lethality at pupal stage was observed in this genetic combination. This lethality might be due to leaky ectopic expression of *miR-965* in other tissues.

5.3.3.1 Characterization of abnormal segmentation in *miR-965* mutants

I characterized the types of segmentation defects observed in *miR-965* mutant and grouped them into three categories:

a) Lack of tissue: This defect is characterized by loss of cuticular tissue within or between segments (Fig 30d). This defect was the most commonly observed defect in *miR-965* mutants. Approximately 80% of flies showed this defect (Fig 30e). This defect was sometimes present along with the other defects, mentioned below.
b) Fusion of segments: This defect is marked by ambiguous inter-segmental boundaries, where one segment fused with adjacent segment without any defined demarcation between them (Fig 30d). This defect was observed in approximately 10-12% of *miR-965* mutant flies (Fig 30e).
c) Polarity defect: Abdominal segments have a well-defined anterior – posterior polarity, with the anterior part of the tergite having a light colour and the presence of few small bristles. The posterior part of the tergite has dark pigmentation and big bristles pointing into the posterior direction. The *miR-965* mutant showed polarity defects, marked by the presence of pigment and direction of bristles in reverse position (Fig 30c,d). Approximately 20-25% of *miR-965* mutant flies showed this kind of defect (Fig 30e), but this defect was always observed with lack of tissue defect or fusion of segments.

I also quantified the presence of segmentation defects for each abdominal segment from first to last segment. The 3rd abdominal segment was the most affected segment with 60-70% occurrence of deformed segmentation, followed by 4th, 5th and 6th

segment. Sometimes defects occurred in more than one segment simultaneously (Fig 30f). Segmentation defects were never observed in the first and last segments.

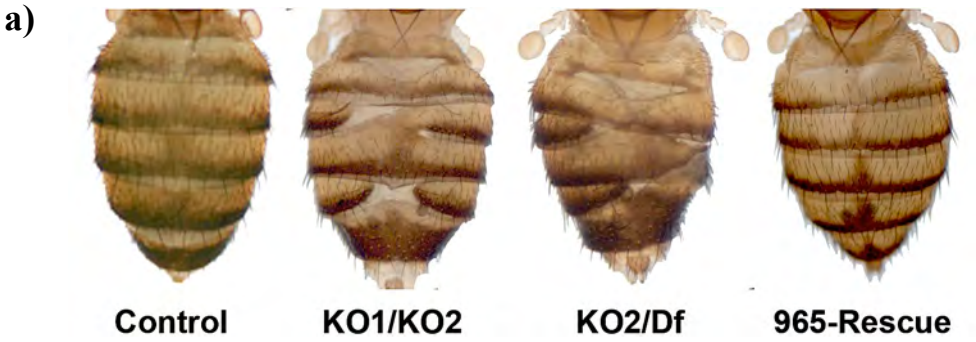
a)
Control
KO1/KO2
KO2/Df
965-Rescue

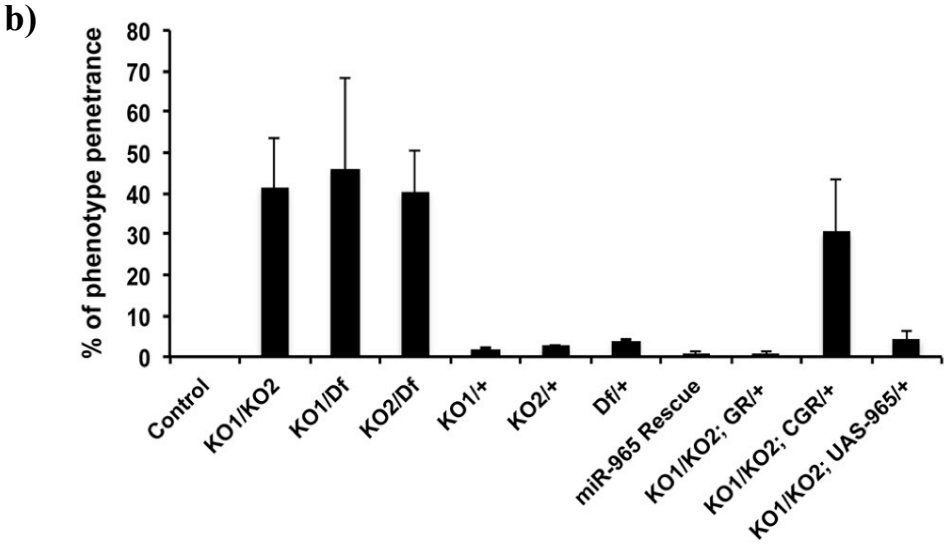
b)
% of phenotype penetrance
0
10
20
30
40
50
60
70
80
Control
KO1/KO2
KO1/Df
KO2/Df
KO1/+
KO2/+
Df/+
miR-965 Rescue
KO1/KO2; GR/+
KO1/KO2; CGR/+
KO1/KO2; UAS-965/+

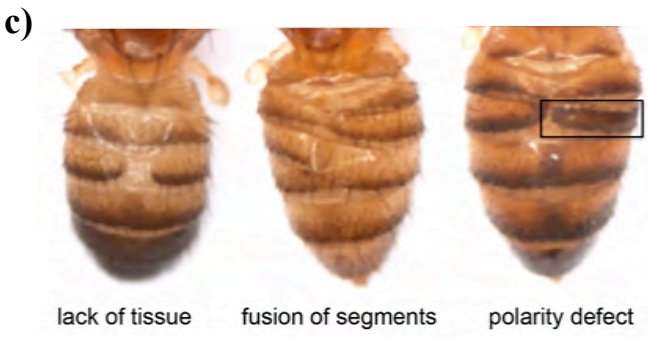
c)
lack of tissue
fusion of segments
polarity defect


d)
KO1/KO2
Wild Type

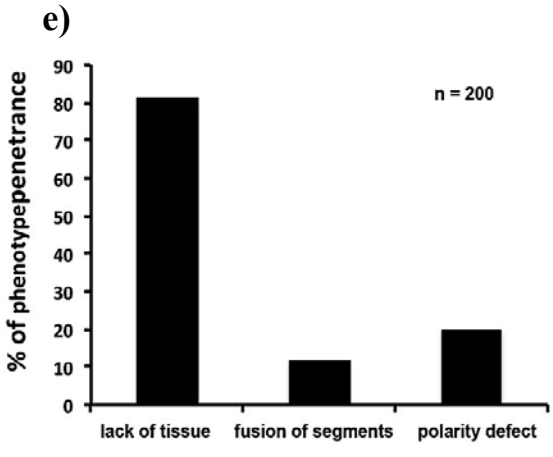
e)
% of phenotypepenetrance
0
10
20
30
40
50
60
70
80
90
n = 200
lack of tissue
fusion of segments
polarity defect

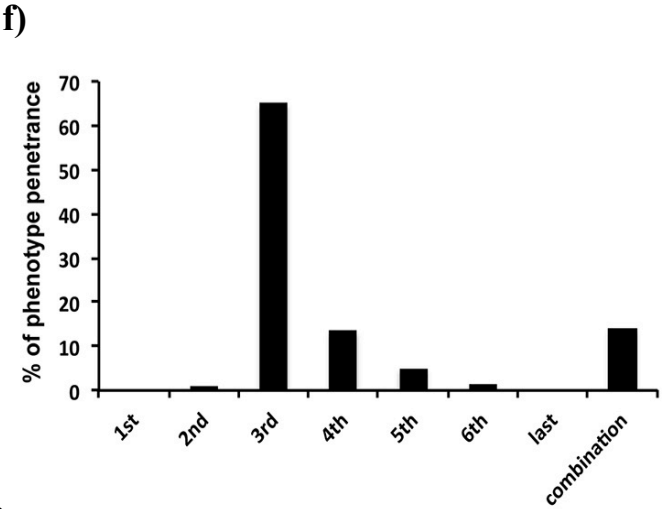
f)
% of phenotype penetrance
0
10
20
30
40
50
60
70
1st
2nd
3rd
4th
5th
6th
last
combination

Figure 30: Abdominal segmentation defect of *miR-965* mutants

a) Images of abdomens of adult flies, showing abdominal segmentation defects in *miR-965* mutants (KO1/KO2, KO2/Df) and normal segmentation in *miR-965* rescue and control flies. *miR-965* rescue represents *miR-965* RMCE rescue.
b) Graph showing penetrance of abnormal segmentation defects in the flies of indicated genotypes. *miR-965* mutants (KO1/KO2, KO1/Df, KO2/Df) showed 30-50% penetrance compared to 2-4% penetrance in all heterozygous (KO1/+, KO2/+, Df/+), *miR-965* Rescue (RMCE rescue), GR (genomic rescue) and leaky *miR-965*-UAS flies. CGR represents control for genomic rescue with 30-40% penetrance of segmentation defects in adult flies.
c) Images of *miR-965* mutant flies showing three kinds of defects, lack of tissue (left panel), fusion of segments (middle panel) and polarity defect (right panel).
d) Magnified view of polarity defect of Fig C (right panel). *miR-965* mutant (left panel) showing big bristles oriented in both directions as compared to wild type (right panel), having bristles pointing in one direction.
e) Graph showing penetrance for three kinds of segmentation defects observed in *miR-965* mutant flies, shown in Fig C. n=200.
f) Graph showing penetrance of segmentation defects in different abdominal segments of *miR-965* mutant. n=200

5.4 Characterization of *miR-965* mutant segmentation at the histoblast level

To explore the origin of the defects, I decided to look for morphological and physiological changes in the histoblast cells, which could possibly be responsible for deformed adult segmentations of *miR-965* mutants. I characterized defects during early division phase and late growth/migration phase of histoblast development. I made use of *escargot (esg)*-GAL4 driving UAS-GFP to visualize changes during histoblast development in mutants. The *esg* gene is expressed from embryonic till late pupal stage in the histoblast cells (Hayashi et al 1993). The *miR-965* mutant showed segmentation defects on the dorsal side (tergite) of segments. Therefore, I studied anterior and posterior dorsal histoblast nests (precursor of tergite) to discern the cause of defects in *miR-965* mutant.

5.4.1 Defects during division phase of histoblast development in *miR-965* mutants

I used *esg*-GAL4 driving nuclear UAS-GFP in mutant, control and rescue background to score morphology of cells and their number during the first three synchronous divisions, from 0hrs to 8hrs APF. The *miR-965* mutants showed the following defects during early histoblast division phase:

a) Abnormal morphology of histoblast cells at 0hrs APF: Histoblast cells in the *miR-965* mutants lost their normal round shaped morphology and appeared more elongated in shape, when observed at 0hrs to 1hrs APF (Fig 31a,b). Histoblast cells acquired normal round shape in *miR-965* rescue (Fig 31c).
b) Asynchronous division of histoblast cells: The *miR-965* mutants showed asymmetrical and asynchronous cell division of histoblast cells during first three divisions of early mitotic phase. Unlike synchronous divisions of all

histoblast cells in each dorsal nest in control, the *miR-965* mutants seemed to have continuous and asymmetrical divisions of histoblast cells (Fig 31b), which resulted in increased number of cells as well as occurrence of different size of cells in the histoblast nests. The *miR-965* Rescue restored normal synchronous pattern of cell divisions in the histoblast nests (Fig 31c).

c) Apoptosis of histoblast cells: The *miR-965* mutants often showed apoptosis in the histoblast nests during early division phase, which was generally not observed in control and *miR-965* rescue (Fig 31d).

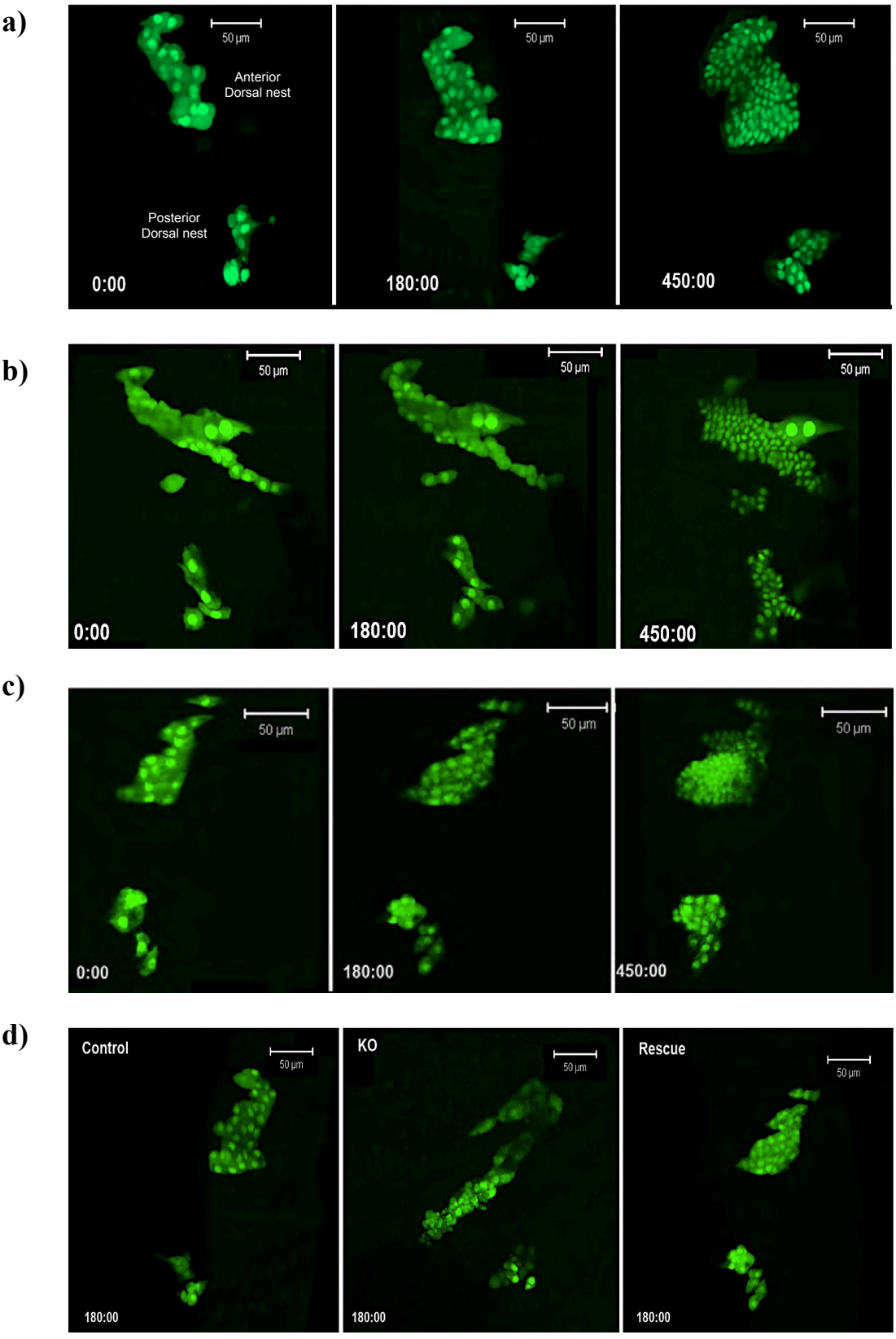
a)
50 µm
Anterior
Dorsal nest
Posterior
Dorsal nest
0:00
180:00
450:00
b)
0:00
180:00
450:00
c)
0:00
180:00
450:00
d)
Control
KO
Rescue
180:00

Figure 31: Defects of histoblast cells in *miR-965* mutant during early division phase

a) Time-lapse images of control pupa at 0hrs, 3hrs, 7.5hrs APF, showing three synchronous cell divisions and almost equal size of histoblast cells in the anterior and posterior dorsal nests. Histoblast cells are visualized by *esg*-GAL4 driving nuclear UAS-GFP. Scale bar- 50μM
b) Time-lapse images of *miR-965* mutant pupa at 0hrs, 3hrs, 7.5hrs APF, showing asynchronous cell divisions and asymmetric shape of the histoblast cells. Histoblast are visualized by *esg*-GAL4 driving nuclear UAS-GFP, recombined on the same chromosome with *miR-965* mutant. Scale bar- 50μM.
c) Time-lapse images of *miR-965* RMCE rescue pupa at 0hrs, 3hrs, 7.5hrs APF, showing synchronous cell divisions of histoblast cells. Histoblast cells are visualized by esg-GAL4 driving nuclear UAS-GFP, recombined on the same chromosome with *miR-965* RMCE rescue. Scale bar- 50μM.
d) Images showing histoblast cells in the *miR-965* mutant (KO, middle panel) undergoing apoptosis in the dorsal nest, marked by bright green and very small fragmented nuclei of histoblast cells. No apoptosis observed in control (left panel) and *miR-965* Rescue (right panel) at 3hrs APF. Scale bar- 50μM.

5.4.2 Defects during growth and migration phase of histoblast development in *miR-965* mutants

To detect defects during the growth and migration phases of histoblast development, I analyzed *miR-965* mutant pupae from 15hrs APF onwards, using *esg*-GAL4 driving cytoplasmic UAS-GFP in the mutant background. There were two obvious defects, observed in *miR-965* mutants:

a) Presence of LECs in the histoblast nests: LECs at the periphery of histoblast nest undergo apoptosis following growth and spreading of the histoblast cells. In *miR-965* mutant, some LECs were resistant to apoptosis and hence maintained their original position between growing histoblast cells. LECs were easily spotted inside the histoblast nest because of their big nuclei and strong expression of *esg*, when they persist in the nest for too long (Fig 32a).

b) Slow and aberrant migration of histoblast nest: In the *miR-965* mutant, dorsal histoblast nests moved very slowly and aberrantly during migration phase of histoblast development. Presence of LECs within the nests also seemed to resist the normal movement of histoblast nests. Certain segments in *miR-965* mutants had delayed spreading relative to the adjacent normally moving histoblast nests, hence, resulted in a histoblast cells free gap within the segment at the end of pupariation This might contribute towards the lack of tissue (most common defect observed) defect in the *miR-965* mutants (Fig 32b,c).

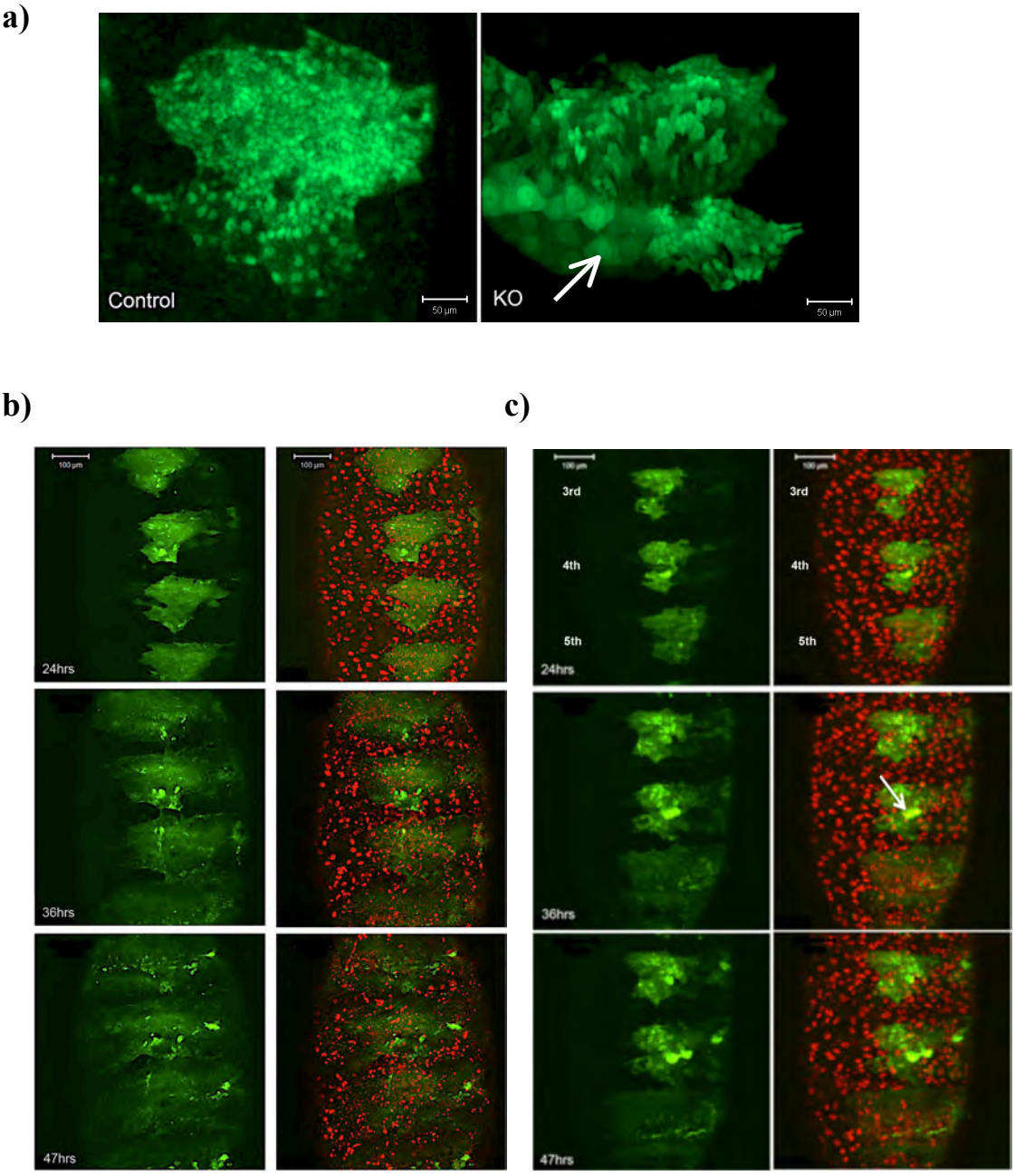

Figure 32: Defects during growth and migration phase of histoblast development in *miR-965* mutant

a) Images showing fused anterior and posterior dorsal histoblast nests in control (left panel) and *miR-965* mutant (KO, right panel) at 21hrs APF. Presence of big LECs (shown with arrow) within histoblast nest is conspicuous in the *miR-965* mutant, compared to equal size histoblast cells without any LECs, in the control. Scale bar- 50µM.

b) Time-lapse images from control showing growth and migration at 24hrs, 36hrs and 47hrs APF, using *esg*-GAL4 driving cytoplasmic UAS-GFP. Note that segments are fully covered with histoblast cells by 47hrs APF. Scale bar- 100μM.

c) Time-lapse images from the *miR-965* mutant, showing presence of LECs (bright green with big nucleus shown by arrow) within migrating histoblast nests and slow migration of 3rd and 4th histoblast nests, compared to normal migration of 5th histoblast nests at 24hrs, 36hrs and 47hrs APF, using *esg*-GAL4 driving cytoplasmic UAS-GFP. Scale bar- 100μM.

5.4.3 Overexpression of *miR-965* in histoblast cells

I overexpressed *miR-965* in the histoblast cells using *esg*-GAL driving UAS-*miR-965*. *UAS-miR-965* transgene was generated by introducing 158bp *miR-965* hairpin into the flies. Events during early stage of histoblast development were visualized using *esg*-GAL4 driving nuclear UAS-GFP simultaneously with *UAS-miR-965*.

Histoblast cells overexpressing *miR-965* showed arrested or delayed cell divisions, with few histoblast cells undergoing one or two rounds of division from 0hrs to 8hrs APF. This resulted in a very small number of histoblast cells in the nest at the end of division phase (Fig 33a). Pupae overexpressing *miR-965* in histoblast cells could not survive beyond 15hrs APF (Fig 33b).

a)

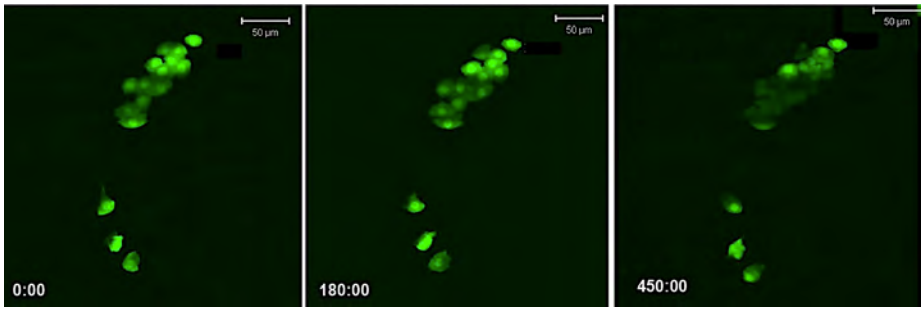

b)

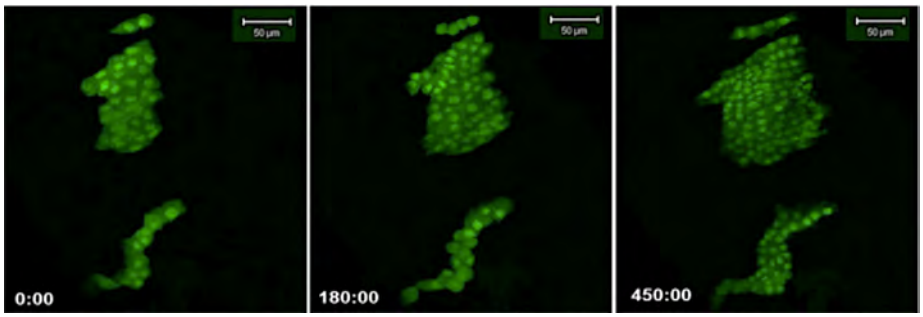

c)

Figure 33: Overexpression of *miR-965* in the histoblast cells

a) Time-lapse images at 0hrs, 3hrs and 7.5hrs APF, showing arrested/delayed cell division of histoblast cells by overexpressing *miR-965* (UAS-*miR-965*) using *esg*-GAL4 driving nuclear GFP. Scale bar- 50µM
b) Time-lapse images of control pupa at 0hrs, 3hrs and 7.5hrs APF, showing synchronous cell division of histoblast cells using *esg*-GAL4 driving nuclear GFP. Scale bar- 50µM
c) Image showing dead pupa at ~15hrs APF, due to lack of increase in cell numbers in the pupa overexpressing *miR-965*.

5.5 Target search for *miR-965*

Computational predictions of *miR-965* targets, RT-qPCR and luciferase reporter assays were used for finding candidate target(s).

5.5.1 Computational prediction of possible targets of *miR-965*

Targetscan predicted 69 genes as targets of *miR-965*. To narrow down the number of target genes, I looked for strong seed matches among all the candidates using RNA hybrid. An 8-mer site, followed by 7-mer sites, is considered as the strongest site for mRNA targeting. I first considered genes having 8-mer sites and then with 7-mer sites for *miR-965* targeting.

Beside, computational prediction, expression pattern of target genes was also considered. The *miR-965* showed histoblast-specific expression pattern, so I selected the few target genes from computationally prediction target list, which had some known function in histoblast development or abdominal segmentation formation and shared temporal expression with *miR-965*.

Based on these criteria, only 7 genes (*polycomb, string, wingless, homeothorax, Tor, Hsp83, jumu*), plus the host gene *kismet,* were selected for initial target search.

5.5.2 Target search by RT-qPCR

As mentioned previously, upregulation of target genes occur in miRNA mutants. I looked for up-regulation of target transcript levels by qPCR of the 8 selected genes. RNA extracted from 21hrs pupae of mutant, rescue and control was used for qPCR. I looked for genes that showed upregulation in mutant and returned to normal level in rescue pupae. Out of the 8 genes analyzed, I found two genes, *string (stg)* and *wingless (wg)*, which followed the expected trend in the qPCR (Fig 34a).

5.6 *stg* and *wg* as direct targets of *miR-965*

5.6.1 *stg* and *wg* as direct targets in luciferase reporter assays

The 3' UTRs of both *stg* and *wg,* each contain one strong 8-mer predicted *miR-965* sites (refer as seed 1 for *stg* 3'UTR) (Fig 34b,d). To test whether *stg* and *wg* are direct targets of *miR-965*, luciferase reporters carrying endogenous 3'UTRs of *stg* and *wg* were used. In S2 cells, co-expression of *stg* 3'UTR luciferase reporter with *miR-965* expressing vector, caused ~70% reduction in luciferase activity (Fig 34c), compared to luciferase control vector (vector without *stg* 3'UTR). Approximately 50% reduction in luciferase activity was observed with *wg* 3'UTR, upon co-expression with *miR-965* (Fig 34e).

To show that *stg* and *wg* 3'UTR repression by *miR-965* was mediated by seed sites in respective 3'UTRs, I mutated 8-mer seed sites in both *stg* and *wg* 3'UTRs. Repression of *wg* 3'UTR by *miR-965* was completely relieved by introducing mutations in seed sequence (Fig 34e), however, only ~20% repression by *miR-965* was relieved in the case of mutated *stg* 3'UTR compared to wild type *stg* 3'UTR (Fig 34c). I searched for another putative *miR-965* target seed site in the 3'UTR of *stg,* using RNA hybrid and found a site (refer as seed 2) with significant complementarity between *stg* 3'UTR and *miR-965*, however this complementarity does not follow the rules of the typical miRNA target sites with 5'seed match (Fig 34b). Nevertheless, I mutated this seed site to see if it could influence luciferase reporter activity. No significant increase in luciferase repression was observed with both 8-mer seed 1 and putative seed 2 site mutations, but significant relief of ~40% in luciferase reporter activity of *stg* 3'UTR was observed, when the sequence between the two sites were also mutated (Fig 34b), however, I could not achieve complete relief from repression of mutated *stg* 3'UTR by *miR-965*. This might possibly be due to changes in the

secondary structure of *stg* 3'UTR, caused by introduction of mutations in the wild type genomic sequence. In conclusion, luciferase reporter results indicated that both *stg* and *wg* are direct targets of *miR-965.*

5.6.2 *miR-965* regulate *stg* expression in histoblast nests

I introduced *stg* wild type 3'UTR and *stg* 3'UTR with multiple mutations (same as used for luciferase reporter assay above) into GFP expression constructs. GFP was ubiquitously expressed from the tubulin promoter. Expression of GFP should be down regulated in *miR-965* expressing cells because of targeting of *stg* 3'UTR attached to it. Anterior and posterior dorsal histoblast nests showed lack of GFP from 15hrs APF, thus indicating *miR-965* mediated repression of wild type *stg* 3'UTR in the histoblast nests (Fig 34f). No repression of GFP was observed in the histoblast nests expressing *stg* 3'UTR having multiple mutations (Fig 34g). These results indicated that *stg* is a direct target of *miR-965 in vivo*.

No specific pattern was obtained in the histoblast nests for *wg* 3'UTR GFP reporter from 15hrs APF till 30hrs APF. It might be possible that *wg* plays a role in the later stages of histoblast development, which eventually form dorsal tergite surface of segment.

a)

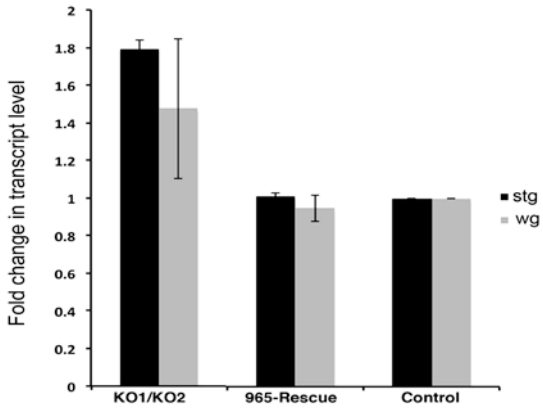
Fold change in transcript level
2
1.8
1.6
1.4
1.2
1
0.8
0.6
0.4
0.2
0
KO1/KO2
965-Rescue
Control
stg
wg

b)


seed 2
seed 1
CCGACATTACGCCTAAGTGATGCCAGATGTACCCTATATGATCA
AAGATCTATCGTTTAAGAGTTGAAAGTTGTAAACTTCTACGCTTA
5' stg 3'UTR..CUAU CGUUU 3'
5' stg 3'UTR...UACGCUUA 3'
3'miR-965.....GAUA GCGAA 5'
C
3'miR-965..... AUGCGAAU 5'

c)

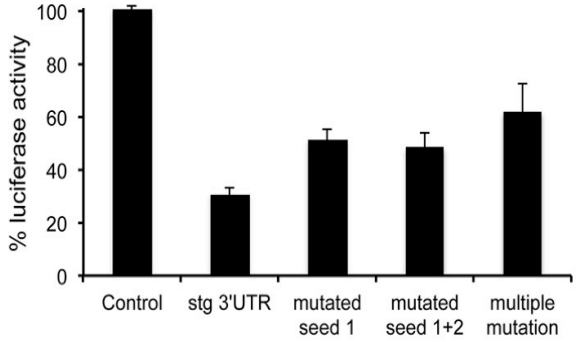
% luciferase activity
100
80
60
40
20
0
Control
stg 3'UTR
mutated seed 1
mutated seed 1+2
multiple mutation

d)


TATGATCA
TACGCTTA
5'wg 3'UTR....UACGCUUA 3'
3'miR-965.....UAGCGAAU 5'

e)

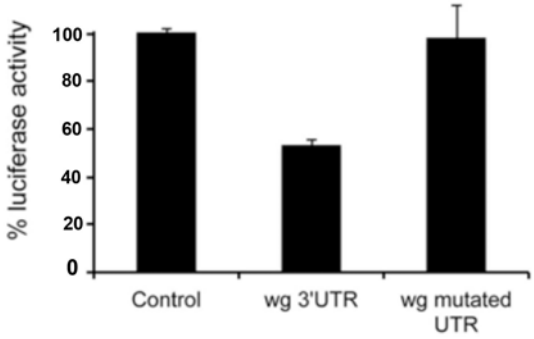
% luciferase activity
100
80
60
40
20
0
Control
wg 3'UTR
wg mutated UTR

f)

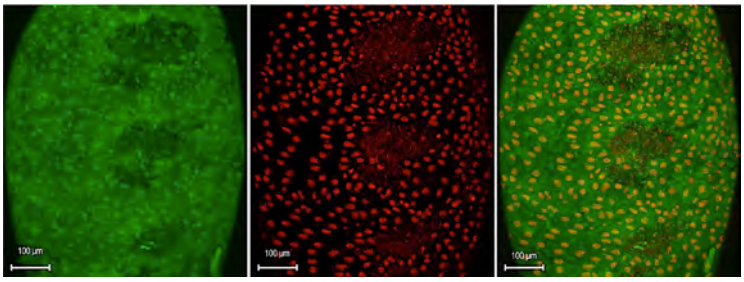
stg 3'UTR-GFP
H2-RFP
merged

g)

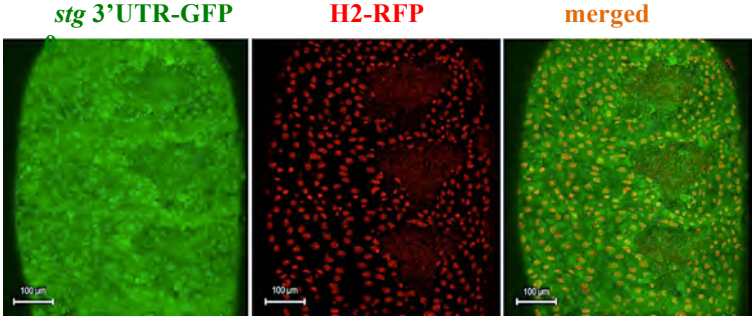
multiple mutated
stg 3'UTR-GFP
H2-RFP
merged

Figure 34: *stg* and *wg* as direct targets of *miR-965*

a) RT-qPCR showing upregulation of *stg* (black) and *wg* (grey) transcripts in 21hrs old pupa samples of mutant (KO1/KO2), rescue and control. *stg* and *wg* transcript levels in *miR-965* RMCE rescue were comparable to control. qPCRs were done on RNA extracted from three independent samples and data were normalized to rp49.
b) Sequence of 3'UTR of *stg*, showing 8-mer site (seed 1) and putative second site (seed 2) match with *miR-965*. Mutated nucleotides are indicated in red.
c) Luciferase reporter assay showing effect of *miR-965* expression on the luciferase reporters containing wild type *stg* 3'UTR, 3'UTR with mutations in one seed (seed1), mutations in two seeds (seed1+2) and mutations in both seed and sequence between them (multiple mutation). Data were normalized to renilla luciferase reporters. Data represent average of three independent experiments. $p<0.01$ comparing luciferase activity of wild type *stg* 3'UTR with mutated seed1 and multiple mutated 3'UTR. $p=0.5$, comparing mutated seed1 with mutated seed 1+2 3'UTR.
d) Sequence of *wg* 3'UTR showing seed match with *miR-965*. Mutated nucelotides are shown in red.
e) Luciferase reporter assay showing effect of *miR-965* expression on the luciferase reporters containing wild type *wg* 3'UTR and seed mutated *wg* 3'UTR. Data represent average of three independent experiments. $p<0.01$, comparing luciferase reporter activity of *wg* 3'UTR with mutated 3'UTR.
f) Images showing strong *stg* 3'UTR repression by *miR-965* by lack of GFP in the histoblast nests at 21hrs APF (left panel). *stg* 3'UTR-GFP is driven ubiquitously by tubulin promoter. Middle panel represents H2-RFP for marking small histoblast nuclei and big LEC nuclei. Scale bar-100μM.
g) Images showing no repression of mutated *stg* 3'UTR by *miR-965* in the histoblast nests at 22hrs APF. Note that mutated 3'UTR used here is same as multiple mutated *stg* 3'UTR used in the luciferase assay. Scale bar-100μM.

5.7 Phenocopy of *miR-965* abdominal segmentation defects by overexpression of target genes

5.7.1 Overexpression of *stg* to phenocopy *miR-965* mutant adult segmentation defects

I overexpressed *stg* in the histoblast cells, using *esg*-GAL4 driving *UAS-stg*. I observed similar kinds of adult abdominal segmentation defects as in *miR-965* mutants (Fig 35a). Penetrance of phenotype between *miR-965* mutant and flies with *stg* overexpression was also similar, when grown under similar conditions of temperature and humidity (Fig 35b). Abdominal segmentation defects in *stg* overexpression flies were quantified for the three kinds of defects - lack of tissue, fusion of segments and polarity defect. Lack of tissue was the most prominent defect observed in ~85% of flies. Fusion of segments and polarity defects were never present alone, but always accompanied with lack of tissue defect (Fig 35c). Polarity defect was least penetrant defect, rarely shown by *stg* overexpression flies.

I also looked for defects at the histoblast level, using *esg*-GAL4 driving UAS-GFP in *stg* overexpression background. Defects similar to *miR-965* mutant were observed at different stages of the histoblast development. At early division phase of histoblast development, cells underwent asynchronous division and had increased numbers of cells in each histoblast nests. Histoblast cells undergoing apoptosis were also observed (Fig 36a). At growth and migration phase, histoblast nests contained LECs within growing histoblast nests. Histoblast nests also moved slowly (Fig 36c) and could not cover whole segment by end of pupariation, hence causing lack of tissues in adult abdominal segments.

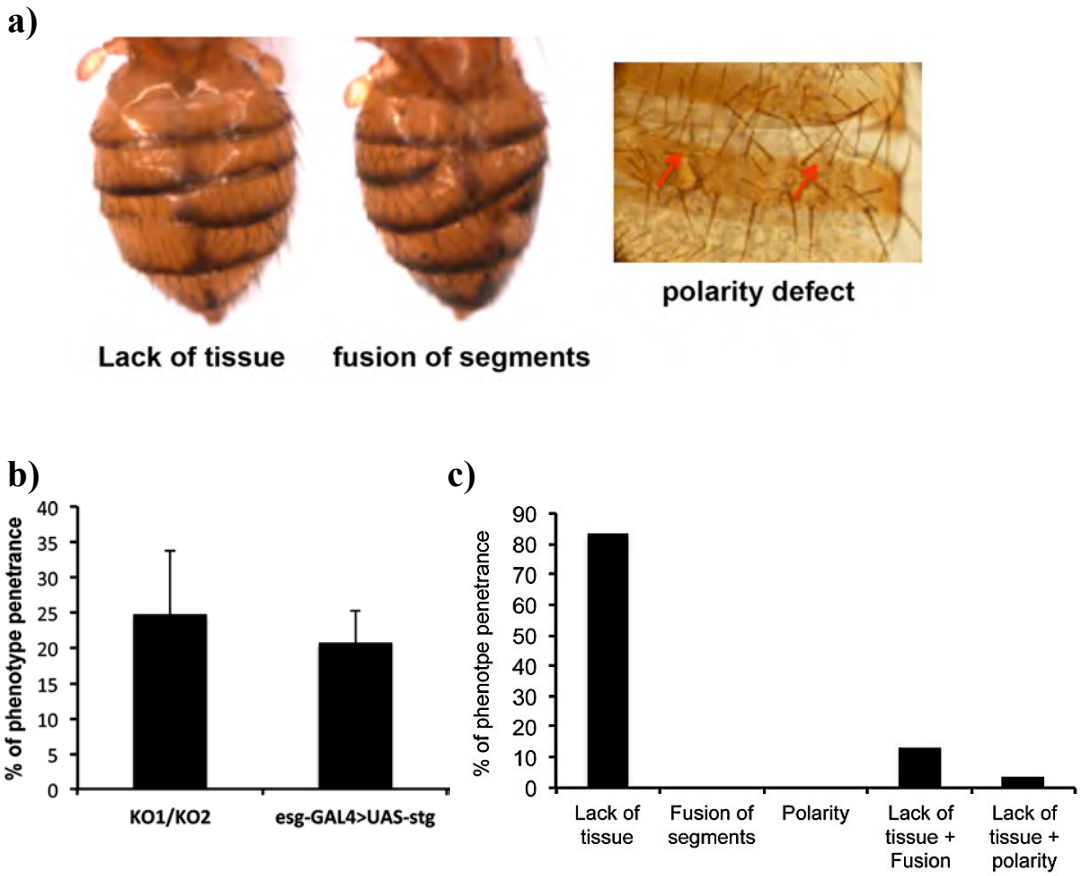

Figure 35: Phenocopy of *miR-965* mutant defects by overexpression of *stg*

a) Images showing adult abdominal segmentation defects (lack of tissues, fusion of segments and polarity defect) in flies overexpressing *stg* in the histoblast cells.
b) Graph showing penetrance of adult abdominal segmentation defects in *miR-965* mutant and flies overexpressing *stg* in histoblast cells.
c) Graph showing penetrance of three kinds of defects in flies overexpressing *stg*. ~80% flies showed lack of tissue alone and 20% showed lack of tissue defect with fusion of segments or polarity defect.

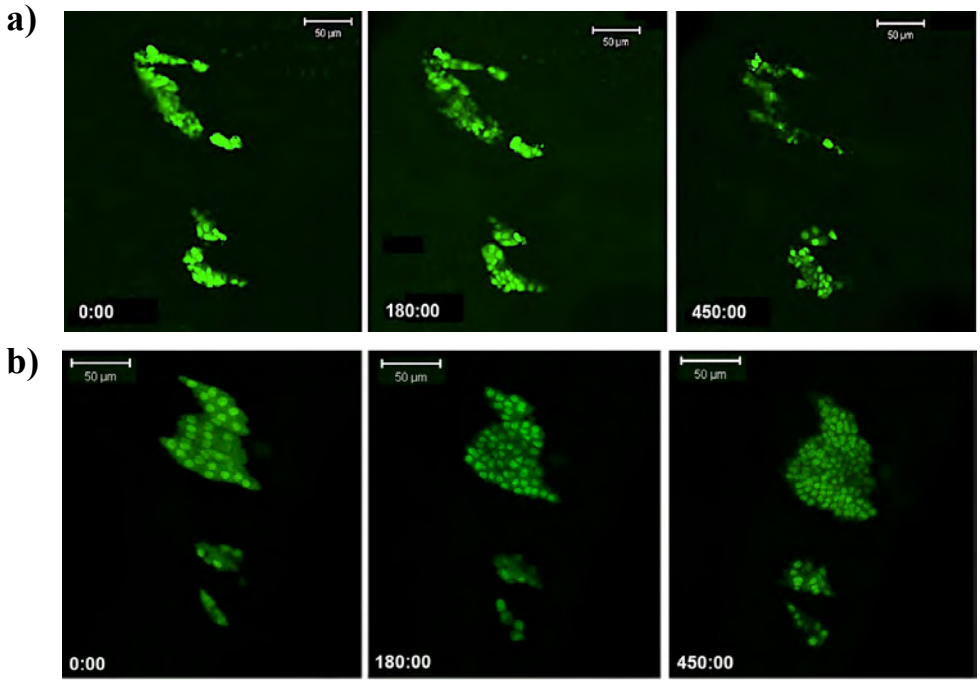
a)
50 µm
0:00
180:00
450:00
b)
50 µm
0:00
180:00
450:00

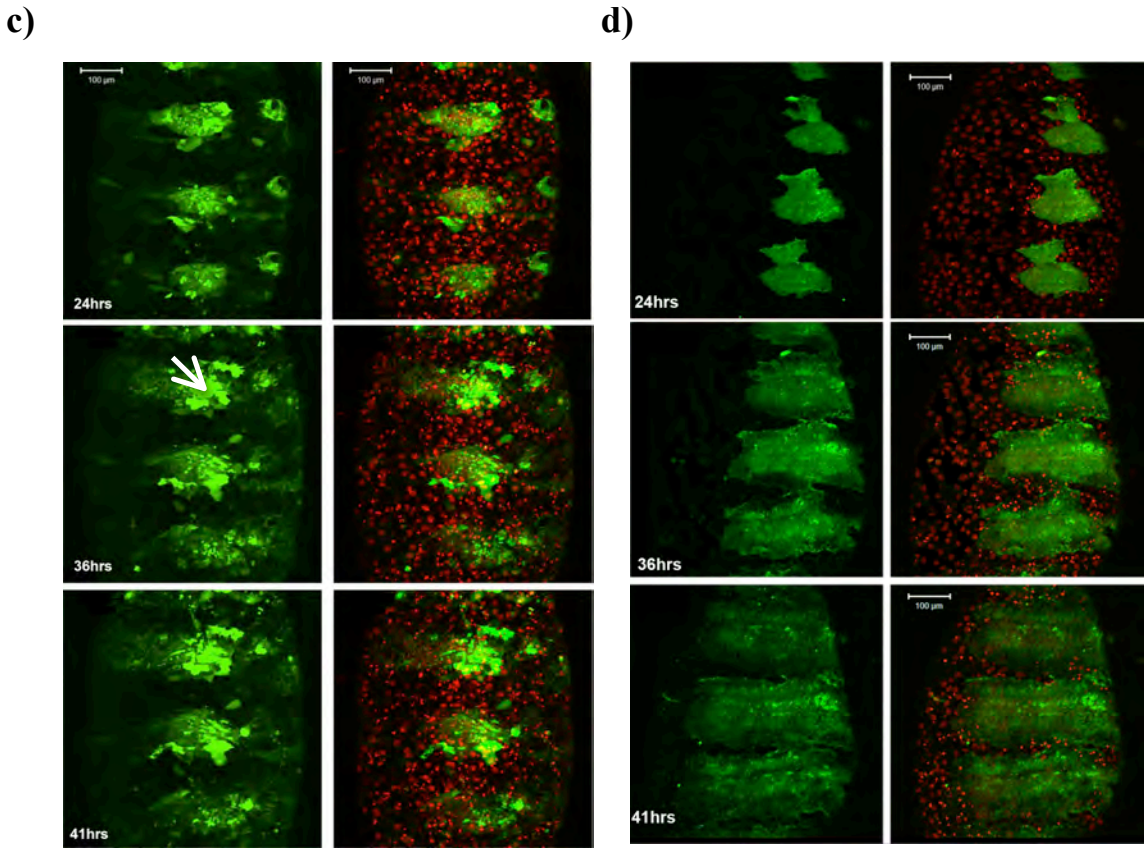
c)
d)
100 µm
24hrs
36hrs
41hrs

Figure 36: Phenocopy of *miR-965* mutant defects by overexpression of *stg* at the histoblast level

a) Time-lapse images of pupa overexpressing *stg* in histoblast cells at 0hrs, 3hrs, 7.5hrs APF, showing asynchronous cell divisions and asymmetric histoblast cells in the nest. Histoblast cells are visualized by *esg*-GAL4 driving nuclear UAS-GFP in *stg* overexpression background. Apoptotic cells in the nest are shown by bright green GFP and by presence of small and fragmented nuclei. Scale bar- 50μM.
b) Time-lapse images of control pupa at 0hrs, 3hrs and 7.5hrs APF, showing synchronous cell division of histoblast cells using *esg*-GAL4 driving nuclear GFP. Scale bar- 50μM.
c) Time-lapse images of pupa overexpressing *stg* in the histoblast cells at 24hrs, 36hrs and 41hrs APF showing slow and aberrant movement of histoblast nests. Bright GFP within nests indicates apoptosis resistant LECs (shown by arrow). Note that upper segment migrated faster than lower two segments. Scale bar – 100μM.
d) Time-lapse images of control pupa at 24hrs, 36hrs and 41hrs APF showing migration of histoblast nests using *esg*-GAL4 driving cytoplasmic GFP. Scale bar – 100μM.

5.7.2 Overexpression of *wg* to phenocopy *miR-965* mutant adult segmentation defect

I overexpressed *wg* in the histoblast cells, using *esg*-GAL4 but overexpression of *wg* throughout development proved deleterious for flies and they died during embryogenesis. To overcome this problem, I used a temperature sensitive allele, UAS-*wg(ts*) for *wg* overexpression. This allele maintains normal levels of *wg* activity at 25°C and starts overexpressing *wg* at 16-18°C. The *esg*-GAL4 driving temperature sensitive *UAS-wg* flies were grown at 25°C and shifted to 18°C at third instar larval stage for *wg* overexpression. I observed abdominal segmentation defects in *wg* overexpression flies, though with low penetrance of ~5-10% (Fig 37a,b).

The effect of *wg* overexpression at the histoblast level could not be studied due to inability to maintain 16°C, that is required for the activity of *UAS-wg(ts)* allele. I am currently modifying conditions to study the effect of *wg* overexpression at the histoblast level. Meanwhile, I tried to see any changes in *wg* expression in *miR-965* mutant, using Wg antibody in fixed pupal samples. In *miR-965* mutant, the expression domain of *wg* expanded slightly as compared to centrally localized expression of *wg* inside the histoblast nests (Fig 37c).

a)

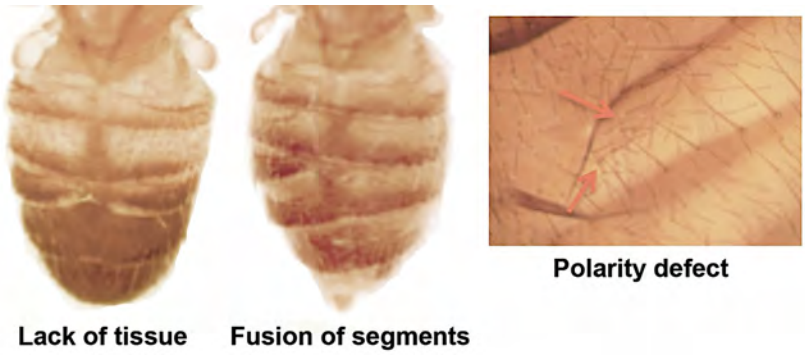
Lack of tissue
Fusion of segments
Polarity defect

b)

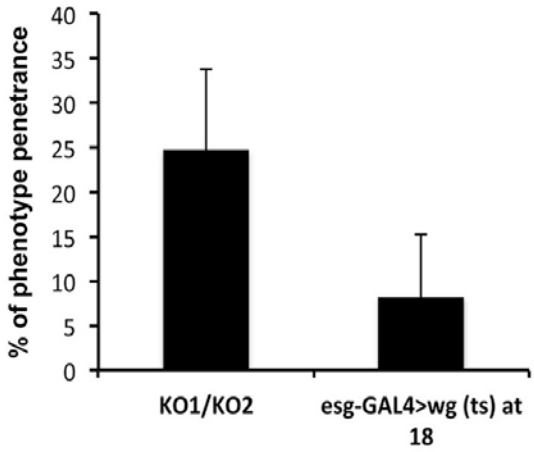
% of phenotype penetrance
40
35
30
25
20
15
10
5
0
KO1/KO2
esg-GAL4>wg (ts) at 18

c)

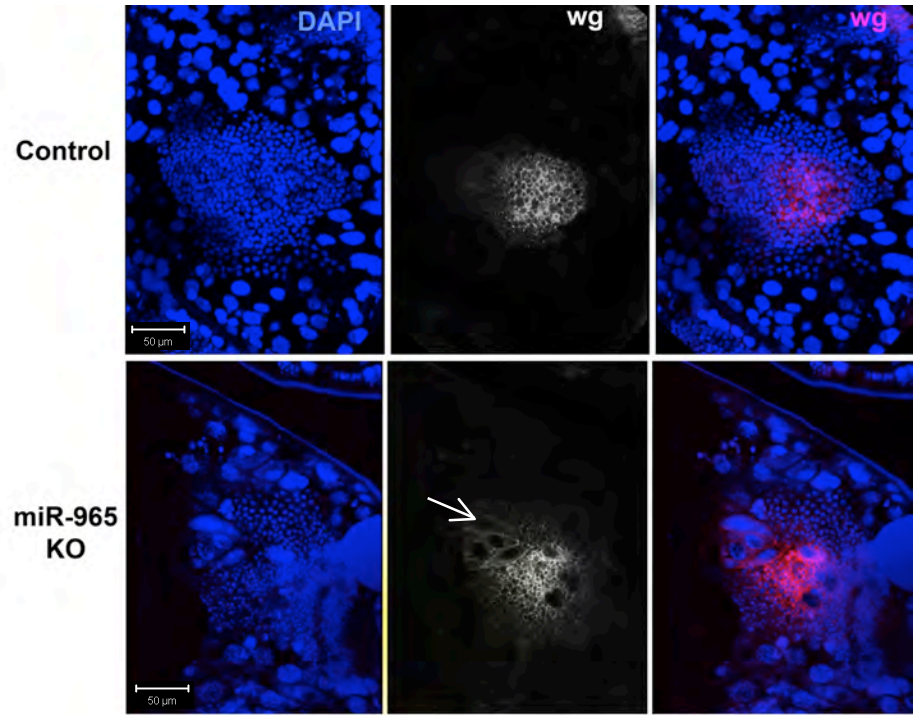
Control
miR-965 KO
DAPI
wg
wg
50 µm
50 µm

Figure 37: Abdominal segmentation defects of *wg* overexpression and *wg* expression in *miR-965* mutant

a) Images showing abdominal segmentation defects (lack of tissue, fusion of segments and polarity defects) in adult flies overexpressing *wg* in histoblast cells, using temperature sensitive *UAS-wg* allele.
b) Graph showing penetrance of abdominal defects in flies overexpressing *wg* in histoblasts and in *miR-965* mutants.
c) Images showing increased expression in *miR-965* mutant histoblast nests at 21hrs APF compared to control, using Wg antibody (grey in middle panel and red in right panel). DAPI (blue) marks the nuclei of histoblasts and LECs. Histoblast cells are recognized by their small nuclei, compared to big nuclei of LECs. Presence of LECs in histoblast nest in *miR-965* mutant is conspicuous (shown by arrow).

5.8 Confirmation of *stg* and *wg* as biological targets of *miR-965*

If abnormal adult segmentation were caused by overexpression of either *stg* or *wg* or both, reducing *stg* or *wg* expression levels in *miR-965* mutant would be expected to rescue its segmentation defects.

For reducing levels of *stg* in *miR-965* mutant background, I used three different *stg* mutant alleles (stg^{4}, $stg^{DG05404}$, $stg^{EY12388}$). Abnormal adult segmentation of *miR-965* mutant was significantly rescued by reducing *stg* levels in the *miR-965* mutant (Fig 38a).

For reducing level of *wg* specifically at pupal stage, I used a temperature sensitive *wg* mutant allele (wg^{IL114}) in the *miR-965* mutant background. The wg^{IL114} mutant allele behaves like wild type at 18°C and as a null mutant at 25°C. Mild rescue with reduction in *wg* level was observed in *miR-965* mutant ($p=0.59$). However, the penetrance of the deformed segmentation phenotype was greatly reduced by lowering both *stg* and *wg* levels together in *miR-965* mutant (Fig 38a).

These genetic results indicated that majority of abnormal adult segmentation was contributed by the lack of targeting of *stg* by *miR-965* and to a lesser extent by *wg* in *Drosophila melanogaster.*

a)

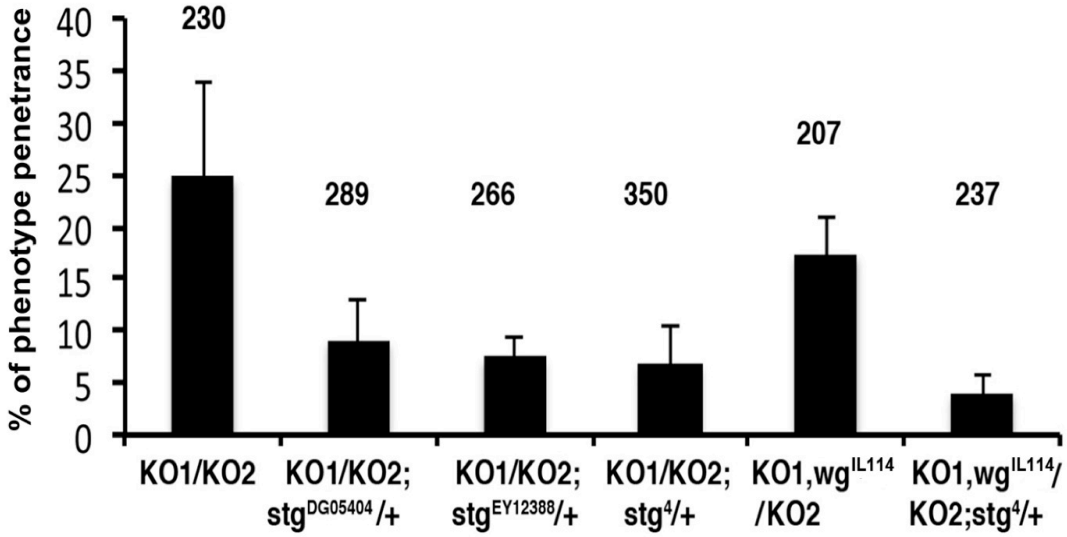

Figure 38: *stg* and *wg* as targets of *miR-965 in vivo*

a) Graph showing penetrance of segmentation defects in *miR-965* mutant (KO1/KO2), with reduced *stg* levels using *stg* mutant alleles ($stg^{DG05404}$, $stg^{EY12388}$, stg^{4}) and reduced *wg* level using temperature sensitive *wg* null allele (wg^{IL114}) in *miR-965* mutant (KO1/KO2) background. $p<0.5$, when comparing *miR-965* mutant (KO1/KO2) with three different *stg* mutant alleles KO1/KO2; $stg^{DG05404}$, KO1/KO2; $stg^{EY12388}$, KO1/KO2; stg^{4}.
$p=0.59$, comparing *miR-965* mutant (KO1/KO2) with KO1/KO2; wg^{IL114} allele and $p=0.18$, comparing *miR-965* mutant (KO1/KO2) with KO1, wg^{IL114}/KO2; $stg^{4.}$

5.9 Discussions

The abdominal epithelium of *Drosophila* represents a good *in vivo* model system for analyzing processes like cell proliferation, cell replacement and cell death. The adult abdominal epithelium is formed by abdominal histoblast cells, which replace the larval epidermal cells (LECs) during metamorphosis. The histoblasts are originated as a small group of cells during embryogenesis and remain dormant till pupal stage. At onset of the pupal stage, ecdysone activates *string (stg)* transcription to induce proliferation of histoblast cells (Ninov et al 2009).

Here, I have shown that *miR-965* represses *stg* transcript during histoblast development in order to form normal abdominal segments. In *miR-965* mutant, Stg is overexpressed making cells to undergo precocious and asynchronous cell divisions. This resulted in increased number of cells and cells with asymmetric shape at 0hrs APF. Overexpression of *miR-965* resulted in repression of stg, thus preventing histoblast cells to enter into division phase, which eventually resulted in the early death of pupa.

According to the RNA sequencing data (Ruby et al 2007b), *miR-965* expresses strongly during larval stage and decreases at the pupal stage. In concordance to this observation, no *miR-965* expression was observed during early division phase in pupae, using a *miR-965* GFP sensor. Therefore, I conclude that *miR-965* represses *stg* expression during larval stage and prevents histoblast cells from entering into a proliferative phase before pupariation. In the pupa, during early division phase, *miR-965* is not expressed, allowing expression of *stg,* required for rapid divisions of

histoblasts. *miR-965* is expressed in the histoblast nests during growth and migration phase and fine-tunes the *stg* levels, required for slow divisions during this period.

During the growth and migration phase, the rate of cell divisions decreases and cells need to grow and spread. *stg 3'UTR* GFP reporters have shown that *stg* is repressed by *miR-965* in the migrating histoblast nests and this repression was abrogated when *miR-965* targeting sites were mutated. Therefore, *miR-965* controls expression of *stg* during migration phase to restrict rapid cell divisions and allows cells to grow and migrate.

An increase in cell size accompanied by cell divisions is required to cause apoptosis in the surrounding LECs (Nakajima et al 2011). In *miR-965* mutant, *stg* overexpression might have hampered normal growth process of histoblast cells by making them divide during growth and migration phase and hence, disturbing normal histoblast migration and LEC removal. Abnormal migration and cell death was evident from the aberrant spreading of histoblasts and presence of LECs inside the nests during growth phase.

As mentioned earlier that ecdysone at the onset of pupariation triggers *stg* activation (Ninov et al 2009), and our results showed that the *miR-965* represses stg. I did a preliminary study to test if there is any relationship between ecdysone, *stg* and *miR-965* and my results showed that knockdown of ecdysone receptor resulted in the upregulation of *miR-965*. Based on these results, I can hypothesize that ecdysone at the onset of pupariation activates *stg* expression by repressing *miR-965*.

Wg has been shown to promote identity of tergite and sternite by interacting with *EGFR* receptor (DER) (Shirras & Couso 1996), which plays an important role during growth and migration phase. *Wg* also antagonize *dpp* in the histoblast nests to define dorsal-ventral boundaries. Differential cell adhesion properties of cells with *Wg/DER* signaling give rise to tergites and sternites, whereas *dpp* signaling forms soft pleural tissues, hence *wg* and *dpp* help in defining anterior posterior boundaries of each segment (Kopp et al 1999, Shirras & Couso 1996). In *miR-965* mutant, *wg* expression was observed to be upregulated, therefore it might be possible that misregulation of *wg* in histoblast nests changed its interactions with *dpp* and resulted in the lack of defined boundaries of segments. This might be responsible for polarity defects observed in *miR-965* mutant. In addition, overexpression of *wg* might also change adhesive properties of cells, which might have caused persistence of LECs inside histoblast nests.

In summary, I have shown that *miR-965* mediated regulation of *stg* and *wg* during histoblast development is important for the formation of uniform adult abdominal segments. Lack of this regulation changed the properties of histoblast cells during different phases of development and subsequently caused abnormal segmentation in adults.

REFERENCES:

Aboobaker AA, Tomancak P, Patel N, Rubin GM, Lai EC. 2005. Drosophila microRNAs exhibit diverse spatial expression patterns during embryonic development. *Proceedings of the National Academy of Sciences of the United States of America* 102: 18017-22

Altuvia Y, Landgraf P, Lithwick G, Elefant N, Pfeffer S, et al. 2005. Clustering and conservation patterns of human microRNAs. *Nucleic acids research* 33: 2697-706

Aravin AA, Lagos-Quintana M, Yalcin A, Zavolan M, Marks D, et al. 2003. The small RNA profile during Drosophila melanogaster development. *Developmental cell* 5: 337-50

Arber S, Han B, Mendelsohn M, Smith M, Jessell TM, Sockanathan S. 1999. Requirement for the homeobox gene Hb9 in the consolidation of motor neuron identity. *Neuron* 23: 659-74

Bagga S, Bracht J, Hunter S, Massirer K, Holtz J, et al. 2005. Regulation by let-7 and lin-4 miRNAs results in target mRNA degradation. *Cell* 122: 553-63

Bak LK, Schousboe A, Waagepetersen HS. 2006. The glutamate/GABA-glutamine cycle: aspects of transport, neurotransmitter homeostasis and ammonia transfer. *J Neurochem* Aug;98(3):641-53.

Behm-Ansmant I, Rehwinkel J, Doerks T, Stark A, Bork P, Izaurralde E. 2006. mRNA degradation by miRNAs and GW182 requires both CCR4:NOT deadenylase and DCP1:DCP2 decapping complexes. *Genes Dev* 20: 1885-98

Bellocchio EE, Reimer RJ, Fremeau RT, Jr., Edwards RH. 2000. Uptake of glutamate into synaptic vesicles by an inorganic phosphate transporter. *Science* 289: 957-60

Berezikov E, Cuppen E, Plasterk RH. 2006. Approaches to microRNA discovery. *Nat Genet* 38 Suppl: S2-7

Besson MT, Re DB, Moulin M, Birman S. 2005. High affinity transport of taurine by the Drosophila aspartate transporter dEAAT2. *The Journal of biological chemistry* 280: 6621-6

Besson MT, Soustelle L, Birman S. 1999. Identification and structural characterization of two genes encoding glutamate transporter homologues differently expressed in the nervous system of Drosophila melanogaster. *FEBS letters* 443: 97-104

Besson MT, Soustelle L, Birman S. 2000. Selective high-affinity transport of aspartate by a Drosophila homologue of the excitatory amino-acid transporters. *Current biology : CB* 10: 207-10

Betel D, Wilson M, Gabow A, Marks DS, Sander C. 2008. The microRNA.org resource: targets and expression. *Nucleic acids research* 36: D149-53

Biemar F, Zinzen R, Ronshaugen M, Sementchenko V, Manak JR, Levine MS. 2005. Spatial regulation of microRNA gene expression in the *Drosophila* embryo. *Proceedings of the National Academy of Sciences of the United States of America* 102: 15907-11

Bohnsack MT, Czaplinski K, Gorlich D. 2004. Exportin 5 is a RanGTP-dependent dsRNA-binding protein that mediates nuclear export of pre-miRNAs. *RNA* 10: 185-91

Boulland JL, Qureshi T, Seal RP, Rafiki A, Gundersen V, et al. 2004. Expression of the vesicular glutamate transporters during development indicates the widespread corelease of multiple neurotransmitters. *The Journal of comparative neurology* 480: 264-80

Brand AH, Perrimon N. June1, 1993. Targeted gene expression as a mean of altering cell fates and generating dominant phenotypes. *Development* 118: 401-415

Brennecke J, Hipfner DR, Stark A, Russell RB, Cohen SM. 2003. bantam encodes a developmentally regulated microRNA that controls cell proliferation and regulates the proapoptotic gene hid in *Drosophila*. *Cell* 113: 25-36

Brennecke J, Stark A, Russell RB, Cohen SM. 2005. Principles of microRNA-target recognition. *PLoS biology* 3: e85

Brenner JL, Jasiewicz KL, Fahley AF, Kemp BJ, Abbott AL. 2010. Loss of individual microRNAs causes mutant phenotypes in sensitized genetic backgrounds in C. elegans. *Current biology : CB* 20: 1321-5

Brusa R, Zimmermann F, Koh DS, Feldmeyer D, Gass P, et al. 1995. Early-onset epilepsy and postnatal lethality associated with an editing-deficient GluR-B allele in mice. *Science* 270: 1677-80

Cai X, Hagedorn CH, Cullen BR. 2004. Human microRNAs are processed from capped, polyadenylated transcripts that can also function as mRNAs. *RNA* 10: 1957-66

Calin GA, Dumitru CD, Shimizu M, Bichi R, Zupo S, et al. 2002. Frequent deletions and down-regulation of micro- RNA genes miR15 and miR16 at 13q14 in chronic lymphocytic leukemia. *Proceedings of the National Academy of Sciences of the United States of America* 99: 15524-9

Caponi S, Funel N, Frampton AE, Mosca F, Santarpia L, et al. 2012. The good, the bad and the ugly: a tale of miR-101, miR-21 and miR-155 in pancreatic

intraductal papillary mucinous neoplasms. *Annals of oncology : official journal of the European Society for Medical Oncology / ESMO*

Caygill EE, Johnston LA. 2008. Temporal regulation of metamorphic processes in Drosophila by the let-7 and miR-125 heterochronic microRNAs. *Current biology : CB* 18: 943-50

Chen JF, Mandel EM, Thomson JM, Wu Q, Callis TE, et al. 2006. The role of microRNA-1 and microRNA-133 in skeletal muscle proliferation and differentiation. *Nat Genet* 38: 228-33

Chen PE, Geballe MT, Stansfeld PJ, Johnston AR, Yuan H, et al. 2005a. Structural features of the glutamate binding site in recombinant NR1/NR2A N-methyl-D-aspartate receptors determined by site-directed mutagenesis and molecular modeling. *Molecular pharmacology* 67: 1470-84

Chen PY, Manninga H, Slanchev K, Chien M, Russo JJ, et al. 2005b. The developmental miRNA profiles of zebrafish as determined by small RNA cloning. *Genes Dev* 19: 1288-93

Chen W, Aoki C, Mahadomrongkul V, Gruber CE, Wang GJ, et al. 2002. Expression of a variant form of the glutamate transporter GLT1 in neuronal cultures and in neurons and astrocytes in the rat brain. *The Journal of neuroscience : the official journal of the Society for Neuroscience* 22: 2142-52

Chen YW, Weng R, Cohen SM. 2011. Protocols for use of homologous recombination gene targeting to produce microRNA mutants in Drosophila. *Methods in molecular biology* 732: 99-120

Chendrimada TP, Finn KJ, Ji X, Baillat D, Gregory RI, et al. 2007. MicroRNA silencing through RISC recruitment of eIF6. *Nature* 447: 823-8

Chendrimada TP, Gregory RI, Kumaraswamy E, Norman J, Cooch N, et al. 2005. TRBP recruits the Dicer complex to Ago2 for microRNA processing and gene silencing. *Nature* 436: 740-4

Cheng LC, Pastrana E, Tavazoie M, Doetsch F. 2009. miR-124 regulates adult neurogenesis in the subventricular zone stem cell niche. *Nature neuroscience* 12: 399-408

Chin LJ, Ratner E, Leng S, Zhai R, Nallur S, et al. 2008. A SNP in a let-7 microRNA complementary site in the KRAS 3' untranslated region increases non-small cell lung cancer risk. *Cancer research* 68: 8535-40

Coller J, Parker R. 2004. Eukaryotic mRNA decapping. *Annual review of biochemistry* 73: 861-90

Conn PJ, Pin JP. 1997. Pharmacology and functions of metabotropic glutamate receptors. *Annual review of pharmacology and toxicology* 37: 205-37

Contractor A, Mulle C, Swanson GT. 2011. Kainate receptors coming of age: milestones of two decades of research. *Trends in neurosciences* 34: 154-63

Cull-Candy S, Brickley S, Farrant M. 2001. NMDA receptor subunits: diversity, development and disease. *Current opinion in neurobiology* 11: 327-35

Cummings E, Donohoe G, Hargreaves A, Moore S, Fahey C, et al. 2012. Mood congruent psychotic symptoms and specific cognitive deficits in carriers of the novel schizophrenia risk variant at MIR-137. *Neuroscience letters*

Currie DA, Truman JW, Burden SJ. 1995. Drosophila glutamate receptor RNA expression in embryonic and larval muscle fibers. *Developmental dynamics : an official publication of the American Association of Anatomists* 203: 311-6

D'Alessandra Y, Devanna P, Limana F, Straino S, Di Carlo A, et al. 2010. Circulating microRNAs are new and sensitive biomarkers of myocardial infarction. *European heart journal* 31: 2765-73

D'Onofrio M, Cuomo L, Battaglia G, Ngomba RT, Storto M, et al. 2001. Neuroprotection mediated by glial group-II metabotropic glutamate receptors requires the activation of the MAP kinase and the phosphatidylinositol-3-kinase pathways. *J Neurochem* 78: 435-45

Daikhin Y and Yudkoff M. 2000. Compartmentation of Brain Glutamate Metabolism in Neurons and Glia. *American Society for Nutritional Sciences.* 1026s-1031s.

Daniels RW, Collins CA, Gelfand MV, Dant J, Brooks ES, et al. 2004. Increased expression of the *Drosophila* vesicular glutamate transporter leads to excess glutamate release and a compensatory decrease in quantal content. *The Journal of neuroscience : the official journal of the Society for Neuroscience* 24: 10466-74

Daniels RW, Miller BR, DiAntonio A. 2011. Increased vesicular glutamate transporter expression causes excitotoxic neurodegeneration. *Neurobiology of disease* 41: 415-20

Dill H, Linder B, Fehr A, Fischer U. 2012. Intronic miR-26b controls neuronal differentiation by repressing its host transcript, ctdsp2. *Genes Dev* 26: 25-30

Dingledine R, Borges K, Bowie D, Traynelis SF. 1999. The glutamate receptor ion channels. *Pharmacological reviews* 51: 7-61

Disbrow JK, Gershten MJ, Ruth JA. 1982. Uptake of L-[3H] glutamic acid by crude and purified synaptic vesicles from rat brain. *Biochemical and biophysical research communications* 108: 1221-7

Doench JG, Sharp PA. 2004. Specificity of microRNA target selection in translational repression. *Genes Dev* 18: 504-11

Eliasof S, Arriza JL, Leighton BH, Amara SG, Kavanaugh MP. 1998. Localization and function of five glutamate transporters cloned from the salamander retina. *Vision research* 38: 1443-54

Esau C, Davis S, Murray SF, Yu XX, Pandey SK, et al. 2006. miR-122 regulation of lipid metabolism revealed by in vivo antisense targeting. *Cell metabolism* 3: 87-98

Esquela-Kerscher A, Trang P, Wiggins JF, Patrawala L, Cheng A, et al. 2008. The *let-7* microRNA reduces tumor growth in mouse models of lung cancer. *Cell cycle* 7: 759-64

Eulalio A, Behm-Ansmant I, Schweizer D, Izaurralde E. 2007. P-body formation is a consequence, not the cause, of RNA-mediated gene silencing. *Mol Cell Biol* 27: 3970-81

Farh KK, Grimson A, Jan C, Lewis BP, Johnston WK, et al. 2005. The widespread impact of mammalian MicroRNAs on mRNA repression and evolution. *Science* 310: 1817-21

Fazi F, Rosa A, Fatica A, Gelmetti V, De Marchis ML, et al. 2005. A minicircuitry comprised of microRNA-223 and transcription factors NFI-A and C/EBPalpha regulates human granulopoiesis. *Cell* 123: 819-31

Feldmeyer D, Kask K, Brusa R, Kornau HC, Kolhekar R, et al. 1999. Neurological dysfunctions in mice expressing different levels of the Q/R site-unedited AMPAR subunit GluR-B. *Nature neuroscience* 2: 57-64

Filipowicz W, Bhattacharyya SN, Sonenberg N. 2008. Mechanisms of post-transcriptional regulation by microRNAs: are the answers in sight? *Nat Rev Genet* 9: 102-14

Floor E, Leventhal PS, Schaeffer SF. 1990. Partial purification and characterization of the vacuolar H(+)-ATPase of mammalian synaptic vesicles. *J Neurochem* 55: 1663-70

Forstemann K, Horwich MD, Wee L, Tomari Y, Zamore PD. 2007. *Drosophila* microRNAs are sorted into functionally distinct argonaute complexes after production by dicer-1. *Cell* 130: 287-97

Forstemann K, Tomari Y, Du T, Vagin VV, Denli AM, et al. 2005. Normal microRNA maturation and germ-line stem cell maintenance requires *Loquacious*, a double-stranded RNA-binding domain protein. *PLoS Biol* 3: e236

Friedman JM, Jones PA. 2009. MicroRNAs: critical mediators of differentiation, development and disease. *Swiss medical weekly* 139: 466-72

Furuta A, Rothstein JD, Martin LJ. 1997. Glutamate transporter protein subtypes are expressed differentially during rat CNS development. *The Journal of neuroscience : the official journal of the Society for Neuroscience* 17: 8363-75

Gammelsaeter R, Coppola T, Marcaggi P, Storm-Mathisen J, Chaudhry FA, et al. 2011. A role for glutamate transporters in the regulation of insulin secretion. *PLoS One* 6: e22960

Gauwerky CE, Huebner K, Isobe M, Nowell PC, Croce CM. 1989. Activation of MYC in a masked t(8;17) translocation results in an aggressive B-cell leukemia. *Proceedings of the National Academy of Sciences of the United States of America* 86: 8867-71

Girmatsion Z, Biliczki P, Bonauer A, Wimmer-Greinecker G, Scherer M, et al. 2009. Changes in microRNA-1 expression and IK1 up-regulation in human atrial fibrillation. *Heart rhythm : the official journal of the Heart Rhythm Society* 6: 1802-9

Gong WJ, Golic KG. 2003. Ends-out, or replacement, gene targeting in Drosophila. *Proceedings of the National Academy of Sciences of the United States of America* 100: 2556-61

Gregg RG, Metzenberg AB, Hogan K, Sekhon G, Laxova R. 1991. Waisman syndrome, a human X-linked recessive basal ganglia disorder with mental retardation: localization to Xq27.3-qter. *Genomics* 9: 701-6

Gregory RI, Chendrimada TP, Cooch N, Shiekhattar R. 2005. Human RISC couples microRNA biogenesis and posttranscriptional gene silencing. *Cell* 123: 631-40

Gregory RI, Chendrimada TP, Shiekhattar R. 2006. MicroRNA biogenesis: isolation and characterization of the microprocessor complex. *Methods in molecular biology* 342: 33-47

Grignol V, Fairchild ET, Zimmerer JM, Lesinski GB, Walker MJ, et al. 2011. miR-21 and miR-155 are associated with mitotic activity and lesion depth of borderline melanocytic lesions. *British journal of cancer* 105: 1023-9

Grimson A, Farh KK, Johnston WK, Garrett-Engele P, Lim LP, Bartel DP. 2007. MicroRNA targeting specificity in mammals: determinants beyond seed pairing. *Molecular cell* 27: 91-105

Grishok A, Pasquinelli AE, Conte D, Li N, Parrish S, et al. 2001. Genes and mechanisms related to RNA interference regulate expression of the small temporal RNAs that control *C. elegans* developmental timing. *Cell* 106: 23-34

Groth AC, Fish M, Nusse R, Calos MP. 2004. Construction of transgenic Drosophila by using the site-specific integrase from phage phiC31. *Genetics* 166: 1775-82

Guo H, Ingolia NT, Weissman JS, Bartel DP. 2010. Mammalian microRNAs predominantly act to decrease target mRNA levels. *Nature* 466: 835-40

Hatfield SD, Shcherbata HR, Fischer KA, Nakahara K, Carthew RW, Ruohola-Baker H. 2005. Stem cell division is regulated by the microRNA pathway. *Nature* 435: 974-8

Hayashi S, Hirose S, Metcalfe T, Shirras AD. 1993. Control of imaginal cell development by the escargot gene of Drosophila. *Development* 118: 105-15

Hendrickson DG, Hogan DJ, McCullough HL, Myers JW, Herschlag D, et al. 2009. Concordant regulation of translation and mRNA abundance for hundreds of targets of a human microRNA. *PLoS Biol* 7: e1000238

Huettner JE. 2003. Kainate receptors and synaptic transmission. *Progress in neurobiology* 70: 387-407

Hutvagner G, McLachlan J, Pasquinelli AE, Balint E, Tuschl T, Zamore PD. 2001. A cellular function for the RNA-interference enzyme Dicer in the maturation of the let-7 small temporal RNA. *Science* 293: 834-8

Hutvagner G, Zamore PD. 2002a. A microRNA in a multiple-turnover RNAi enzyme complex. *Science* 297: 2056-60

Hutvagner G, Zamore PD. 2002b. RNAi: nature abhors a double-strand. *Current opinion in genetics & development* 12: 225-32

Iacovelli L, Capobianco L, Iula M, Di Giorgi Gerevini V, Picascia A, et al. 2004. Regulation of mGlu4 metabotropic glutamate receptor signaling by type-2 G-protein coupled receptor kinase (GRK2). *Molecular pharmacology* 65: 1103-10

Ibanez-Ventoso C, Vora M, Driscoll M. 2008. Sequence relationships among *C. elegans, D. melanogaster* and human microRNAs highlight the extensive conservation of microRNAs in biology. *PLoS One* 3: e2818

Iorio MV, Ferracin M, Liu CG, Veronese A, Spizzo R, et al. 2005. MicroRNA gene expression deregulation in human breast cancer. *Cancer research* 65: 7065-70

Jiang F, Ye X, Liu X, Fincher L, McKearin D, Liu Q. 2005. Dicer-1 and R3D1-L catalyze microRNA maturation in *Drosophila*. *Genes Dev* 19: 1674-9

Jing Q, Huang S, Guth S, Zarubin T, Motoyama A, et al. 2005. Involvement of microRNA in AU-rich element-mediated mRNA instability. *Cell* 120: 623-34

John B, Enright AJ, Aravin A, Tuschl T, Sander C, Marks DS. 2004. Human MicroRNA targets. *PLoS Biol* 2: e363

Karres JS, Hilgers V, Carrera I, Treisman J, Cohen SM. 2007. The conserved microRNA miR-8 tunes atrophin levels to prevent neurodegeneration in Drosophila. *Cell* 131: 136-45

Kashani A, Betancur C, Giros B, Hirsch E, El Mestikawy S. 2007. Altered expression of vesicular glutamate transporters VGLUT1 and VGLUT2 in Parkinson disease. *Neurobiology of aging* 28: 568-78

Kawahara Y, Ito K, Sun H, Aizawa H, Kanazawa I, Kwak S. 2004. Glutamate receptors: RNA editing and death of motor neurons. *Nature* 427: 801

Kertesz M, Iovino N, Unnerstall U, Gaul U, Segal E. 2007. The role of site accessibility in microRNA target recognition. *Nat Genet* 39: 1278-84

Ketting RF, Fischer SE, Bernstein E, Sijen T, Hannon GJ, Plasterk RH. 2001. Dicer functions in RNA interference and in synthesis of small RNA involved in developmental timing in *C. elegans*. *Genes Dev* 15: 2654-9

Khvorova A, Reynolds A, Jayasena SD. 2003. Functional siRNAs and miRNAs exhibit strand bias. *Cell* 115: 209-16

Kim CH, Chung HJ, Lee HK, Huganir RL. 2001. Interaction of the AMPA receptor subunit GluR2/3 with PDZ domains regulates hippocampal long-term depression. *Proceedings of the National Academy of Sciences of the United States of America* 98: 11725-30

Kim DS, Kwak SE, Kim JE, Won MH, Choi HC, et al. 2005. Bilateral enhancement of excitation via up-regulation of vesicular glutamate transporter subtype 1, not subtype 2, immunoreactivity in the unilateral hypoxic epilepsy model. *Brain research* 1055: 122-30

Kim J, Inoue K, Ishii J, Vanti WB, Voronov SV, et al. 2007. A MicroRNA feedback circuit in midbrain dopamine neurons. *Science* 317: 1220-4

Kim VN. 2005. MicroRNA biogenesis: coordinated cropping and dicing. *Nature reviews. Molecular cell biology* 6: 376-85

Kiriakidou M, Nelson PT, Kouranov A, Fitziev P, Bouyioukos C, et al. 2004. A combined computational-experimental approach predicts human microRNA targets. *Genes Dev* 18: 1165-78

Klein ME, Lioy DT, Ma L, Impey S, Mandel G, Goodman RH. 2007. Homeostatic regulation of MeCP2 expression by a CREB-induced microRNA. *Nature neuroscience* 10: 1513-4

Koch HP, Kavanaugh MP, Esslinger CS, Zerangue N, Humphrey JM, et al. 1999. Differentiation of substrate and nonsubstrate inhibitors of the high-affinity, sodium-dependent glutamate transporters. *Molecular pharmacology* 56: 1095-104

Kopp A, Blackman RK, Duncan I. 1999. Wingless, decapentaplegic and EGF receptor signaling pathways interact to specify dorso-ventral pattern in the adult abdomen of *Drosophila*. *Development* 126: 3495-507

Krek A, Grun D, Poy MN, Wolf R, Rosenberg L, et al. 2005. Combinatorial microRNA target predictions. *Nat Genet* 37: 495-500

Kwon C, Han Z, Olson EN, Srivastava D. 2005. MicroRNA-1 influences cardiac differentiation in *Drosophila* and regulates Notch signaling. *Proceedings of the National Academy of Sciences of the United States of America* 102: 18986-91

Lagos-Quintana M, Rauhut R, Lendeckel W, Tuschl T. 2001. Identification of novel genes coding for small expressed RNAs. *Science* 294: 853-8

Lagos-Quintana M, Rauhut R, Yalcin A, Meyer J, Lendeckel W, Tuschl T. 2002. Identification of tissue-specific microRNAs from mouse. *Current biology : CB* 12: 735-9

Lal A, Navarro F, Maher Ca, Maliszewski LE, Yan N, et al. 2009. miR-24 Inhibits cell proliferation by targeting E2F2, MYC, and other cell-cycle genes via binding to "seedless" 3'UTR microRNA recognition elements. *Molecular cell* 35: 610-25

Lall S, Grun D, Krek A, Chen K, Wang YL, et al. 2006. A genome-wide map of conserved microRNA targets in C. elegans. *Current biology : CB* 16: 460-71

Laneve P, Gioia U, Andriotto A, Moretti F, Bozzoni I, Caffarelli E. 2010. A minicircuitry involving REST and CREB controls miR-9-2 expression during human neuronal differentiation. *Nucleic acids research* 38: 6895-905

Lau NC, Lim LP, Weinstein EG, Bartel DP. 2001. An abundant class of tiny RNAs with probable regulatory roles in *Caenorhabditis elegans*. *Science* 294: 858-62

Lee HW, Lee EH, Ha SY, Lee CH, Chang HK, et al. 2012. Altered expression of microRNA miR-21, miR-155, and let-7a and their roles in pulmonary neuroendocrine tumors. *Pathology international* 62: 583-91

Lee RC, Ambros V. 2001. An extensive class of small RNAs in *Caenorhabditis elegans*. *Science* 294: 862-4

Lee RC, Feinbaum RL, Ambros V. 1993. The *C. elegans* heterochronic gene lin-4 encodes small RNAs with antisense complementarity to lin-14. *Cell* 75: 843-54

Lee Y, Kim M, Han J, Yeom KH, Lee S, et al. 2004. MicroRNA genes are transcribed by RNA polymerase II. *EMBO J* 23: 4051-60

Lewis BP, Burge CB, Bartel DP. 2005. Conserved seed pairing, often flanked by adenosines, indicates that thousands of human genes are microRNA targets. *Cell* 120: 15-20

Lewis BP, Shih IH, Jones-Rhoades MW, Bartel DP, Burge CB. 2003. Prediction of mammalian microRNA targets. *Cell* 115: 787-98

Li MZ, Elledge SJ. 2007. Harnessing homologous recombination *in vitro* to generate recombinant DNA via SLIC. *Nat Methods* 4: 251-6

Liguz-Lecznar M, Skangiel-Kramska J. 2007. Vesicular glutamate transporters (VGLUTs): the three musketeers of glutamatergic system. *Acta neurobiologiae experimentalis* 67: 207-18

Liu N, Landreh M, Cao K, Abe M, Hendriks GJ, et al. 2012. The microRNA miR-34 modulates ageing and neurodegeneration in Drosophila. *Nature* 482: 519-23

Llave C, Xie Z, Kasschau KD, Carrington JC. 2002. Cleavage of Scarecrow-like mRNA targets directed by a class of *Arabidopsis* miRNA. *Science* 297: 2053-6

Lu J, Getz G, Miska EA, Alvarez-Saavedra E, Lamb J, et al. 2005. MicroRNA expression profiles classify human cancers. *Nature* 435: 834-8

Madhavan MM, Madhavan K. 1980. Morphogenesis of the epidermis of adult abdomen of *Drosophila*. *Journal of embryology and experimental morphology* 60: 1-31

Madhavan MM and Schneidermann, H. A. 1977. Histological analysis of the dynamics of growth of imaginal discs and histoblast nests during the larval development of *Drosophila melanogaster*. *Roux's Arch, Dev. Biol.* 183: 269–305

Mahr A, Aberle H. 2006. The expression pattern of the *Drosophila* vesicular glutamate transporter: a marker protein for motoneurons and glutamatergic centers in the brain. *Gene expression patterns : GEP* 6: 299-309

Makeyev EV, Zhang J, Carrasco MA, Maniatis T. 2007. The MicroRNA miR-124 promotes neuronal differentiation by triggering brain-specific alternative pre-mRNA splicing. *Molecular cell* 27: 435-48

Maniataki E, Mourelatos Z. 2005. A human, ATP-independent, RISC assembly machine fueled by pre-miRNA. *Genes Dev* 19: 2979-90

Mansfield JH, Harfe BD, Nissen R, Obenauer J, Srineel J, et al. 2004. MicroRNA-responsive 'sensor' transgenes uncover Hox-like and other developmentally regulated patterns of vertebrate microRNA expression. *Nat Genet* 36: 1079-83

Mark KA, Quinton MS, Russek SJ, Yamamoto BK. 2007. Dynamic changes in vesicular glutamate transporter 1 function and expression related to methamphetamine-induced glutamate release. *The Journal of neuroscience : the official journal of the Society for Neuroscience* 27: 6823-31

Maroney PA, Yu Y, Nilsen TW. 2006. MicroRNAs, mRNAs, and translation. *Cold Spring Harbor symposia on quantitative biology* 71: 531-5

Matranga C, Tomari Y, Shin C, Bartel DP, Zamore PD. 2005. Passenger-strand cleavage facilitates assembly of siRNA into Ago2-containing RNAi enzyme complexes. *Cell* 123: 607-20

Mattie MD, Benz CC, Bowers J, Sensinger K, Wong L, et al. 2006. Optimized high-throughput microRNA expression profiling provides novel biomarker assessment of clinical prostate and breast cancer biopsies. *Molecular cancer* 5: 24

Mattson MP. 2003. Excitotoxic and excitoprotective mechanisms: abundant targets for the prevention and treatment of neurodegenerative disorders. *Neuromolecular medicine* 3: 65-94

Meijer HA, Kong YW, Lu WT, Wilczynska A, Spriggs RV, Robinson SW, Godfrey JD, Willis AE, and Bushell M. 2013. Translational Repression and eIF4A2 activity are critical for MicroRNA-mediated gene regulation. *Science* 5 April: Vol. 340 no. 6128 pp. 82-85

Mayer ML. 2011. Emerging models of glutamate receptor ion channel structure and function. *Structure* 19: 1370-80

Meyer WJ, Schreiber S, Guo Y, Volkmann T, Welte MA, Muller HA. 2006. Overlapping functions of argonaute proteins in patterning and morphogenesis of *Drosophila* embryos. *PLoS genetics* 2: e134

Miranda KC, Huynh T, Tay Y, Ang YS, Tam WL, et al. 2006. A pattern-based method for the identification of MicroRNA binding sites and their corresponding heteroduplexes. *Cell* 126: 1203-17

Moriyama Y, Yamamoto A. 1995. Vesicular L-glutamate transporter in microvesicles from bovine pineal glands. Driving force, mechanism of chloride anion activation, and substrate specificity. *The Journal of biological chemistry* 270: 22314-20

Morozova N, Zinovyev A, Nonne N, Pritchard LL, Gorban AN, Harel-Bellan A. 2012. Kinetic signatures of microRNA modes of action. *RNA* 18: 1635-55

Murchison EP, Stein P, Xuan Z, Pan H, Zhang MQ, et al. 2007. Critical roles for Dicer in the female germline. *Genes Dev* 21: 682-93

Naito S UT. 1985. Characterization of glutamate uptake into synaptic vesicles. *Journal of neurochemistry* 44: 99-109

Nakajima Y, Kuranaga E, Sugimura K, Miyawaki A, Miura M. 2011. Nonautonomous apoptosis is triggered by local cell cycle progression during epithelial replacement in Drosophila. *Mol Cell Biol* 31: 2499-512

Nielsen AF, Leuschner PJ, Martinez J. 2007. Not miR-ly a splicing factor: hnRNP A1 succumbs to microRNA temptation. *Nature structural & molecular biology* 14: 572-3

Ninov N, Chiarelli DA, Martin-Blanco E. 2007. Extrinsic and intrinsic mechanisms directing epithelial cell sheet replacement during Drosophila metamorphosis. *Development* 134: 367-79

Ninov N, Manjon C, Martin-Blanco E. 2009. Dynamic control of cell cycle and growth coupling by ecdysone, EGFR, and PI3K signaling in Drosophila histoblasts. *PLoS Biol* 7: e1000079

Noren Hooten N, Abdelmohsen K, Gorospe M, Ejiogu N, Zonderman AB, Evans MK. 2010. microRNA expression patterns reveal differential expression of target genes with age. *PLoS One* 5: e10724

Nottrott S, Simard MJ, Richter JD. 2006. Human let-7a miRNA blocks protein production on actively translating polyribosomes. *Nature structural & molecular biology* 13: 1108-14

Okamura K, Hagen JW, Duan H, Tyler DM, Lai EC. 2007. The mirtron pathway generates microRNA-class regulatory RNAs in Drosophila. *Cell* 130: 89-100

Okamura K, Ishizuka A, Siomi H, Siomi MC. 2004. Distinct roles for Argonaute proteins in small RNA-directed RNA cleavage pathways. *Genes Dev* 18: 1655-66

Olney, JW (1969). "Brain lesions, obesity, and other disturbances in mice treated with monosodium glutamate.". *Science* **164** (3880): 719–21.

Olney JW. 2003. Excitotoxicity, apoptosis and neuropsychiatric disorders. *Current opinion in pharmacology* 3: 101-9

Osada H, Takahashi T. 2011. let-7 and miR-17-92: small-sized major players in lung cancer development. *Cancer science* 102: 9-17

Petersen CP, Bordeleau ME, Pelletier J, Sharp PA. 2006. Short RNAs repress translation after initiation in mammalian cells. *Molecular cell* 21: 533-42

Pillai RS, Bhattacharyya SN, Artus CG, Zoller T, Cougot N, et al. 2005. Inhibition of translational initiation by Let-7 MicroRNA in human cells. *Science* 309: 1573-6

Pulikkan JA, Dengler V, Peramangalam PS, Peer Zada AA, Muller-Tidow C, et al. 2010. Cell-cycle regulator E2F1 and microRNA-223 comprise an autoregulatory negative feedback loop in acute myeloid leukemia. *Blood* 115: 1768-78

Rehmsmeier M, Steffen P, Hochsmann M, Giegerich R. 2004. Fast and effective prediction of microRNA/target duplexes. *RNA* 10: 1507-17

Reinhart BJ, Slack FJ, Basson M, Pasquinelli AE, Bettinger JC, et al. 2000. The 21-nucleotide let-7 RNA regulates developmental timing in *Caenorhabditis elegans*. *Nature* 403: 901-6

Reinhart BJ, Weinstein EG, Rhoades MW, Bartel B, Bartel DP. 2002. MicroRNAs in plants. *Genes Dev* 16: 1616-26

Reisberg B, Doody R, Stoffler A, Schmitt F, Ferris S, et al. 2003. Memantine in moderate-to-severe Alzheimer's disease. *The New England journal of medicine* 348: 1333-41

Rhoades MW, Reinhart BJ, Lim LP, Burge CB, Bartel B, Bartel DP. 2002. Prediction of plant microRNA targets. *Cell* 110: 513-20

Rodriguez A, Griffiths-Jones S, Ashurst JL, Bradley A. 2004. Identification of mammalian microRNA host genes and transcription units. *Genome research* 14: 1902-10

Roseland CR, Schneiderman HA. 1979. Regulation and metamorphosis of the abdominal histoblasts of *Drosophila melanogaster. Wilhelm Roux's archives of developmental biology* Volume 186, Issue 3, pp 235-265

Ruby JG, Jan CH, Bartel DP. 2007a. Intronic microRNA precursors that bypass Drosha processing. *Nature* 448: 83-6

Ruby JG, Stark A, Johnston WK, Kellis M, Bartel DP, Lai EC. 2007b. Evolution, biogenesis, expression, and target predictions of a substantially expanded set of *Drosophila* microRNAs. *Genome research* 17: 1850-64

Ruzzo A, Canestrari E, Galluccio N, Santini D, Vincenzi B, et al. 2011. Role of KRAS let-7 LCS6 SNP in metastatic colorectal cancer patients. *Annals of oncology : official journal of the European Society for Medical Oncology / ESMO* 22: 234-5

Ryan B, Musazzi L, Mallei A, Tardito D, Gruber SH, et al. 2009. Remodelling by early-life stress of NMDA receptor-dependent synaptic plasticity in a gene-environment rat model of depression. *The international journal of neuropsychopharmacology / official scientific journal of the Collegium Internationale Neuropsychopharmacologicum* 12: 553-9

Sagara Y, Schubert D. 1998. The activation of metabotropic glutamate receptors protects nerve cells from oxidative stress. *The Journal of neuroscience : the official journal of the Society for Neuroscience* 18: 6662-71

Saito K, Ishizuka A, Siomi H, Siomi MC. 2005. Processing of pre-microRNAs by the Dicer-1-Loquacious complex in *Drosophila* cells. *PLoS Biol* 3: e235

Sandmann T, Cohen SM. 2007. Identification of novel *Drosophila melanogaster* microRNAs. *PLoS One* 2: e1265

Schmitt A, Asan E, Lesch KP, Kugler P. 2002. A splice variant of glutamate transporter GLT1/EAAT2 expressed in neurons: cloning and localization in rat nervous system. *Neuroscience* 109: 45-61

Schuster CM, Ultsch A, Schloss P, Cox JA, Schmitt B, Betz H. 1991. Molecular cloning of an invertebrate glutamate receptor subunit expressed in *Drosophila* muscle. *Science* 254: 112-4

Schwarz DS, Hutvagner G, Du T, Xu Z, Aronin N, Zamore PD. 2003. Asymmetry in the assembly of the RNAi enzyme complex. *Cell* 115: 199-208

Seitz H, Tushir JS, Zamore PD. 2011. A 5'-uridine amplifies miRNA/miRNA* asymmetry in Drosophila by promoting RNA-induced silencing complex formation. *Silence* 2: 4

Shigemoto R, Kinoshita A, Wada E, Nomura S, Ohishi H, et al. 1997. Differential presynaptic localization of metabotropic glutamate receptor subtypes in the rat hippocampus. *The Journal of neuroscience : the official journal of the Society for Neuroscience* 17: 7503-22

Shirras AD, Couso JP. 1996. Cell fates in the adult abdomen of *Drosophila* are determined by wingless during pupal development. *Dev Biol* 175: 24-36

Siliprandi R, Lipartiti M, Fadda E, Sautter J, Manev H. 1992. Activation of the glutamate metabotropic receptor protects retina against N-methyl-D-aspartate toxicity. *European journal of pharmacology* 219: 173-4.

Simcox AA, Hersperger E, Shearn A, Whittle JR, Cohen SM. 1991. Establishment of imaginal discs and histoblast nests in *Drosophila. Mech Dev* 34(1):11-20.

Smits KM, Paranjape T, Nallur S, Wouters KA, Weijenberg MP, et al. 2011. A let-7 microRNA SNP in the KRAS 3'UTR is prognostic in early-stage colorectal cancer. *Clinical cancer research : an official journal of the American Association for Cancer Research* 17: 7723-31

Spillson AB, Russell JW. 2003. Metabotropic glutamate receptor regulation of neuronal cell death. *Experimental neurology* 184 Suppl 1: S97-105

Stark A, Brennecke J, Bushati N, Russell RB, Cohen SM. 2005. Animal MicroRNAs confer robustness to gene expression and have a significant impact on 3'UTR evolution. *Cell* 123: 1133-46

Struhl G, Barbash DA, Lawrence PA. 1997. Hedgehog organises the pattern and polarity of epidermal cells in the *Drosophila* abdomen. *Development* 124: 2143-54

Sutherland GR, Gedeon A, Kornman L, Donnelly A, Byard RW, et al. 1991. Prenatal diagnosis of fragile X syndrome by direct detection of the unstable DNA sequence. *The New England journal of medicine* 325: 1720-2

Takamori S, Rhee JS, Rosenmund C, Jahn R. 2000. Identification of a vesicular glutamate transporter that defines a glutamatergic phenotype in neurons. *Nature* 407: 189-94

Thermann R, Hentze MW. 2007. *Drosophila* miR2 induces pseudo-polysomes and inhibits translation initiation. *Nature* 447: 875-8

Tomari Y, Du T, Zamore PD. 2007. Sorting of *Drosophila* small silencing RNAs. *Cell* 130: 299-308

Tordera RM, Pei Q, Sharp T. 2005. Evidence for increased expression of the vesicular glutamate transporter, VGLUT1, by a course of antidepressant treatment. *J Neurochem* 94: 875-83

Touret M, Parrot S, Denoroy L, Belin MF, Didier-Bazes M. 2007. Glutamatergic alterations in the cortex of genetic absence epilepsy rats. *BMC neuroscience* 8: 69

Townley-Tilson WH, Callis TE, Wang D. 2010. MicroRNAs 1, 133, and 206: critical factors of skeletal and cardiac muscle development, function, and disease. *The international journal of biochemistry & cell biology* 42: 1252-5

Tsang J, Zhu J, van Oudenaarden A. 2007. MicroRNA-mediated feedback and feedforward loops are recurrent network motifs in mammals. *Molecular cell* 26: 753-67

Tzschentke TM. 2002. Glutamatergic mechanisms in different disease states: overview and therapeutical implications - an introduction. *Amino acids* 23: 147-52

Valencia-Sanchez MA, Liu J, Hannon GJ, Parker R. 2006. Control of translation and mRNA degradation by miRNAs and siRNAs. *Genes Dev* 20: 515-24

van Rooij E, Sutherland LB, Liu N, Williams AH, McAnally J, et al. 2006. A signature pattern of stress-responsive microRNAs that can evoke cardiac hypertrophy and heart failure. *Proceedings of the National Academy of Sciences of the United States of America* 103: 18255-60

van Rooij E, Sutherland LB, Qi X, Richardson JA, Hill J, Olson EN. 2007. Control of stress-dependent cardiac growth and gene expression by a microRNA. *Science* 316: 575-9

Varghese J, Cohen SM. 2007. microRNA miR-14 acts to modulate a positive autoregulatory loop controlling steroid hormone signaling in Drosophila. *Genes Dev* 21: 2277-82

Varghese J, Lim SF, Cohen SM. 2010. *Drosophila* miR-14 regulates insulin production and metabolism through its target, sugarbabe. *Genes Dev* 24: 2748-53

Vincent P, Mulle C. 2009. Kainate receptors in epilepsy and excitotoxicity. *Neuroscience* 158: 309-23

Volinia S, Calin GA, Liu CG, Ambs S, Cimmino A, et al. 2006. A microRNA expression signature of human solid tumors defines cancer gene targets. *Proceedings of the National Academy of Sciences of the United States of America* 103: 2257-61

Wafford KA, Kathoria M, Bain CJ, Marshall G, Le Bourdelles B, et al. 1995. Identification of amino acids in the N-methyl-D-aspartate receptor NR1 subunit that contribute to the glycine binding site. *Molecular pharmacology* 47: 374-80

Wakiyama M, Takimoto K, Ohara O, Yokoyama S. 2007. Let-7 microRNA-mediated mRNA deadenylation and translational repression in a mammalian cell-free system. *Genes Dev* 21: 1857-62

Wang QZ, Lv YH, Gong YH, Li ZF, Xu W, et al. 2012. Double-stranded Let-7 mimics, potential candidates for cancer gene therapy. *Journal of physiology and biochemistry* 68: 107-19

Wang X, Proud CG. 2008. A novel mechanism for the control of translation initiation by amino acids, mediated by phosphorylation of eukaryotic initiation factor 2B. *Mol Cell Biol* 28: 1429-42

Weng R, Chen YW, Bushati N, Cliffe A, Cohen SM. 2009. Recombinase-mediated cassette exchange provides a versatile platform for gene targeting: knockout of miR-31b. *Genetics* 183: 399-402

Wienholds E, Kloosterman WP, Miska E, Alvarez-Saavedra E, Berezikov E, et al. 2005. MicroRNA expression in zebrafish embryonic development. *Science* 309: 310-1

Wightman B, Ha I, Ruvkun G. 1993. Posttranscriptional regulation of the heterochronic gene lin-14 by lin-4 mediates temporal pattern formation in C. elegans. *Cell* 75: 855-62

Wojcik SM, Rhee JS, Herzog E, Sigler A, Jahn R, et al. 2004. An essential role for vesicular glutamate transporter 1 (VGLUT1) in postnatal development and control of quantal size. *Proceedings of the National Academy of Sciences of the United States of America* 101: 7158-63

Wolosker H, Rocha JB, Engelender S, Panizzutti R, De Miranda J, de Meis L. 1997. Sarco/endoplasmic reticulum Ca2+-ATPase isoforms: diverse responses to acidosis. *The Biochemical journal* 321 (Pt 2): 545-50

Wu L, Fan J, Belasco JG. 2006. MicroRNAs direct rapid deadenylation of mRNA. *Proceedings of the National Academy of Sciences of the United States of America* 103: 4034-39

Wu Q, Clark MS, Palmiter RD. 2012. Deciphering a neuronal circuit that mediates appetite. *Nature* 483: 594-7

Wuchty S, Fontana W, Hofacker IL, Schuster P. 1999. Complete suboptimal folding of RNA and the stability of secondary structures. *Biopolymers* 49: 145-65

Yang M, Shen H, Qiu C, Ni Y, Wang L, et al. 2012. High expression of miR-21 and miR-155 predicts recurrence and unfavourable survival in non-small cell lung cancer. *European journal of cancer*

Yekta S, Shih IH, Bartel DP. 2004. MicroRNA-directed cleavage of HOXB8 mRNA. *Science* 304: 594-6

Yi JH, Hazell AS. 2006. Excitotoxic mechanisms and the role of astrocytic glutamate transporters in traumatic brain injury. *Neurochemistry international* 48: 394-403

Yi R, Qin Y, Macara IG, Cullen BR. 2003. Exportin-5 mediates the nuclear export of pre-microRNAs and short hairpin RNAs. *Genes Dev* 17: 3011-6

Yoo AS, Greenwald I. 2005. LIN-12/Notch activation leads to microRNA-mediated down-regulation of Vav in *C. elegans*. *Science* 310: 1330-3

Zhang W, Winder T, Ning Y, Pohl A, Yang D, et al. 2011. A let-7 microRNA-binding site polymorphism in 3'-untranslated region of KRAS gene predicts response in wild-type KRAS patients with metastatic colorectal cancer treated with cetuximab monotherapy. *Annals of oncology : official journal of the European Society for Medical Oncology / ESMO* 22: 104-9

Zhao Y, Ransom JF, Li A, Vedantham V, von Drehle M, et al. 2007. Dysregulation of cardiogenesis, cardiac conduction, and cell cycle in mice lacking miRNA-1-2. *Cell* 129: 303-17

Zheng GX, Ravi A, Calabrese JM, Medeiros LA, Kirak O, et al. 2011. A latent pro-survival function for the mir-290-295 cluster in mouse embryonic stem cells. *PLoS genetics* 7: e1002054